Dynamical quark loops at low energies and in medium

Benić, Sanjin

Doctoral thesis / Disertacija

2013

Degree Grantor / Ustanova koja je dodijelila akademski / stručni stupanj: **University of Zagreb, Faculty of Science / Sveučilište u Zagrebu, Prirodoslovno-matematički fakultet**

Permanent link / Trajna poveznica: https://urn.nsk.hr/urn:nbn:hr:217:984849

Rights / Prava: In copyright/Zaštićeno autorskim pravom.

Download date / Datum preuzimanja: **2024-04-25**

Repository / Repozitorij:

Repository of the Faculty of Science - University of Zagreb

UNIVERSITY OF ZAGREB
FACULTY OF SCIENCE
PHYSICS DEPARTMENT

Sanjin Benić

Dynamical quark loops
at low energies and in medium

Doctoral Thesis submitted to the Physics Department
Faculty of Science, University of Zagreb
for the academic degree of
Doctor of Natural Sciences (Physics)

Zagreb, 2013.

Sanjin Benić

Dinamičke kvarkovske petlje
na niskim energijama i u mediju

Zagreb, 2013.

This thesis was made under the mentorship of Prof. Dr. Dubravko Klabučar, within University post-graduate studies at Physics Department of Faculty of Science of University of Zagreb.

Ova disertacija izrađena je pod vodstvom prof. dr. sc. Dubravka Klabučara, u sklopu Sveučilišnog poslijediplomskog studija pri Fizičkom odsjeku Prirodoslovno-matematičkoga fakulteta Sveučilišta u Zagrebu.

Acknowledgments

Herewith I would like to express great thanks to my supervisor Prof. Dubravko Klabučar, for his encouragement, constant patience and full support throughout the tick and thin of this research. I am deeply indebt to Prof. David Blaschke for many invitations to Wrocław, as well as to wonderful schools in Dubna and Catania, for countless physics discussions and for leaving a profound and irreducible mark on my professional as well as personal development. This thesis would be impossible without the extraordinary patience of my dear colleague Davor Horvatić with every painful detail of the tedious numerical work. Part of the results presented in this thesis are a product of the work with Dalibor Kekez, Gustavo Contrera and Prof. Michael Buballa - thank you for sharing your time, knowledge and expertize!

I would like to thank my friends and colleagues at the University of Zagreb: Branimir, Luka and Ivica for their help, advice and for numerous exciting discussions on many physics phenomena. I find myself extremely fortunate to have met a host of wonderful physicists within such a short time of doing physics, in particular: Daniel, Jakub, Rafał, Agnieszka and Thomas at Wrocław University who always provided a warm and cheerful atmosphere, Giuseppe who patiently endured many late night discussions, David Alvarez, Martina, Andreas and many more.

I hold deep gratitude, respect and admiration to my family for their love and for their support. Petra, thank you for your infinite love, inspiration and understanding.

University of Zagreb   Doctoral Thesis
Faculty of Science
Physics Department

Dynamical quark loops at low energies and in medium

SANJIN BENIĆ

Faculty of Science, Zagreb

We performed a research of dynamical quark loops as a basis for micro-scopic modelling of low-energy aspects of Quantum Chromodynamics (QCD). Part of research covers the calculation of the anomalous transition of a virtual photon into three pions, within a constituent quark-meson model. We study the possibility of adding the lowest resonances, e. g. the rho and omega mesons. In the second part mesons are built from quark-antiquark loops (Bethe-Salpeter amplitudes). Quark propagators are generated from the associated Dyson-Schwinger gap equation. Research is first focused on the $\eta - \eta'$ complex, which is in direct relationship with the gluonic sector of the theory. Using the Matsubara formalism, the calculation is generalized to finite temperatures, where it is particularly interesting to observe influence of the medium on restoration of $U(1)_A$. Experimental analysis of data from heavy-ion collisions at RHIC requires that the mass of the η' particle significantly reduces at finite temperature, consequently leading to partial restoration of $U(1)_A$ symmetry. Given result is explained by a modification of the Witten-Veneziano relation at finite temperature. General study of quark models at finite temperature and density is a third subject of this research. By calculating the equation of state it is established that covariant quark models suffer from a thermodynamic instability. Inclusion of the Polyakov loop stabilizes the system. Within the non-local Nambu Jona Lasinio model effect of Lorentz symmetry breaking on the phase diagram is investigated. Under certain approximations the hadron dissociation effect is discussed for the π and the σ particle at finite temperature. We

have shown that the meson widths for dissociation into quark-antiquark pairs as functions of temperature are extremely sensitive to the particular way the quark-antiquark interaction is introduced.

Supervisor:	- Prof. dr. sc. Dubravko Klabučar, University of Zagreb
Committee:	1. Doc. dr. sc. Davor Horvatić, University of Zagreb
	2. Prof. dr. sc. Dubravko Klabučar, University of Zagreb
	3. Prof. dr. sc. Mirko Planinić, University of Zagreb
	4. Prof. dr. sc. David Blaschke, Wrocław University
	5. Dr. sc. Dalibor Kekez, Senior Research Associate, Ruđer Bošković Institute
Replacements:	1. Dr. sc. Tihomir Surić, Senior Research Associate, Ruđer Bošković Institute
	2. Prof. dr. sc. Ivica Picek, University of Zagreb
Thesis accepted:	2013.

Sveučilište u Zagrebu   Doktorska disertacija
Prirodoslovno-matematički fakultet
Fizički odsjek

Dinamičke kvarkovske petlje na niskim energijama i u mediju

Sanjin Benić

Prirodoslovno-matematički fakultet, Zagreb

Istražili smo dinamičke kvarkovske petlje kao temelja za mikroskopsko modeliranje niskoenergetske kvantne kromodinamike (QCD, od engl. Quantum Chromodynamics). Dio istraživanja pokriva računanje anomalnog prijelaza virtualnog fotona u tri piona, unutar konstituentnog kvarkovskog modela. Izučava se mogućnost doprinosa najnižih rezonanci, kao npr. ρ i ω mezona. U drugom dijelu mezoni se grade iz kvark-antikvark petlji (Bethe-Salpeter amplituda). Kvarkovski propagatori generiraju se iz pripadne Dyson-Schwinger jednadžbe procjepa. U fokusu istraživanja je $\eta - \eta'$ kompleks koji je izravnoj vezi s gluonskim sektorom teorije. Pomoću Matsubarinog formalizma račun se generalizira na konačne temperature, gdje je posebice interesantno promotriti utjecaj medija na obnavljanje $U(1)_A$. Analiza eksperimentalnih rezultata sa sudarivača teških iona na RHIC-u nalaže da se masa η' čestice znatno reducira na konačnoj temperaturi, što posljedično vodi na djelomi cnu restauraciju $U(1)_A$ simetrije. Dani rezultat se obrazlaže modifikacijom Witten-Veneziano relacije na konačnoj temperaturi. Generalno izučavanje kvarkovskih modela na konačnoj temperaturi i gustoći je treća stavka ovog istraživanja. Računanjem jednadžbe stanja ustanovljuje se da kovarijantni kvarkovski modeli pate od termodinamičke nestabilnosti. Tek uključenje Polyakovljeve petlje stabilizira sustav. Unutar nelokalnih Nambu–Jona-Lasinio modela efekt lomljenja Lorentzove simetrije na fazni dijagram je istražen. Unutar određenih aproksimacija diskutira se disocijacija hadrona za π i σ česticu na konačnoj temperaturi. Pokazano je da širina mezona za disocijaciju u kvark-antkvark par kao funkcija

temperature je izrazito osjetljiva na način na koji se efektivna kvark-antikvark interakcija uvodi u sistem.

Contents

Introduction

The main object of this Thesis is to explore the role of dynamical quarks in modeling a variety of QCD observables, in the vacuum, as well as in the medium.

In Chapter 1 we briefly review selected properties of QCD. The following Chapter 2 calculates the anomalous process $\gamma^* \to \pi^+\pi^0\pi^-$ in the quark-level linear sigma model. As a novelty, we generalize the model by introducing vector mesons, in order to meet the requirements of experiments exploring high momentum range of the corresponding $\gamma^* \to \pi^+\pi^0\pi^-$ form factor.

Chapter 3 serves to introduce technical aspects of the bound state formalism to be used in the next two chapters. The $\eta - \eta'$ complex is studied in Chapter 4, where the Witten-Veneziano relation in medium is closely inspected. We have found that in order to accommodate the recent analysis of experimental results on the η' multiplicity, Witten-Veneziano relation should be modified at finite temperature.

In the final two Chapters 5 and 6, we explore the thermodynamics of the covariant quark models, introduced in Chapter 3. We study the $T - \mu$ phase diagram of the model.

Our calculations show that covariant models are thermodynamically unstable. We have found that the system is partially stabilized by the Polyakov loop.

In the last Chapter 6 of this Thesis, we study meson dissociation as a physical mechanism for in-medium deconfinement. Under certain approximations, we were able to calculate the structure of the quark-antiquark polarization loop in the complex energy plane. Results reveal a great sensitivity to the particular form of the effective gluon interaction used.

1

Selected overview of QCD

Quantum Chromodynamics (QCD) is a $SU(3)$ quantum gauge theory of quarks and gluons. The seeds of QCD were sown back in 1964 when Gell Mann made order in the hadron zoo with the introduction of quarks in the famous Eightfold Way [1]. Thus, the flavor degree of freedom was born.

Color was a theoretical construct to explain the existence of states such as the Δ^{++} resonance. Containing three up quarks with the same spin orientation, this state did not obey the Pauli principle. Deep inelastic scattering at SLAC [2, 3] put the theory to test, confirming that quarks come in $N_c = 3$ colors.

Embedding of quarks in a quantum gauge theory, where they interact through intermediate gluons was developed in 1973 independently by Pati and Salam [4], Fritsch, Gell–Mann and Leutwyler [5], and Weinberg [6].

Explicitly, the classical QCD Lagrangian for N_f flavors reads

$$\mathscr{L} = -\sum_{i=1}^{N_f} \bar{q}(\gamma^\mu \mathscr{D}_\mu + m_i)q - \frac{1}{2}\mathrm{Tr}(F^{\mu\nu}F_{\mu\nu}) + \frac{\theta}{16\pi^2}\mathrm{Tr}(\tilde{F}^{\mu\nu}F_{\mu\nu}) \,, \qquad (1.1)$$

where q are the quark and $F_{\mu\nu}$ gauge fields. The interaction is generated by the covariant derivative

$$\mathscr{D}_\mu = \partial_\mu + ig A_\mu \qquad (1.2)$$

but also by the non-Abelian strucure of the theory

$$F_{\mu\nu} = \partial_\mu A_\nu - \partial_\nu A_\mu + g[A_\mu, A_\nu] \,, \qquad (1.3)$$

where A_μ are matrices in $SU(3)$ space. Parameters of the theory are the quark masses m_i, the gauge coupling g and the angle θ.

§ 1.1 PROPERTIES

At low energies quarks and gluons exist only in color singlet states: mesons and baryons. The fact that up to now no one has ever spotted a free quark or gluon

5

in a detector is known as *confinement*.

However, at high energies they behave as almost free-particles. This dramatic property, known as *asymptotic freedom*, discovered by Gross, Politzer and Wilczek [7, 8], is understood as a logarithmic decrease

$$\mu^2 \frac{\partial \alpha_s}{\partial \mu^2} = -\frac{1}{4\pi} \left(11 - \frac{2N_f}{3} \right) \alpha_s^2, \quad \alpha_s(\mu^2) = \frac{1}{\frac{1}{4\pi} \left(11 - \frac{2N_f}{3} \right) \log(\mu^2/\Lambda_{\text{QCD}}^2)} \quad (1.4)$$

of the strong coupling constant α_s with the typical momenta in the process μ.

A hint of confining property of QCD is seen already from (1.4), where at the scale $\Lambda_{\text{QCD}} \sim 200$ MeV strong coupling diverges. Of course, perturbation theory itself breaks down at a higher scale - non-perturbative physics becomes important already at least around $4\pi f_\pi \sim 1$ GeV and in practice even higher.

A physical manifestation of the non-perturbative physics is witnessed by the breaking of the approximate chiral symmetry of QCD. Namely in the limit where all N_f quarks have identically vanishing masses, QCD enjoys a global $SU(N_f)_L \times SU(N_f)_R$ chiral symmetry. This is believed to be broken by strong infrared quantum fluctuations down to its vectorial subgroup $SU(N_f)_{L+R}$. The imprint of this *dynamical chiral symmetry breaking* is manifested in the absence of degenerate parity partners in the physical spectrum, as e. g. seen in the splitting between ρ and a_1 mesons. Moreover, that truly strong dynamics is what governs QCD in the IR is witnessed by the presence of a mass gap in the spectrum. For example, instead of the small hyperfine splitting between the π and the ρ state, as expected in weakly coupled system like QED, one observes a huge mass gap of the order of 1 GeV. Finally, the lightness of the pion is a direct consequence of the Goldstone theorem, stating that massless particles always accompany breaking of a continuous global symmetry.

In the real world quarks are not massless, but chiral symmetry is still useful for quarks with masses $m_q \ll \Lambda_{\text{QCD}}$. Thus, Λ_{QCD} plays a special role in determining the *hierarchy* between quarks. As we will be concerned exclusively with physics up to 1 GeV, we will consider only u, d and s quarks, with $m_u \sim 5$ MeV and $m_s \sim 100$ MeV, as relevant degrees of freedom. The effects of much heavier c, b and t quarks can be safely neglected.

§ 1.2 TOOLS

The strong non-linearity of the theory in the IR mandates the usage of non-perturbative techniques to calculate QCD observables. These are lattice QCD theory, functional methods and effective models. Although this work is mostly concentrated on effective models, let us briefly highlight the first two methods as well.

Lattice QCD (lQCD) methods start by discretization of Euclidean spacetime, so that the QCD path integral becomes accessible through Monte-Carlo integration. At this point, this is the only *ab initio* approach for QCD able to put error bars on its output, which is its main merit. As some of its fantastic successes we may single out calculation of the proton mass [9], and the resolution that the quark and gluon plasma emerges at high T and zero density through not through a strict phase transition [11, 10, 12], but a crossover. As one of its most severe challenges, let us single out the infamous sign problem [11]: the high density physics of QCD is not accessible to Monte-Carlo simulations due to the complex fermion determinant.

An alternative in the continuum are the functional methods as e. g. the Dyson-Schwinger equations (DSEs) [13, 14] which are an infinite set of coupled integral equations for the Green functions of the theory, and the functional renormalization group (fRG) techniques [15, 16], constituting an infinite set of coupled differential equations for the Green functions of the theory. For example, we will encounter the DSE for the quark two-point Green function - the propagator. In that case, solving this equation exactly would require an input of the gluon propagator as well as of the quark-gluon vertex. These have their own DSE's to fulfil which in turn require the input of higher n-point Green's functions. Hence the system may never be closed.

Now we ask, how to then extract reliable information from such a system? An honest answer is: there is none - any truncation is an uncontrolled approximation. Nevertheless, a great hope is that these resummations are able to catch the essential non-perturbative element only in a small subset of Greens functions as e. g. dressed propagators and vertices. These can be tested on the lattice, making it possible to identify effects of the truncation, and therefore improve it. On the good side, as they represent continuum approaches, they are able to detect possible infrared divergences, unaccessible to lattice, as well as treat the high density regime. In this work we will not use the fRG equations, but in Chap. 3 we will, to some extent, lay out the relevant properties of the DSE formalism in more detail.

Finally, effective models serve as caricatures of the full theory. However, let us keep in mind that there are extremely successful effective approaches to QCD such as chiral perturbation theory. The reason for this success lies in applying the derivative expansion of the QCD path integral in terms of the Goldstone fields. This is also in principle the only "truly" effective field theory of low energy QCD [17], in the sense of being able to deliver observables with arbitrary accuracy, if the calculation is carried out in an arbitrary order of the derivative expansion.

Why then look for alternative models, if we have a handle on the effective theory? One reason is that we would like to be able to predict the effective cou-

plings of this theory, instead of fitting them to experiment. These couplings should in principle be derived from QCD. But any model of QCD, given in terms of quark and gluons degrees of freedom, has a chance of predicting them as well. Thus, by providing a suitable quark model we are able to learn something about QCD, at least qualitatively. In the words of Thomas Cohen [18]: *While high-quality numerical simulations may allow us to test whether QCD can explain low-energy hadronic phenomena, they will not, by themselves, give much insight into how QCD works in the low-energy regime. Simple intuitive pictures are essential to obtain insight, and models provide such pictures.*

Perhaps an even more convincing reason is that mesons and baryons are correct degrees of freedom only in a certain range of the QCD phase diagram. If the temperature and/or density is high enough they shall disappear from the spectrum. We will have more to say on this in the following Sections.

§ 1.3 CONSTITUENT VS. CURRENT QUARKS

Dynamical chiral symmetry breaking is the mechanism for providing mass to the visible matter in the Universe. Namely, even in massless QCD the proton weighs about 890 MeV.

On the quark level, the Higgs mechanism in the Standard Model gives u and d quarks only small, *current* masses of the order of ~ 5 MeV. The *constituent* quark mass may then be defined as $\sim m_N/3$ or $m_\rho/2$. Its origin are strong self-energy effects within QCD.

In more technical terms, vacuum structure of the fermion propagator is defined by two scalar functions $A(p^2)$ and $B(p^2)$. In Euclidean space it takes the following form

$$S^{-1}(p) = i\not{p}A(p^2) + B(p^2) \,, \tag{1.5}$$

the physical interpretation can be found from the alternative expression

$$S(p) = Z(p^2)\frac{i\not{p} + M(p^2)}{p^2 + M^2(p^2)} \,. \tag{1.6}$$

Here $M(p^2)$ has the meaning of the dynamical mass, while $Z(p^2) = 1/A(p^2)$ is the wave function renormalization.

Lattice calculations of the quark propagator teaches us [19, 20] that both $M(p^2)$ and $Z(p^2)$ alter dramatically in the IR. The dynamical mass strongly increases from its current value of a few MeV at $p^2 \gtrsim 1$ GeV to few hundred MeV at $p^2 \gtrsim 0$, while $Z(p^2)$ can differ from unity by $10 - 20\%$. Such a significant alteration of the quark propagator is an explicit manifestation of strong interactions. The dynamically generated mass is a clear signature of chiral symmetry
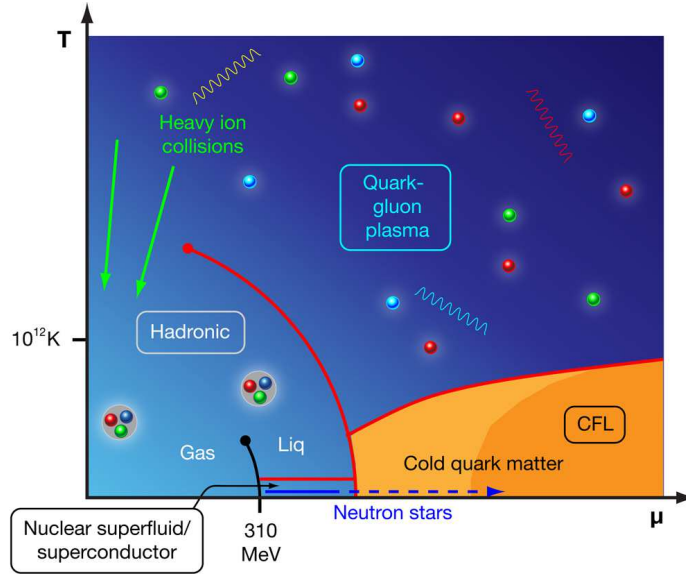
Figure 1.1: A cartoon of the conjectured QCD phase diagram, Fig. by A. Stone-braker.

breaking. Notice that this is unlike anything seen in perturbation theory, where coupling constants (like e. g. the mass) have a typical logarithmic running.

The physical picture of a quark emerging from such a calculation is of the one dressed by a cloud of non-perturbative gluons. From up close ($p^2 \gg \Lambda_{\text{QCD}}^2$), we are able to "see through the gluon cloud" the small current mass. Observing from afar, the gluon cloud renormalizes the quark mass, so that at large distance ($p^2 \ll \Lambda_{\text{QCD}}^2$) what is observed is the quark with a constituent mass.

§ 1.4 PHASE DIAGRAM

It is a fascinating fact that the QCD phase transition is the first phase transition predicted by an elementary particle theory that can be directly tested in a laboratory. Through heavy ion collisions we will come to understand what the Universe was like in its first moments of existence, and what hides in the interior of neutron stars.

QCD phase diagram is given in terms of the temperature T and baryochemical potential μ_B, see Fig. 1.1. At low T and $\mu_B = 0$ resides the mesons. The region at $T = 0$ and low μ_B is the realm of nuclear matter. It is conjectured that, due to the property of asymptotic freedom the high T and/or high μ_B ground

state of is a plasma. First guess on the boundary separating the two worlds is provided by $T \sim \Lambda_{\mathrm{QCD}} \sim 200$ MeV and $\mu_B \sim N_c \Lambda_{\mathrm{QCD}} \sim 1$ GeV.

There are two ways to describe the phase transition in QCD: one is through the melting of various condensates, like e. g. the quark and the gluon condensates, while the other is simply through chemistry - the chemical dissociation of hadrons.

To predict the QCD phase diagram one needs ab initio approaches like lattice or functional methods. To describe the QCD phase diagrams one uses a patchwork of models, each carefully describing a particular phase, provided by the degrees of freedom in a particular phase. These models are then used to also predict the possible boundary lines between the different phases. For a recent review one may consult [21].

In the limit of $m_q \to 0$, the quark condensate

$$\langle \bar{q}q \rangle_0 = -\frac{\partial}{\partial m_q} \log Z \Big|_{m_q=0} , \tag{1.7}$$

where Z is the QCD partition function, is an order parameter of chiral symmetry breaking, and can therefore be used to discern between different phases.

In the limit of $m_q \to \infty$ chiral physics looses its meaning. Quarks are essentially static, external probes of the pure YM system. This provides convenient grounds for characterization of confinement through the free energies of a system of quarks. In particular, for a single static quark, one defines the Polyakov loop Φ [22]

$$\Phi = \frac{1}{N_c} \mathrm{Tr}\left(\mathcal{P} e^{ig \int_0^\beta dx_4 A_4(x)} \right) , \tag{1.8}$$

where A_4 is the temporal gauge field. The name comes from the fact that at finite temperature it describes nothing but the Aharonov-Bohm phase the static quark acquires while traversing the thermal circle. Physically, it is related to the static energy of a free quark F_q

$$\Phi = e^{-\beta F_q} ,$$

so that $\Phi = 0$ at any finite temperature $\beta = 1/T$ represents a confining phase due to infinite free energy cost for having a free quark in the system.

Both the chiral and the deconfinement phase transition, are accompanied with symmetries being broken and restored. In the chirally broken phase massless QCD enjoys the $SU(N_f)_{L+R}$ symmetry, while the chirally restored phase brings back the full $SU(N_f)_L \times SU(N_f)_R$ symmetry. Conversely, in the confining regime the system is $Z(N_c)$ symmetric, where $Z(N_c)$ is the center of $SU(N_c)$. The deconfinement then breaks the $Z(N_c)$ symmetry.

Observe that these descriptions of the system are adequate only in the purely theoretical and opposite limits of $m_q \to 0$ or $m_q \to \infty$. For finite, but small, quark masses, the condensate may still give a valid characterization of the system, it can even show an order parameter behavior if in the massless case the transition is first order, as is the case of $N_f = 3$ [23]. Likewise, for finite but large quark masses, describing the system by the Polyakov loop may still be adequate. For $N_c = 3$ the transition is first order [24], so at finite quark masses we can still have an order parameter behavior. Modern lattice simulations [25] point that the physical u, d and s quarks lie outside of these regions, so that in the physical world there is no real phase transition but a smooth crossover.

From the experimental side, first hints of a new state of matter [26] from CERN-Super Proton Synchrotron (SPS) were confirmed by the Relativistic Heavy Ion Collider (RHIC) at Brookhaven National Laboratory [27] claiming that the quark-gluon plasma behaves like a perfect liquid, with exceptionally small viscosity. A detail underpinning of the thermal properties of QGP is the current program of the the Large Hadron Collider (LHC) [28].

First order phase transitions end up in second order critical end-points after which there is no true phase transition any more. This will happen for the chiral transition if we crank up the quark mass sufficiently, and it will happen for the confinement-deconfinement transition if we lower it. For physical quark masses it is then well established that the transition is neither strictly chiral nor confinement-deconfinement. Lattice calculations reveal that the condensate and the Polyakov loop show a rapid, but a smooth change by proceeding from a low T to a high T phase [25]. The question whether such a behavior persists also at non-zero μ_B, i. e. the search for critical end-point in the QCD phase diagram presents one of the main targets of future heavy ion collisions at Nuclotron based Ion Collider fAcility (NICA) in Dubna and Facility for Antiproton and Ion Research (FAIR) in Darmstadt.

What do we know about the QCD phase diagram at finite μ_B? The low T, and moderate μ_B region reveals a nuclear liquid-gas phase transition. At extremely high μ_B, of the order of 10^8 MeV, perturbative approach becomes admissible. Due to the intrinsic attractive channel in the quark-quark interaction the system develops an instability with respect to Cooper pairing, so that the ground state energy is lowered by forming a color superconductor, provided the temperature is sufficiently low [29, 30].

Whether this Color-Flavor-Locked (CFL) phase, or any of the less symmetric superconducting phases persists to chemical potentials of the order of $1 - 10$ GeV is a big open question. A laboratory for exploring these issues is the interior of a compact star.

The chemical picture of melting hadrons allows a intuitive description of the phase transition. This idea originates back to solid state physics, where the

metal- insulator transition is described via the so called Mott effect. Electrons in an insulator are normally confined to lattice sites. However, if sufficient thermal agitation is provided, they can merge in the continuum, and the material becomes a conductor. It is believed that the same Mott transition might provide the physical interpretation of the QCD phase transition. An attempt to describe it requires a microscopic understanding of the dissociation of hadrons, requiring understanding also of their formation, which basically boils down to understanding confinement. When this is established, the Mott effect is a natural mechanism for in-medium deconfinement. Thus, within the chemical picture, one appreciates the need for a bound state description of hadrons.

How to reconcile these two pictures, i. e. the melting condensates vs. the melting hadron picture? Here is a simplified explanation. Take the pion state, which is the lightest hadron with a mass of 140 MeV. In the quark model picture, the pion is a highly relativistic bound state of two constituent quarks, each with a mass of ~ 300 MeV. This means that the continuum threshold for the pion to Mott dissociate in its constituents is far above its mass. The moral is that such a gap is created by the chiral condensate - when the condensate melts, the threshold will lower until eventually it falls below the pion mass, i. e. the bound state dissociates.

There is a caveat to this simplified picture, as it cannot be applied to e. g. the ρ-meson, which lies very close to the threshold. An even better example would be the excited pion states. Obviously the confining nature of QCD is very important for a proper description.

2

Axial anomaly and $\gamma^* \rightarrow 3\pi$ process

§ 2.1 CHIRAL ANOMALY IN QCD

Of significant importance for particle physics are processes driven by quantum corrections. Prominent examples in the theory of weak interactions are the flavour changing neutral currents [31] in the Standard Model. In fact, there are processes which would simply not occur, or be extremely suppressed, if there was not for their quantum nature, and $\pi^0 \rightarrow \gamma\gamma$ is by far the most famous one, with the branching ratio for the 2γ channel $98.823 \pm 0.0034\%$. This is a process driven by the so-called Adler-Bell-Jackiw (ABJ) quantum anomaly [32, 33]. For a theory like massless quantum electrodynamics, Adler etal. have found that the axial current $J_5^\mu = \bar{\psi}\gamma^\mu\gamma_5\psi$ generated by the fermion field ψ is not conserved, leading to the celebrated result

$$\partial_\mu J_5^\mu = 2\frac{e^2}{16\pi^2}\tilde{F}_{\mu\nu}F^{\mu\nu} \,. \tag{2.1}$$

However, it was quickly realized that in QCD a number of process are anomalous, to list only some of them: $\eta(\eta') \rightarrow \gamma\gamma$, $\gamma^* \rightarrow \pi^+\pi^0\pi^-$, $\eta(\eta') \rightarrow \pi^+\pi^-\gamma$ etc. Rule of thumb is to consider an odd number of pseudoscalar particles and an even number of vector particles. Moreover, purely hadronic processes like $K^+K^- \rightarrow \pi^+\pi^-\pi^0$ are anomalous as well.

Probably the most elegant way to capture all the low-energy effective vertices for these reactions is provided by Wess, Zumino [34] and Witten [35] (WZW) action. By gauging the WZW action one also encounters all the possible radiative meson processes [35].

§ 2.2 EXPERIMENT

It is fair to say that the $\pi^0 \to \gamma\gamma$ process is well understood from the theoretical and experimental point of view. From a theoretical side, its cousin, the $\gamma^* \to 3\pi$, was first analysed by Aviv and Zee [36]. They found that in the low energy and chiral limit the convenient amplitude for this process is

$$A_\gamma^{3\pi} = \frac{e\, N_c}{12\pi^2 f_\pi^3} = 9.72 \pm 0.09 \,\text{GeV}^{-3} \,. \tag{2.2}$$

Of course, this is in complete accordance with the result given by the WZW action.

Experimentally, not much is known. The only measured value for this form-factor was provided back in '86 at Serpukhov [37]. Using the Primakoff effect, i. e. a combination of electromagnetic and strong interaction of the charged pion with a nucleus the experimental value

$$F_\gamma^{3\pi}(\text{expt}) = 12.9 \pm 0.9 \pm 0.5 \,\text{GeV}^{-3} \tag{2.3}$$

was extracted from the corresponding cross section. Clearly there is a discrepancy between this number and the theoretical prediction (2.2).

Due to the fact that (6.28) is not the value of the form-factor at the soft point, but was extracted by assuming a constant form-factor over the momentum range relevant at Serpukhov, a careful reanalysis [38, 39] showed that the actual disagreement is not that drastic, meaning that the value suitable for comparison with theory is

$$F_\gamma^{3\pi}(\text{expt}) = 11.4 \pm 1.3 \,\text{GeV}^{-3} \tag{2.4}$$

Moreover, it was found [39] that the remaining discrepancy is due to very specific kinematics used at Serpukhov allowing for electromagnetic corrections to become even more important than the chiral corrections. It is thus interesting for ongoing and future experiments like CEBAF at J-Lab [40] and COMPASS at CERN [41, 42] to make a more detailed prediction for the form-factor.

§ 2.3 CONSTITUENT QUARK MODEL COUPLED TO VECTOR MESONS

A usual treatment of the anomaly through a fermion loop is via axial vertices. Anomaly is then seen in the linear UV divergence in the amplitude. However, thanks to the Veltman-Sutherland (VS) theorem [43, 44] we are allowed to use pseudoscalar instead of axial vertices [45, 46, 47].

For the calculation of the form-factor we use a constituent quark loop (CQL) model, by coupling pions to pseudoscalar quark bilinears [47], [48, 49, 50, 51], [46, 52]. These present a class of quark-level linear σ models. In principle they can be derived from e. g. a quark model with one gluon exchange, the simplest being the NJL model, by partial integration of the quark degrees of freedom. The obvious disadvantage of this approach is a lack of confinement[1], hence the additional prescription is to use quarks only as virtual particles.

In experiments like the COMPASS experiment, higher energies are accessible, so that the lowest resonances, like the ρ, may appear in the process. For example, it is well known that the process $\eta' \to 2\pi\gamma$ generates a sharp ρ peak in its dipion spectrum [53]. Both the $\eta(\eta') \to 2\pi\gamma^{(*)}$ are to be measured on WASA at COSY [54, 55]. The $K^-\gamma^* \to K^-\pi^0$ to be measured on CEBAF is also expected to be influenced by the lightest resonances. Thus we are invited to couple also the lowest lying vector states, the ρ triplet and the ω to the CQL model. In the specific problem at hand we postulate that the pion pair might come via decay of a vector resonance.

The relevant terms of the effective Lagrangian is given by [2]

$$\mathscr{L}_{\text{eff}} = -\bar{q}(\slashed{\partial} + M_q + \dots)q + \mathscr{L}_{\text{int}} + \mathscr{L}_{\text{VMD2}} + \mathscr{L}_{\rho\pi\pi} , \qquad (2.5)$$

where $q = (u, d)^T$, M_q is the constituent mass.

The term $\mathscr{L}_{\text{int}}$ is given by

$$\mathscr{L}_{\text{int}} = -2ig_{\pi\bar{q}q}\bar{q}\gamma_5\pi q + ig_{\rho\bar{q}q}\bar{q}\gamma^\mu\rho_\mu q , \qquad (2.6)$$

where $\pi = \pi_a t_a$ with $t_a = \tau_a/2$ being the isospin Pauli matrices. The vector fields are $\rho^\mu = \rho_a^\mu t_a + \omega^\mu t_0$ and $t_0 = \tau_0/2$, $\tau_0 = \text{diag}(1, 1)$.

Even though in principle the $\rho \to \pi\pi$ decay can be calculated from $\mathscr{L}_{\text{int}}$, this quark triangle can be approximated by an effective point interaction, due to its weak momentum dependence [50]. This way only the effective coupling

$$\mathscr{L}_{\rho\pi\pi} = 2iG_{\rho\pi\pi}\text{Tr}([\pi, (\partial_\mu\pi)]\rho^\mu) , \qquad (2.7)$$

is of relevance to us. Finally, electromagnetism is introduced via vector meson dominance (more precisely, its second version VMD2) [56], which is basically

---

[1]A very qualitative explanation for this simplification goes as following: low-lying hadrons, with which we are concerned here, are ground states of quarks bound by some potential. In the low-energy regime, the probability to excite quarks is small. Therefore it is not important if the potential well for them is finite, or infinite, i. e. confining.

[2]The Minkowski metric used in this calculation is $\eta_{\mu\nu} = \text{diag}(\eta_{00}, \eta_{11}, \eta_{22}, \eta_{33}) = \text{diag}(-1, 1, 1, 1)$.
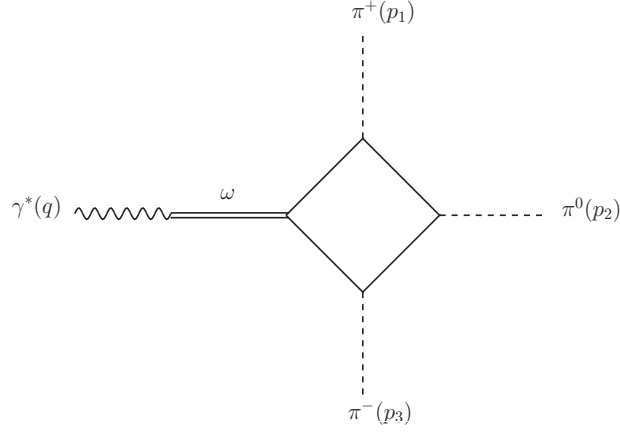
Figure 2.1: One of the six box diagrams.

saying that the hadronic contribution to the photon polarization tensor is saturated by vector mesons. An effective Lagrangian encompassing this property is

$$\mathcal{L}_{\text{VMD2}} = \frac{em_\rho^2}{g_{\rho\gamma}} A^\mu \left(\rho_\mu^0 + \frac{1}{3} \omega_\mu \right) .$$ (2.8)

The couplings that include vector mesons, are all assumed to satisfy vector meson universality [49], i. e.

$$g_{\rho\bar{q}q} = G_{\rho\pi\pi} = g_{\rho\gamma} \equiv g_\rho .$$ (2.9)

We have assumed the ideal $\omega - \phi$ mixing responsible for a factor of $1/3$ in (2.8). The stated approach is then abbreviated as the CQL-VMD model.

Notice that in this prescription photons couple to quarks only through an intermediate resonance. The quark box diagram depicted in Fig. 2.1, provides the same amplitude as the one with a direct coupling to the photon, if the photon is close to the mass shell, due to a convenient cancellation

$$\frac{em_\rho^2}{g_{\rho\gamma}} \times \frac{1}{m_\rho^2} \times g_{\rho\bar{q}q} \simeq e$$ (2.10)

in the amplitude. An almost on-shell photon is pertinent for all the relevant experiments, so we will be restricted to that case.

With vector mesons in the picture, additional diagram becomes relevant, where the quark box is replaced by a quark triangle, so that the two legs of a quark box are replaced by a vector meson, see Fig. 2.2.
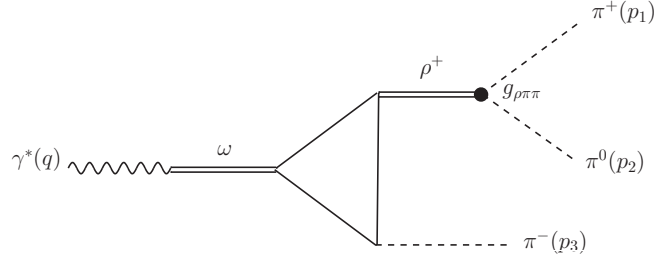
Figure 2.2: One of the six resonant triangle diagrams.

§ 2.4 WEINBERG-TOMOZAWA TERM

Applying Feynman rules leads to the following invariant amplitude

$$\mathcal{M}_\gamma^{3\pi} = \epsilon_\mu(\mathbf{q},\sigma)\, p_{1\nu}\, p_{2\rho}\, p_{3\lambda}\, \varepsilon^{\mu\nu\rho\lambda}\, F_\gamma^{3\pi}(p_1,p_2,p_3)\,, \qquad (2.11)$$

where kinematics is given by $\gamma^*(q) \to \pi^+(p_1)\pi^0(p_2)\pi^-(p_3)$, and $\epsilon_\mu(\mathbf{q},\sigma)$ is the photon polarization vector with polarization σ. It is convenient to introduce Mandelstam variables $s = -(p_1 + p_2)^2$, $t = -(p_2 + p_3)^2$, $u = -(p_1 + p_3)^2$.

The box and the triangle contributions to the form-factor $F_\gamma^{3\pi}$ read

$$F_\Diamond(p_1,p_2,p_3) = \frac{1}{3}\frac{eN_c}{6\pi^2}\frac{g_{\pi\bar{q}q}^3}{M_q^3}\frac{m_\rho^2}{m_\rho^2 + q^2}$$
$$\times \left[\widetilde{D}_0(p_1,p_2,p_3) + \widetilde{D}_0(p_1,p_3,p_2) + \widetilde{D}_0(p_2,p_1,p_3)\right], \quad (2.12)$$

$$F_\triangle^{\text{res}}(p_1,p_2,p_3) = \frac{1}{2}\frac{eN_c}{6\pi^2}\frac{g_{\pi\bar{q}q}}{M_q}\frac{g_{\rho\bar{q}q}^2}{m_\rho^2}\frac{m_\rho^2}{m_\rho^2 + q^2}$$
$$\times \left[\frac{m_\rho^2}{m_\rho^2 - s}\widetilde{C}_0(p_1,p_2) + \frac{m_\rho^2}{m_\rho^2 - t}\widetilde{C}_0(p_2,p_3) + \frac{m_\rho^2}{m_\rho^2 - u}\widetilde{C}_0(p_1,p_3)\right], \quad (2.13)$$

where $\widetilde{C}_0 = (2! M_q^2/i\pi^2)C_0$ and $\widetilde{D}_0 = (3! M_q^4/i\pi^2)D_0$, where $C_0(D_0)$ is the standard 't Hooft–Veltman [57] scalar three(four)–point function. In the soft-point and chiral limit where $\widetilde{C}_0, \widetilde{D}_0 \to 1$

$$F_\triangle^{\text{res}} \to \frac{3}{2}\frac{eN_c}{12\pi^2}\frac{1}{f_\pi^3} = \frac{3}{2}A_\gamma^{3\pi}\,, \qquad F_\Diamond \to \frac{eN_c}{12\pi^2}\frac{1}{f_\pi^3} = A_\gamma^{3\pi}\,, \qquad (2.14)$$
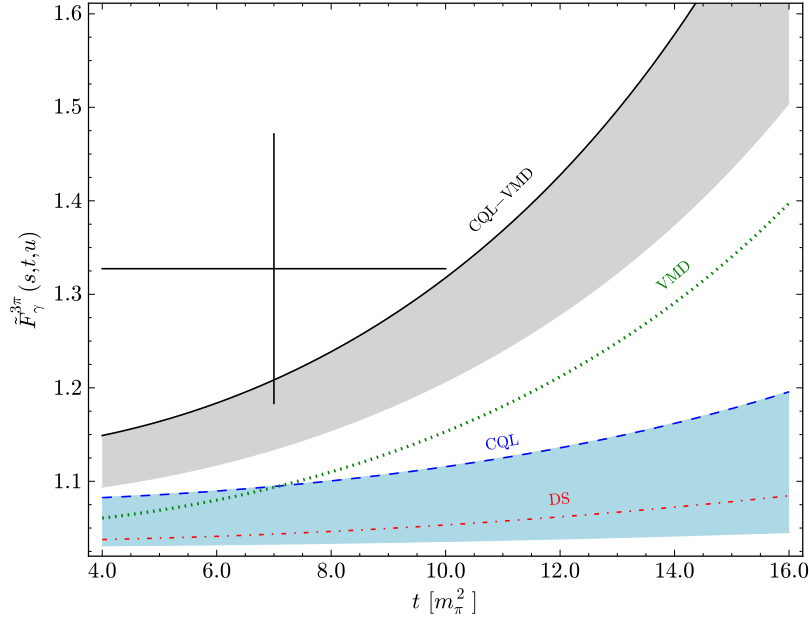
Figure 2.3: The form factors $\tilde{F}_\gamma^{3\pi}(s, t, u)$ from various approaches are depicted as functions of t. The upper shaded stripe covers the results of CQL–VMD approach for constituent masses between $M_q = 360$ MeV (corresponding to the solid black curve marking the upper edge of that stripe) and M_q equal to the DS scale $\Lambda = 565.69$ MeV of Ref. [71] (corresponding to the lower edge of that stripe). The lower shaded stripe covers the results of the "pure" CQL model [46] for the same M_q interval. A comparison is made with results of the "modified" VMD [61, 70] (green dotted curve) and of DS (in GIA) [71] (red dash-dotted curve). The exhibited Serpukhov point [37] is actually the average value extracted from the total cross-section.

where Kawarabayashi-Suzuki-Fayyazuddin-Riazuddin (KSFR) and Goldberger-Treiman (GT) relations

$$\frac{g_{\rho\pi\pi}^2}{m_\rho^2} = \frac{1}{2f_\pi^2}, \quad \frac{g_{\pi\bar{q}q}}{M_q} = \frac{1}{f_\pi}, \tag{2.15}$$

have been employed, respectively.

Clearly, the additional interactions spoils the WZW anomaly constraint. The problem of obtaining the correct form-factor value for the $\gamma^* \to 3\pi$ process when vector mesons are involved is known for quite some time [58, 59, 60, 61, 62].

We have proposed [63] to remedy this issue by introducing a quark level

non-resonant Weinberg-Tomozawa term [64, 65] in the effective Lagrangian

$$2ig_{\rho\pi\pi}\text{Tr}([\pi,(\partial_\mu\pi)]\rho^\mu) \to 2i\text{Tr}([\pi,(\partial_\mu\pi)](g_{\rho\pi\pi}\rho^\mu - ig_{\pi\pi\bar{q}q}J^\mu)) \tag{2.16}$$

where $J^\mu = t_a J_a^\mu$, $J_a^\mu = \bar{q}\gamma^\mu t_a q$, and $g_{\pi\pi\bar{q}q}$ is fixed precisely in a way to respect the $\gamma^* \to 3\pi$ WZW constraint, i.e., in a way that it cancels the resonance part in the soft-point limit *completely*, yielding $g_{\pi\pi\bar{q}q} = \frac{1}{2f_\pi^2}$. In terms of meson degrees of freedom, this means that the resonant contribution from the intermediate vector meson with $Q^2 = 0$ is absent. This is reasonable as it would correspond to a constant meson propagator $1/m_\rho^2$, and this in turn corresponds to a point interaction in the coordinate space. In the present case, it would correspond to a ρ-meson propagating *zero* distance from its $q\bar{q}$ vertex before turning into two pions, i.e., to a $q\bar{q}$ vertex producing two pions *immediately*, since here Q^2 is either s, t, or u, depending on the two-pion channel coupled to ρ. Contrary to that, two pions can come from a vector $q\bar{q}$ vertex only via a truly propagating intermediate ρ meson (with transferred momentum $Q^2 \neq 0$), while there is no direct conversion of quarks and antiquarks into the two-pion vector current.

This is the reason why our previous calculation has led to the spurious soft–point contribution $\frac{3}{2} A_\gamma^{3\pi}$ (2.14): in the resonant graphs, the part

$$\bar{q}\gamma^\mu t_a q \to \text{intermediate } \rho_a^\mu \to \epsilon_{abc}\pi_b \partial^\mu \pi_c$$

yields simply[3] the "vector $q\bar{q} \to 2\pi$ form factor"

$$\mathcal{F}_\rho^V(Q^2) \propto g_{\rho q\bar{q}} \frac{1}{Q^2 + m_\rho^2} g_{\rho\pi\pi} = \frac{m_\rho^2}{2f_\pi^2} \frac{1}{Q^2 + m_\rho^2}, \tag{2.17}$$

which is, nevertheless, wrong as it stands because it contains the contribution of the intermediate ρ with $Q^2 = 0$. The correct vector $q\bar{q} \to 2\pi$ form factor can be obtained by subtracting this contribution:

$$\begin{aligned}
\mathcal{F}^V(Q^2) &= \mathcal{F}_\rho^V(Q^2) - \mathcal{F}_\rho^V(0) \propto g_{\rho q\bar{q}} \frac{1}{Q^2 + m_\rho^2} g_{\rho\pi\pi} - g_{\rho q\bar{q}} \frac{1}{m_\rho^2} g_{\rho\pi\pi} \\
&= \frac{1}{2f_\pi^2} \frac{-Q^2}{Q^2 + m_\rho^2},
\end{aligned} \tag{2.18}$$

i.e., the resonant contributions depend on Q^2 essentially as in for example the Dyson-Schwinger substructure considerations such as [66] and [67] (see esp. their Eqs. (30) and (34)).

---

[3] – thanks to vanishing of the transverse part of ρ propagators when contracted with Levi–Civitas from the traces of PVV triangles. The second equality is from the KSFR relation.

With this modification the total triangle contribution $F_\triangle = F_\triangle^{\text{res}} + F_\triangle^{\text{WT}}$ to the amplitude reads

$$F_\triangle(p_1, p_2, p_3) = \frac{1}{2} \frac{eN_c}{6\pi^2} \frac{g_{\pi\bar{q}q}}{M_q} \frac{g_{\rho\bar{q}q}^2}{m_\rho^2} \frac{m_\rho^2}{m_\rho^2 + q^2}$$

$$\times \left[\frac{s}{m_\rho^2 - s} \widetilde{C}_0(p_1, p_2) + \frac{t}{m_\rho^2 - t} \widetilde{C}_0(p_2, p_3) + \frac{u}{m_\rho^2 - u} \widetilde{C}_0(p_1, p_3) \right], \quad (2.19)$$

so that the complete form factor given as $F_\gamma^{3\pi} = F_\triangle + F_\Diamond$ respects the WZW constraint. In the chiral and soft-point limit where $\widetilde{C}_0 \to 1$, and by using the GT and KSFR relation (2.15) one is lead precisely to the Terent'ev phenomenological form [68, 69].

In total, we have succeeded in building up an amplitude which incorporates a coupling of the vector meson that vanishes in the IR limit. However, a weak point of this approach is that the WT term should not be considered on the Lagrangian level, as it would spoil the KSFR relation [62]. On the positive side, it is physically appealing that a more founded Dyson-Schwinger approach offers an elaborate support of our subtraction [66].

§ 2.5 RESULTS

Here we present the results for the calculated form factor for selected kinematics, and also for the total cross section with the nucleus due to the Primakoff effect.

The Figs. 6.5, 2.4 show the "normalized" form factor $\widetilde{F}_\gamma^{3\pi} = F_\gamma^{3\pi} / A_\gamma^{3\pi}$. For constituent u and d masses we use $M_q \approx m_p/3 \approx 330$ MeV, but we also allow this value to vary. The 't Hooft–Veltman integrals, C_0 and D_0, were calculated numerically for the case where the photon can be taken on–shell $q^2 \approx 0$ (pertinent in all experiments [37]), and for

- Primakoff type experiments, [37, 41, 42], where all pions are on shell, so that $s + t + u = 3m_\pi^2$, and where we take $u = m_\pi^2$ for definiteness.

- CEBAF experiment [40], where the third pion (π^-) is off-shell. The kinematical range explored at CEBAF will be mostly in the s channel, and the amplitudes themselves have a weak dependence on the virtuality of π^-, so we take $p_3^2 \approx m_\pi^2$. Now $s + t + u = m_\pi^2$, and we also fix $t = -m_\pi^2$.

Comparison of form-factors calculated in the CQL and CQL-VMD approach first reveals that the presence of the resonance increases its value at non-zero momenta. Second, by increasing M_q one decreases value for $\widetilde{F}^{3\pi}$ at a particular
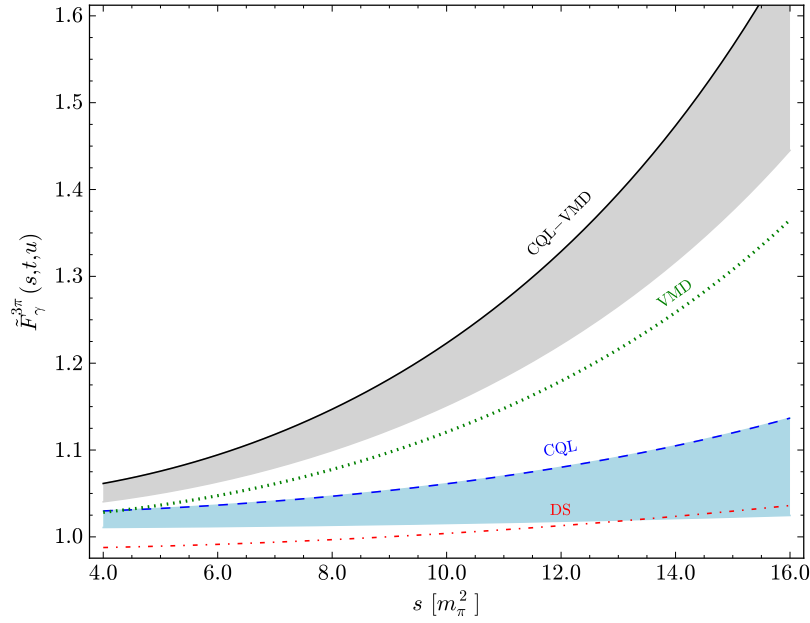
Figure 2.4: Same as previous Fig. 6.5, but for the CEBAF kinematics, where the two outgoing and on-shell pions are π^+ and π^0. The form factor is thus given as the function of their invariant mass squared, the s-variable. For the off-shell pion, π^-, we use $p_3^2 = m_\pi^2$. We also fix $t = -m_\pi^2$.

momenta, simply because that is the only mass scale in the loop. The overall parabolic trend of the curves is due to the fact that a series expansion reveals [71] that the $\mathcal{O}(p^2)$ term in the form-factor is, up to pion virtuality, a constant of the order of m_π^2.

The DS approach yields an especially weak momentum dependence of the amplitude [71]. In the DS, the mass is generated dynamically, so that the mass is a function of momenta (see Eq. 1.6). Hence, the scale of this running Λ, which in turn originates from a specific effective gluon interaction, is what scales the form-factor momentum dependence, and not the constituent quark mass, which one may conveniently denote as running mass at zero momenta. It turns out this scale is somewhat larger than the usual constituent quark mass used in the CQL model, the value of Ref. [71] is $\Lambda = 565.69$ MeV. The lower end of the lower stripe shown in Figs. 6.5, 2.4 is a CQL calculation with $M_q = \Lambda = 565.69$ MeV, presenting a direct manifestation of this effect.

Extraction of the form-factor from the experiment at Serpukhov required additional assumption about the amplitude, namely that the value of the form-factor is constant in the kinematical range considered. It is then best to be
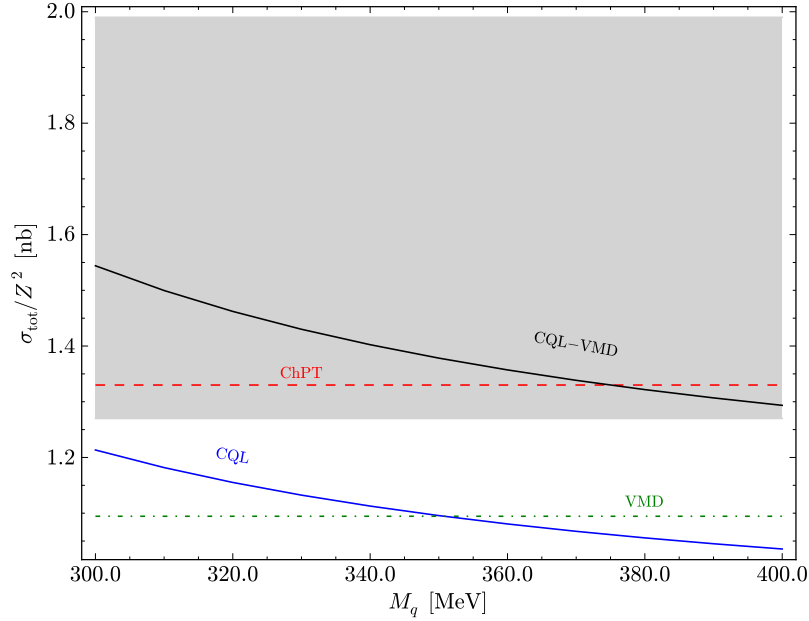
Figure 2.5: Total cross sections for various M_q predicted by CQL is depicted by the lower solid curve, while CQL–VMD yielded the upper solid curve. The (constant) value predicted by VMD alone is depicted by the dotted line, and the ChPTh prediction of 1.33 ± 0.03 nb [39], is given by the dashed line. The experimental cross-section is denoted by the grey area.

cautious, and compare with experiment only the actual measured Primakoff cross-section. The measurements on various targets (with eZ being the nucleus charge) yielded [37]

$$\sigma_{\text{tot}}/Z^2 = 1.63 \pm 0.23 \pm 0.13 \,\text{nb} \, ,$$

which is represented by the grey area in Fig. 2.5, where it is compared with the theoretical predictions of VMD and, for various constituent quark masses M_q between 300 MeV and 400 MeV, of the CQL and CQL–VMD approaches. The fact that the cross section is larger in CQL–VMD is of course reflecting the presence of the resonance. The former is not compatible with the (admittedly scarce) experimental data, but its vector-meson extension, the CQL–VMD approach, is. In spite of this, an alternative approach using Chiral Perturbation Theory (ChPTh) fulfills the experimental constraint once the loop and electromagnetic corrections are carefully taken into account [39]. Thus, at least in the kinematical regime covered by Serpukhov alternative explanations, without introduction of vector mesons are also possible.

In COMPASS experiment, where higher momentum range is explored, it is expected that vector mesons will play a role. Experiments exploring anomalous process for heavier particles like $\eta(\eta') \to 2\pi\gamma$ decays [54, 55] will reach vector resonances, and therefore a study of the $\gamma^* \to 3\pi$ vertex that includes vector mesons makes a convenient benchmark. Moreover, the CQL–VMD approach is numerically simple, allowing for a large range of kinematics to explore, and therefore serving as a useful first step towards a more complete *ab initio* approach, as e. g. [66].

3

Bound state formalism in medium

The central object of our study in the following sections is the thermodynamics of an effective model of QCD. We will in particular be interested in the chiral phase transition, thermodynamic quantities like e. g. the pressure, as well as thermal behavior of meson masses. They can be obtained from various models - here we choose to work in a bound state approach aiming to construct mesons from their $\bar{q}q$ substructure. Clearly such an approach should be non-perturbative, as a resummation of an infinite class of diagrams is required to construct a bound state. Typically one uses an infinite sum of ladder diagrams, see Fig. 3.1, leading to the ladder Bethe-Salpeter equation (BSE). As these present planar diagrams, one can motivate this truncation through a large N_c expansion [72]. In the following we highlight important points of this approach.

§ 3.1 SEPARABLE DYSON-SCHWINGER MODEL

Quark Dyson-Schwinger equation   The first building block is the quark propagator, which is obtained from its DSE [13, 14]

$$S^{-1}(p) = S_0^{-1}(p) + \int \frac{d^4q}{(2\pi)^4} g^2 D_{\mu\nu}((p-q)^2)\gamma_\mu\frac{\lambda_a}{2}S(q)\Gamma_\nu^a(p,q) , \qquad (3.1)$$

also sometimes known as the gap equation. The free quark propagator, denoted as $S_0(p)$, is

$$S_0(p) = (i\not{p} + m)^{-1} , \qquad (3.2)$$

while $D_{\mu\nu}((p-q)^2)$ is the dressed gluon propagator, and $\Gamma_\nu^a(p,q)$ the dressed quark-gluon vertex. Note that the DSE's are usually solved in Euclidean space.
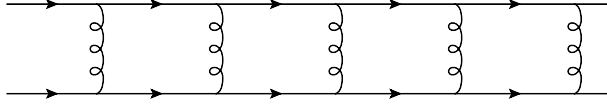
This system is truncated as follows:

Figure 3.1: An illustration of a class of ladder diagrams required to build a bound state in a field theoretic formalism.

- $\Gamma_\mu^a(p,q)$ is replaced by $\gamma_\mu \frac{\lambda_a}{2}$ which is the bare vertex. This is the popular rainbow truncation [13, 14].

- We work in the Feynman-like gauge, where

$$g^2 D_{\mu\nu}((p-q)^2) = \delta_{\mu\nu} D_{\text{eff}}(p^2, q^2, p\cdot q) \,, \tag{3.3}$$

  only due to its simplicity. With this one sacrifices Slavnov-Taylor identities, but still hopes that for model calculations this is not a big issue [78].

- The resulting effective gluon propagator is defined through its Chebyshev expansion. It turns out that the DSE (3.1) is sensitive only to the zeroth and first moment of this expansion [78]. This allows the following form of D_{eff}, the effective gluon propagator

$$D_{\text{eff}}(p^2, q^2, p\cdot q) = D_0 \mathscr{F}_0(p^2)\mathscr{F}_0(q^2) + D_1 (p\cdot q)\mathscr{F}_1(p^2)\mathscr{F}_1(q^2) \,, \tag{3.4}$$

  Constants $D_{0,1}$, together with the form-factors $\mathscr{F}_{0,1}(p^2)$, then specify the zeroth and first Chebyshev moments. A trucation with only the zeroth moment is dubbed rank-1, while including both the zeroth and the first we call rank-2. Note that the prefactor $D_{0,1}$ basically allows the choice $\mathscr{F}_{0,1}(0) = 1$.

These truncations constitute the so-called separable model of QCD [73, 74, 76, 78]. With this machinery at hand it is a simple task to project out of (3.1) the equations for scalar and vectorial part of the quark propagator (1.5)

$$p^2 A(p^2) = p^2 + \frac{8}{3} \int \frac{d^4 q}{(2\pi)^4} D_{\text{eff}}((p-q)^2)(p\cdot q) \frac{A(q^2)}{q^2 A^2(q^2) + B^2(q^2)} \,, \tag{3.5}$$

$$B(p^2) = m + \frac{16}{3} \int \frac{d^4 q}{(2\pi)^4} D_{\text{eff}}((p-q)^2) \frac{B(q^2)}{q^2 A^2(q^2) + B^2(q^2)} \,. \tag{3.6}$$

With the separable case (3.4) one can go much further. Namely, the profile of $A(p^2)$ and $B(p^2)$ is completely determined by just two numbers, viz.

$$A(p^2) = 1 + a\mathscr{F}_1(p^2), \qquad B(p^2) = m + b\mathscr{F}_0(p^2) \,, \tag{3.7}$$

where a, b are calculated from the two coupled integral equations

$$a = \frac{2D_1}{3} \int \frac{d^4q}{(2\pi)^4} \mathscr{F}_1(q^2) \frac{q^2 A(q^2)}{q^2 A^2(q^2) + B^2(q^2)} \,, \tag{3.8}$$

$$b = \frac{16D_0}{3} \int \frac{d^4q}{(2\pi)^4} \mathscr{F}_0(q^2) \frac{B(q^2)}{q^2 A^2(q^2) + B^2(q^2)} \,. \tag{3.9}$$

This is the main merit of the separable approach. Chiral symmetry breaking then means obtaining $b \neq 0$ from this set of equations.

Bethe-Salpeter equation The second step is to use the quark propagator calculated from (3.8)-(3.9) in the BSE. The homogenous BSE in the ladder truncation is defined as follows

$$-\lambda(P^2)\Gamma_{f\bar{f}'}(p, P) = \frac{4}{3} \int \frac{d^4q}{(2\pi)^4} g^2 D_{\mu\nu}((p-q)^2)\gamma_\mu S_f(q_+)\Gamma_{f\bar{f}'}(q, P) S_{\bar{f}'}(q_-)\gamma_\nu \,. \tag{3.10}$$

Here $\Gamma_{f\bar{f}'}(p, P)$ is the meson momentum space wave function and $q_\pm = q \pm P/2$ with P being the meson momentum. The homogenous BSE is valid on-shell where $\lambda(P^2 = -m_M^2) = 1$, and m_M is the meson mass. Together with the DSE, this so-called rainbow-ladder approximation is shown to respect the Goldstone theorem [13]. With it, usual corollaries of chiral physics follow, such as the famous Gell-Mann-Oakes-Renner (GMOR) relation

$$m_\pi^2 f_\pi^2 = -\frac{m_u + m_d}{2} \langle \bar{q}q \rangle_0 \,, \tag{3.11}$$

where $\langle \bar{q}q \rangle_0$ is the quark condensate in the chiral limit.

We will be exclusively interested in the pseudoscalar and scalar channel. For the separable approximation, in the notation of Ref. [79] the bound state amplitude takes the following form [78, 79]

$$\Gamma_{f\bar{f}'}(p, P) = \gamma_5[iE(P^2) + P\!\!\!/E(P^2)]\mathscr{F}_0(p^2) \,. \tag{3.12}$$

The pseudoscalar BSE is then a 2×2 eigenvalue problem $\mathscr{K}(P^2)V = \lambda(P^2)V$ where $V = (E, F)$, the kernel $K_{ij}(P^2)$ is

$$\mathscr{K}_{ij}(P^2) = -\frac{4D_0}{3} \int \frac{d^4q}{(2\pi)^4} \mathscr{F}_0^2(q^2) \text{Tr}[\hat{t}_i S_f(q_+) t_j S_{\bar{f}}(q_-)] \,, \tag{3.13}$$

and $t = (i\gamma_5, \gamma_5 P\!\!\!/)$ and $\hat{t} = (i\gamma_5, -\gamma_5 P\!\!\!/ /(2P^2))$.

Sometimes, we will truncate the BSE system with only the leading covariant. Then, the BSE equation reads

$$\frac{9}{2D_0} = \Pi_M(P^2) = d_q \int \frac{d^4q}{(2\pi)^4} \mathscr{F}_0^2(q^2) \frac{K_M(q^2, P^2, q \cdot P)}{\mathscr{D}(q_+^2)\mathscr{D}(q_-^2)} \,, \tag{3.14}$$

where we have conveniently defined the quark-antiquark polarization loop $\Pi_M(P^2)$ and where $\mathscr{D}(p^2) = p^2 A^2(p^2) + B^2(p^2)$, and

$$K_M(q^2, P^2, q \cdot P) = (p_+ \cdot p_-) A(p_+^2) A(p_-^2) \pm B(p_+^2) B(p_-^2) .$$

One understands these formulas on-shell, i. e. $P^2 = -m_M^2$. The (plus) minus sign in the last formula stands for $(M = \pi)$ $M = \sigma$ meson states [78].

§ 3.2 EFFECTIVE ACTION

Effective action Γ will be needed when evaluating quantities like e. g. the pressure, entropy, as it is equivalent to the thermodynamic potential. Within the 2PI formalism [80] it takes the following form

$$\Gamma[S] = -\text{TrLog}(S^{-1}) + \text{Tr}(\Sigma S) + \Gamma_2[S] , \tag{3.15}$$

where $\Sigma = S - S_0$ and Γ_2 contains all 2PI diagrams. Trace is performed over all degrees of freedom: momentum, spin, flavor and color. For simplicity we work with N_f equal flavors. The rainbow approximation is defined by $\Gamma_2[S] = -\frac{1}{2}\text{Tr}(\Sigma S)$, where Σ is specified so that [13]

$$\Gamma_2[S] = -\frac{N_f}{2} V_4 4 \int \frac{d^4 p}{(2\pi)^4} \int \frac{d^4 q}{(2\pi)^4} \text{Tr}[\gamma_\mu S(p) \gamma_\nu S(q)] g^2 D_{\mu\nu}((p-q)^2) , \tag{3.16}$$

where only the Dirac trace is left. In Feynman-like gauge we have

$$\Gamma_2[S] = -16 N_c N_f V_4 \int \frac{d^4 p}{(2\pi)^4} \int \frac{d^4 q}{(2\pi)^4} D_{\text{eff}}(p^2, q^2, p \cdot q)$$
$$\times \frac{(p \cdot q) A(p^2) A(q^2) + 2 B(p^2) B(q^2)}{[p^2 A^2(p^2) + B^2(p^2)][q^2 A^2(q^2) + B^2(q^2)]} .$$

In the separable approach (3.4), the two integrals factorize, so that

$$\Gamma_2 = -V_4 N_f \left(\frac{9a^2}{D_1} + \frac{9b^2}{8D_0} \right) , \tag{3.17}$$

where (3.8) and (3.9) were used. The first term in (3.15) is easily evaluated leading to the vacuum energy

$$\Omega = \frac{\Gamma}{V_4} = \Omega_{\text{cond}} + \Omega_{\text{zpt}} = N_f \left(\frac{9a^2}{D_1} + \frac{9b^2}{8D_0} \right) - \frac{d_q}{2} \int \frac{d^4 p}{(2\pi)^4} \log\left[p^2 A^2(p^2) + B^2(p^2) \right] , \tag{3.18}$$

where $d_q = 2 \times 2 \times N_f \times N_c$ are the physical number of degrees of freedom. In the last expression the zero-point vacuum energy Ω_{zpt} needs to be regularized by subtracting the zero-point energy of a free quark with mass m

$$\Omega_{\text{zpt}}^{\text{reg}} = -\frac{d_q}{2} \int \frac{d^4 p}{(2\pi)^4} \log\left[\frac{p^2 A^2(p^2) + B^2(p^2)}{p^2 + m^2}\right] . \tag{3.19}$$

This also gives meaning to this quantity:

$$\Omega_{\text{reg}} = \Omega_{\text{cond}} + \Omega_{\text{zpt}}^{\text{reg}} , \tag{3.20}$$

is the energy difference between the non-perturbative and perturbative vacuum, similar to the bag constant. By extremizing the vacuum energy Ω w. r. t. to a, b one arrives at (3.8), (3.9).

It is not always possible to create a non-perturbative, chirally broken vacuum, i. e. the one with $b \neq 0$. This depends on the parameters of the theory. In practice, a sufficient strength in the scalar channel is usually needed. Analogous to the Higgs mechanism, the coefficient in front of the b^2 term in (3.18) needs to negative. This leads to the following requirement

$$1 = g_c \frac{d_q}{\Lambda_0^2} \int \frac{d^4 p}{(2\pi)^4} \frac{\mathscr{F}_0^2(p^2)}{p^2} , \tag{3.21}$$

where, for simplicity, $a = 0$ (no non-trivial wave function renormalization). We have made the following abbreviation $g = 2D_0\Lambda_0^2/9$ for the coupling and the index c stands for its critical value, so that any larger coupling does lead to a chirally broken vacuum. It is now easy to interpret this result as a requirement on the integrated strength of the effective gluon interaction.

In an NJL-type description with $\mathscr{F}_0(p^2) \to \theta(\Lambda_0^2 - \mathbf{p}^2)$ and a sharp 4D cutoff Λ_0 we have $g_c = \frac{4\pi^2}{d_q}$. A Gaussian type form-factor $\mathscr{F}_0(p^2) = e^{-p^2/\Lambda_0^2}$ needs a stronger coupling $g_c^{\text{Gauss}} = 2g_c^{\text{NJL}}$, while for a family of Lorentzians

$$\mathscr{F}_0(p^2) = [1 + p^2/\Lambda_0^2]^{-k}, \qquad \mathscr{F}_0(p^2) = [1 + (p^2/\Lambda_0^2)^k]^{-1} , \tag{3.22}$$

one ends up with $g_c^{\text{Lor}} = (2k-1)g_c^{\text{NJL}}$ and

$$g_c^{\text{Lor}} = \frac{k^2}{k-1} \frac{\sin(\pi/k)}{\pi} g_c^{\text{NJL}} ,$$

respectively. In the latter case for $k \to \infty$ we are back at $g_c^{\text{Lor}} \to g_c^{\text{NJL}}$. The moral of this analysis is that a smooth form-factor needs a stronger coupling to compensate the lack of integrated strength.

§ 3.3 FINITE TEMPERATURE AND CHEMICAL POTENTIAL

Discussion of in-medium physics proceeds with the so-called Matsubara formalism, see e. g. [77]. It boils down to the correspondence between path integrals from quantum field theory, and partition functions from statistical physics. The correspondence states that the path integral is equivalent to the partition function provided the field theory lives in compact Euclidean time with $\beta = 1/T$ being the circumference of the compact time direction. The accompanying boundary conditions for the fields are

- periodic, if the fields are bosonic,

- anti-periodic for fermion fields.

Thus gauge fields satisfy $A_\mu(\mathbf{x}, \tau + \beta) = A_\mu(\mathbf{x}, \tau)$, while for matter $\psi(\mathbf{x}, \tau + \beta) = -\psi(\mathbf{x}, \tau)$ holds.

In momentum space a discrete spectra appears, also known as Matsubara frequencies[1]. A simple prescription for proceeding to finite T for fermions is then

$$p_4 \to \omega_n = (2n+1)\pi T \qquad \int_{-\infty}^{\infty} \frac{dp_4}{2\pi} \to T \sum_{n=-\infty}^{\infty} , \tag{3.23}$$

where ω_n are the fermionic Matsubara frequencies. For bosons one uses $p_4 \to \nu_n = 2n\pi T$.

In accordance with the fact that the operator

$$\int d^3 x \psi^\dagger(x)\psi(x) , \tag{3.24}$$

is the fermion number, chemical potential μ is added as a constant background field, so that $p_4 \to p_4 - i\mu$. In total for Euclidean four momentum $p = (\mathbf{p}, p_4)$ we will use the following notation at finite T and μ: $\tilde{p}_n = (\mathbf{p}, \tilde{\omega}_n) = (\mathbf{p}, \omega_n - i\mu)$.

In medium, Lorentz invariance is broken, giving the following form for the quark propagator

$$S^{-1}(\tilde{p}_n) = i\boldsymbol{\gamma} \cdot \mathbf{p} A(\tilde{p}_n^2) + i\gamma_4 \tilde{p}_n C(\tilde{p}_n^2) + B(\tilde{p}_n^2) . \tag{3.25}$$

Plugging in (3.1) and making the corresponding projections to scalar functions one arrives at

$$A(\tilde{p}_n^2) = 1 + a\mathscr{F}_1(\tilde{p}_n^2) , \qquad B(\tilde{p}_n^2) = m + b\mathscr{F}_0(\tilde{p}_n^2) , \qquad C(\tilde{p}_n^2) = 1 + c\mathscr{F}_1(\tilde{p}_n^2) , \tag{3.26}$$

---

[1]They are exact analogues of the Kaluza-Klein modes in theories with extra dimension.

where the in medium analogues of (3.8) and (3.9) are

$$a = \frac{8D_1}{9} T \sum_{n=-\infty}^{\infty} \int \frac{d^3q}{(2\pi)^3} \mathscr{F}_1(\tilde{q}_n^2) \frac{A(\tilde{q}_n^2)}{\mathbf{q}^2 A^2(\tilde{q}_n^2) + \tilde{\omega}_n^2 C^2(\tilde{q}_n^2) + B^2(\tilde{q}_n^2)} \,, \tag{3.27}$$

$$b = \frac{16D_0}{3} T \sum_{n=-\infty}^{\infty} \int \frac{d^3q}{(2\pi)^3} \mathscr{F}_0(\tilde{q}_n^2) \frac{B(\tilde{q}_n^2)}{\mathbf{q}^2 A^2(\tilde{q}_n^2) + \tilde{\omega}_n^2 C^2(\tilde{q}_n^2) + B^2(\tilde{q}_n^2)} \,. \tag{3.28}$$

With addition of

$$c = \frac{8D_1}{3} T \sum_{n=-\infty}^{\infty} \int \frac{d^3q}{(2\pi)^3} \mathscr{F}_1(\tilde{q}_n^2) \frac{C(\tilde{q}_n^2)}{\mathbf{q}^2 A^2(\tilde{q}_n^2) + \tilde{\omega}_n^2 C^2(\tilde{q}_n^2) + B^2(\tilde{q}_n^2)} \,, \tag{3.29}$$

the system of equations is closed.

Accordingly, the vacuum energy is augmented to

$$\Omega_{\text{reg}} = \Omega_{\text{cond}} + \Omega_{\text{kin}}^{\text{reg}} \,, \tag{3.30}$$

where

$$\Omega_{\text{cond}} = N_f \left(\frac{27}{4D_1} a^2 + \frac{9}{8D_0} b^2 + \frac{9}{4D_1} c^2 \right) \,, \tag{3.31}$$

$$\Omega_{\text{kin}}^{\text{reg}} = -\frac{d_q}{2} T \sum_{n=-\infty}^{+\infty} \int \frac{d^3p}{(2\pi)^3} \log \left[\frac{\mathbf{p}^2 A^2(\tilde{p}_n^2) + \tilde{\omega}_n^2 C^2(\tilde{p}_n^2) + B^2(\tilde{p}_n^2)}{\tilde{p}_n^2 + m^2} \right] \,. \tag{3.32}$$

To evaluate the pressure, one needs to add the thermodynamic potential also of the free Fermi gas [77], which we call $\Omega_{\text{reg}}^{\text{free}}$

$$\Omega_{\text{reg}}^{\text{free}} = -\frac{d_q}{2} \int \frac{d^3p}{(2\pi)^3} \left\{ \log \left[1 + e^{-\beta(E-\mu)} \right] + \log \left[1 + e^{-\beta(E+\mu)} \right] \right\} \,. \tag{3.33}$$

since the regularization (3.32) subtracts not only the vacuum, but also the thermal energy. Here $E = \sqrt{\mathbf{p}^2 + m^2}$. Thus,

$$\Omega_{\text{reg}} \to \Omega_{\text{cond}} + \Omega_{\text{kin}}^{\text{reg}} + \Omega_{\text{free}}^{\text{reg}} \,. \tag{3.34}$$

Pressure is given as $p = -\Omega_{\text{reg}} + \Omega_0$ where with the constant Ω_0 we achieve zero pressure in the vacuum. From the pressure various thermodynamic quantities follow, as e. g. the entropy

$$s = \frac{dp}{dT} \,, \tag{3.35}$$

or the number density

$$n = \frac{dp}{d\mu} \,. \tag{3.36}$$

The phase transition is inferred by observing the behaviour of the quark condensate

$$\langle \bar{q} q \rangle = -\frac{\partial \Omega}{\partial m} \,, \tag{3.37}$$

with the phase transition point obtained from the peak of the chiral susceptibility

$$\chi = \frac{\partial \langle \bar{q} q \rangle}{\partial m} \,. \tag{3.38}$$

For future reference it is useful to provide pressure of free massless quarks

$$p_{\text{SB}}^q = N_c N_f \left[\frac{7\pi^2}{180} + \frac{1}{6} \left(\frac{\mu}{T} \right)^2 + \frac{1}{12\pi^2} \left(\frac{\mu}{T} \right)^4 \right] T^4 \,, \tag{3.39}$$

and massless quarks and gluons

$$p_{\text{SB}} = p_{\text{SB}}^q + (N_c^2 - 1) \frac{\pi^2}{45} T^4 \,. \tag{3.40}$$

Polarization loop (3.14) is augmented to

$$\Pi_M(\nu_m, |\mathbf{P}|) = d_q T \sum_{n=-\infty}^{\infty} \int \frac{d^3 p}{(2\pi)^3} \mathscr{F}_0^2(\tilde{p}_n^2) \frac{K_M(\tilde{\omega}_n^2, \mathbf{p}^2, \nu_m^2, \mathbf{P}^2)}{\mathscr{D}((\tilde{\omega}_n^+)^2, (\mathbf{p}^+)^2) \mathscr{D}((\tilde{\omega}_n^-)^2, (\mathbf{p}^-)^2)} \,. \tag{3.41}$$

with

$$K_M(\tilde{\omega}_n^2, \mathbf{p}^2, \nu_m^2, \mathbf{P}^2) = (\tilde{\omega}_n^+ \tilde{\omega}_n^-) C((\tilde{p}_n^+)^2) C((\tilde{p}_n^-)^2)$$
$$+ (\mathbf{p}^+ \cdot \mathbf{p}^-) A((\tilde{p}_n^+)^2) A((\tilde{p}_n^-)^2) \pm B((\tilde{p}_n^+)^2) B((\tilde{p}_n^-)^2) \,. \tag{3.42}$$

The meson 4-momentum is $P_m = (\nu_m, \mathbf{P})$, where $\nu_m = 2m\pi T$ are the bosonic Matsubara frequencies. Furthermore, $\tilde{\omega}_n^\pm = \tilde{\omega}_n \pm \nu_m/2$, and $\mathbf{p}^\pm = \mathbf{p} \pm \mathbf{P}/2$ and

$$\mathscr{D}(-z^2, \mathbf{p}^2) = \mathbf{p}^2 A^2(-z^2 + \mathbf{p}^2) - z^2 C^2(-z^2 + \mathbf{p}^2) + B^2(-z^2 + \mathbf{p}^2) \,. \tag{3.43}$$

§ 3.4 RELATION TO OTHER APPROACHES

There are many similar bound state approaches to the separable model, as the Instanton Liquid Model (ILM) [81, 82], see also [83, 84, 74, 75], the global color model[2] [86] and the Nambu-Jona–Lasinio (NJL) model [87, 88]. In fact, Eq. (3.9)

---

[2]A nice summary of the relation of the global color model with the separable model, NJL and similar approaches can be found in [85].

in the limit of point-like gluon interaction, i. e. with a profile $\mathscr{F}_0(p^2) \to \theta(\Lambda_0^2 - \mathbf{p}^2)$ Eq. (3.9) matches the famous NJL gap equation. Furthermore, the same limit for the truncated BSE defines the random phase approximation ladder for the quark-antiquark polarization loop. Then the separable model can be thought of as a non-local version of the NJL (nlNJL) model [83, 89].

This relation also serves to put the separable model in perhaps a more transparent context of the nlNJL. Notably, solving the DSE corresponds to solving nlNJL in the mean-field approximation, meaning that the a, b, c can be thought of as being mean-fields of some quark-bilinear, i. e. a meson. For example, b has quantum numbers of the $\bar{q}q$ state, i. e. a scalar σ meson. Solving the BSE is equivalent to solving nlNJL up to quadratic fluctuations. Going to higher orders, mesons can interact, and one ends up with the ChPT Lagrangian [90], where all the coefficients can be in principle predicted.

The difference between the ILM and the separable DSE model is that non-local interactions are introduced in a slightly different manner. This does not affect mean-field calculations, but it has an influence on the polarization loop. In the following Sections we will be making explicit calculations also in the ILM, and thus it is useful to provide a simple dictionary between the two approaches:

- ILM models have no WFR, thus we can put $a = 0$ in the gap equation Eq. (3.9).

- The form-factors in the remaining gap equation are replaced according to

$$\mathscr{F}_0(p^2) \to r^2(p^2) , \tag{3.44}$$

  where $r(p^2)$ is the analogue form-factor in the ILM model.

- The pre-factor in the integrand of the polarization loop (3.14) is modified as follows

$$\mathscr{F}_0^2(q^2) \to r^2(q_+^2) r^2(q_-^2) . \tag{3.45}$$

There are several ways one can think about the form-factors:

- They define the effective gluon interaction between quarks.

- They are meson wave functions, i .e. their spatial extent has to do with the size of the bound-state. Accordingly, the profile is usually chosen to be a simple Gaussian, or a Lorentzian, i. e. a function with no nodes, reflecting the ground state.

- They act as dynamical regulators. In contrast to the NJL model where explicit cutoff is needed to calculate the integrals (the model is non-re-normalizable), here the profile of the form-factors is scaled to some Λ which is then the analogue of the cutoff.

Non-locality induced by the form-factor has several advantages, see also [91] and Refs. therein:

- confinement might be realized in the sense of quark propagator having no singularities on the Minkowski axes. We will say more on this in Sec. 5.

- No additional cutoffs are needed to define mesons via quark-antiquark loops.

- Anomalies are treated in a consistent way.

There are some minor differences between the separable and the nlNJL model:

- nlNJL insists on covariant Lagrangian interactions also at finite T. This effectively means $a = c$.

- BSE coming from the usual nlNJL interaction contains only the leading covariant, encoded in the pseudoscalar channel. There is no axial channel to describe the subleading covariant as well.

§ 3.5   INTRODUCING THE POLYAKOV LOOP

The separable model is designed as a theory of strongly interacting quarks. Gluons are completely non-dynamical, being used through various model quark interactions, without requirement, say, that they have to satisfy a self-consistent equation of their own. In other words, the system of equations developed so far is not a coupled system of quarks and gluons.

Gluons are also absent from the thermodynamics of the separable model. Looking at the separable model from the perspective of symmetries, it is tempting to develop an analogous effective potential for gluons. One simply needs a symmetry and an order parameter (i. e. a mean field). For a world with no quarks these are the $Z(N_c)$ symmetry and the Polyakov loop (PL) Φ, respectively.

The pioneering work on the coupling of the Polyakov loop to quarks, originates from Gocksch and Ogilvie [93] and Ilgenfritz and Kripfganz [92]. Later, Fukushima adopted their reasoning to a NJL-like model [94]. By the progress of Weise etal. [95, 96] the Polyakov loop has become a standard in local and non-local NJL type models, providing means to statistically suppress quark degrees of freedom at low temperatures.

Ignoring the spatial correlations of the Polyakov loop, Landau theory follows. One possible Landau potential $\mathscr{U}(\Phi, \bar{\Phi})$ is the so-called polynomial form [95]

$$\frac{\mathscr{U}(\Phi, \bar{\Phi})}{T^4} = -\frac{b_2(T)}{2}\bar{\Phi}\Phi - \frac{b_3}{6}(\bar{\Phi}^3 + \Phi^3) + \frac{b_4}{4}(\bar{\Phi}\Phi)^2 \, , \tag{3.46}$$

where the Φ^3 term is responsible for a (weak) first-order phase transition. The T dependent Landau coefficient is

$$b_2(T) = a_0 + a_1\left(\frac{T_0}{T}\right) + a_2\left(\frac{T_0}{T}\right)^2 + a_3\left(\frac{T_0}{T}\right)^3 \, . \tag{3.47}$$

The actual numbers are chosen so that the YM pressure, known from lattice QCD, is reproduced [95]. This yields $a_0 = 6.75$, $a_1 = -1.95$, $a_2 = 2.625$, $a_3 = -7.44$, $b_3 = 0.74$, $b_4 = 7.5$. Alternatively, one uses the so-called logarithmic form [96]

$$\frac{\mathscr{U}(\Phi, \bar{\Phi})}{T^4} = -\frac{a(T)}{2}\bar{\Phi}\Phi + b(T)\log[1 - 6\bar{\Phi}\Phi + 4(\bar{\Phi}^3 + \Phi^3) - 3(\bar{\Phi}\Phi)^2] \, , \tag{3.48}$$

where

$$a(T) = a_0 + a_1\left(\frac{T_0}{T}\right) + a_2\left(\frac{T_0}{T}\right)^2 \, , \qquad b(T) = b_3\left(\frac{T_0}{T}\right)^3 \, , \tag{3.49}$$

and $a_0 = 3.51$, $a_1 = -2.47$, $a_2 = 15.22$, and $b_3 = -1.75$. Note that in the logarithmic parametrization the Φ^3 term has a numerically stronger coefficient which will lead to a stronger first-order phase transition.

Implementing the PL in the quark models, as the separable model, is a simple matter. In the Polyakov gauge [22], one resorts to Cartan fields $A_4 = \phi_3\lambda_3 + \phi_8\lambda_8$, so that from (1.8) we have

$$\Phi = \frac{1}{N_c}\text{tr}_c(\mathscr{P}) \, , \qquad \mathscr{P} = \exp[i\beta(\lambda_3\phi_3 + \lambda_8\phi_8)] \, . \tag{3.50}$$

As the PL is treated as a background field, the impact on the quark sector is in terms of introducing the following modification

$$\tilde{\omega}_n \to \tilde{\omega}_n - i(\phi_3\lambda_3 + \phi_8\lambda_8) \, , \tag{3.51}$$

i. e. the fields ϕ_3 and ϕ_8 act in a sense as color dependent imaginary chemical potentials. The full thermodynamic potential of the system may now be written as

$$\Omega_{\text{reg}}(a, b, c, \Phi, \bar{\Phi}) = \Omega_q(a, b, c) + \mathscr{U}(\Phi, \bar{\Phi}) \, , \tag{3.52}$$

where $\Omega_q = \Omega_{\text{cond}} + \Omega_{\text{reg}}^{\text{kin}} + \Omega_{\text{reg}}^{\text{free}}$ is the quark sector. All the color traces in the quark loops are now non-trivial as well, and amount to summing the diagonal color structure given in (3.51).

§ 3.6 MODELS

Here we provide a list of separable models to be used in subsequent Chapters. The model parameters are usually fitted to satisfy the basic requirements of low energy phenomenology, as e. g. the pion mass, decay constant. If not stated otherwise, since we work in the isospin limit m denotes the u and d quark mass.

Rank-1 Gaussian   For numerical studies the Gaussian rank-1 model is given by the following parameters [97]

$$D_0 \Lambda_0^2 = 128 \, , \qquad \Lambda_0 = 0.687 \, \text{GeV} \, , \qquad m = 0.0096 \Lambda_0 \, , \qquad (3.53)$$

whereas the form-factor is $\mathscr{F}_0(p^2) = e^{-p^2/\Lambda_0^2}$.

For the same form-factor an alternative scheme [98]

$$D_0 \Lambda_0^2 = 92.93 \, , \qquad \Lambda_0 = 750.2 \, \text{MeV} \, , \qquad m = 5.78 \, \text{MeV} \, , \qquad (3.54)$$

will also be used.

Rank-2 Gaussian   Parameters of a rank-2 Gaussian model [98] are given as

$$\mathscr{F}_0(p^2) = e^{-p^2/\Lambda_0^2} \, , \qquad \mathscr{F}_1(p^2) = e^{-p^2/\Lambda_1^2} \, , \qquad (3.55)$$

where

$$D_0 \Lambda_0^2 = 144.14 \, , \qquad \Lambda_0 = 814.42 \, \text{MeV} \, , \qquad m = 5.7 \, \text{MeV} \, , \qquad (3.56)$$

and

$$D_1 \Lambda_1^4 = 113.96 \, , \qquad \Lambda_1 = 1034.5 \, \text{MeV} \, . \qquad (3.57)$$

Rank-2 Gaussian and Woods-Saxon   This is $N_f = 2 + 1$ model [99], with form-factors

$$\mathscr{F}_0(p^2) = e^{-p^2/\Lambda_0^2} \, , \qquad \mathscr{F}_1(p^2) = \frac{1 + e^{-p_0^2/\Lambda_1^2}}{1 + e^{(p^2 - p_0^2)/\Lambda_1^2}} \, , \qquad (3.58)$$

and parameters

$$D_0 \Lambda_0^2 = 219 \, , \qquad \Lambda_0 = 758 \, \text{MeV} \, , \qquad m_u = m_d = 5.5 \, \text{MeV} \, , \qquad m_s = 115 \, \text{MeV} \, , \qquad (3.59)$$

and

$$D_1 \Lambda_1^4 = 40 \, , \qquad \Lambda_1 = 961 \, \text{MeV} \, , \qquad p_0 = 600 \, \text{MeV} \, . \qquad (3.60)$$

Rank-2 Lorentzian   For the Lorentzian [98] we have

$$\mathcal{F}_0(p^2) = \frac{1+\alpha_z}{1+\alpha_z f_z(p^2)} \frac{\alpha_m f_m(p^2) - m\alpha_z f_z(p^2)}{\alpha_m - m\alpha_z}, \qquad \mathcal{F}_1(p^2) = \frac{(1+\alpha_z)f_z(p^2)}{1+\alpha_z f_z(p^2)},$$
(3.61)

where

$$f_m(p^2) = \left[1 + \left(p^2/\Lambda_0^2\right)^{3/2}\right]^{-1}, \qquad f_z(p^2) = \left[1 + p^2/\Lambda_1^2\right]^{-5/2},$$
(3.62)

and $\alpha_m = 309$ MeV, $\alpha_z = -0.3$. The remaining parameters are

$$D_0\Lambda_0^2 = 93.68, \qquad \Lambda_0 = 840\,\text{MeV}, \qquad m_u = m_d = 2.37\,\text{MeV},$$
(3.63)

and

$$D_1\Lambda_1^4 = 109.45, \qquad \Lambda_1 = 1400\,\text{MeV}.$$
(3.64)

Instanton Liquid Model   For the form factor in ILM we also take a Gaussian

$$r(p^2) = e^{-p^2/2\Lambda_0^2},$$

with parameters taken from [75]

$$D_0\Lambda_0^2 = 71.19, \qquad \Lambda_0 = 902.4\,\text{MeV}, \qquad m = 5.8\,\text{MeV}.$$
(3.65)

4

η, η' in medium and the Witten-Veneziano relation

Clasically, besides the standard chiral group $SU(N_f)_L \times SU(N_f)_R$, massless QCD is invariant also under the $U(1)_A$ symmetry, where all the quark fields are simply multiplied by common factor $e^{i\alpha\gamma_5}$. If realized, this symmetry should be reflected in terms of parity doublets. If spontaneously broken, a Goldstone boson should appear in the spectrum. None of this we see realized in nature. The lightest singlet $SU(3)$ pseudoscalar is the η' particle. But, with its mass of almost 1 GeV, it is much to heavy to be considered a Goldstone boson. This is the famous $U(1)_A$ problem [100].

What is then the physical reason why η' is so heavy? It turns out that a on a quantum level, $U(1)_A$ is broken explicitly, since the corresponding Nöther current $J_{5,0}^\mu = \bar{q} t_0 \gamma^\mu \gamma_5 q$ is not conserved

$$\partial_\mu J_{5,0}^\mu = 2N_f \omega(x), \quad \omega(x) = \frac{g^2}{16\pi^2} \text{Tr}(\tilde{F}_{\mu\nu} F^{\mu\nu}) . \tag{4.1}$$

Observe the multi-faceted nature of anomaly: the chiral anomaly is governed by a similar mathematical structure, Eq. (2.1), but the physical manifestation of this relation is very different. While the chiral anomaly is relevant for electromagnetic decays of the pion and the etas, the singlet gluon anomaly is responsible for keeping the η' mass so high. This is a reflection of the fact that while the chiral anomaly is governed by perturbative photon fields, singlet anomaly is driven by gluon fields. These fields are non-perturbative at low energies so the η' channel is strongly polarized by the interaction through the $\tilde{F}F$ operator. In particular, instanton configurations play a crucial role here [101, 102]. Namely, the right hand side of (4.1) is a total divergence, so a modified conservation law can be obtained

$$\partial_\mu \tilde{J}_{5,0}^\mu = 0 , \tag{4.2}$$

where $\tilde{J}^{\mu}_{5,0} = J^{\mu}_{5,0} - K^{\mu}$ and

$$K^{\mu} = 2N_f \epsilon^{\mu\nu\rho\sigma} \frac{g^2}{16\pi^2} \text{Tr}(F^{\nu\rho} A^{\sigma}) \,. \tag{4.3}$$

The axial charge, resulting from (4.2)

$$\tilde{Q}_5 = \int d^3x \, \tilde{J}^0_{5,0} \,, \tag{4.4}$$

is not conserved. If we perform integration over time on the last expression, we get

$$\int_{-\infty}^{\infty} dt \, \frac{d\tilde{Q}_5}{dt} = 2N_f \nu \,, \tag{4.5}$$

where $\nu = \int d^4x \, \omega(x)$ is the topological charge. This means that if there are field configurations with non-zero ν, the quantity $\tilde{Q}_5$ is not conserved, changing by $\Delta Q_5 = 2N_f \nu$ as one proceeds from $t = -\infty$ to $t = +\infty$. This applies to QCD, since, for example, a single instanton has $\nu = 1$. Analogous objects are not to be found if the gauge group is Abelian, as in that case the pure gauge theory is simply a free theory.

§ 4.1   THE WITTEN-VENEZIANO RELATION

The Witten-Veneziano relation (WVR) [103, 104] is a large N_c low energy theorem, stating that the extra mass of the singlet pseudoscalar field η_0 resides in the infrared correlations of the topological charge $\omega(x)$ density, to wit

$$M^2_{\eta'} + M^2_{\eta} - 2M^2_K = \frac{2N_f}{f^2_{\pi}} \chi_{\text{YM}} \,, \tag{4.6}$$

where χ_{YM} is the topological charge susceptibility of the pure YM theory

$$\chi_{\text{YM}} = \int d^4x \langle 0| T(\omega(x)\omega(0))|0\rangle \tag{4.7}$$

For completeness we briefly sketch the derivation of this relation, see also [105]. Augmented by a θ term, with a rescaled coupling $g^2 \to g^2/N_c$ the QCD Lagrangian (1.1) depends only on the combination θ/N_c. This means that in the pure gauge limit, the vacuum energy E_{YM} derives from gluon loops, so its functional dependence on θ has to be

$$E_{\text{YM}}(\theta) = N^2_c F\left(\frac{\theta}{N_c}\right) \,.$$

Taylor expanding around $\theta = 0$

$$E_{\mathrm{YM}} = F(0)N_c^2 + \frac{1}{2}F''(0)\theta^2 + \mathcal{O}\left(\frac{1}{N_c^2}\right), \tag{4.8}$$

we see that the second term is $\mathcal{O}(1)$ with the second Taylor coefficient defining the topological susceptibility (4.7)

$$\frac{d^2 E_{\mathrm{YM}}}{d\theta^2} = \chi_{\mathrm{YM}}. \tag{4.9}$$

The propagator of this correlator is defined as

$$U(p) = \int d^4x\, e^{ipx} \langle 0| T(\mathrm{Tr}(F\tilde{F}(x))\mathrm{Tr}(F\tilde{F}(0)))|0\rangle, \tag{4.10}$$

so that

$$\left(\frac{g^2}{16\pi^2 N_c}\right)^2 U_{\mathrm{YM}}(0) = \chi_{\mathrm{YM}}.$$

Now if we have a massless quark in the system, then it is possible to show that the vacuum energy must not depend on θ. A simple way to understand this is to acknowledge that a massless quark can be chirally rotated - in particular, if we use the $U(1)_A$ anomalous symmetry, then the parameter of this rotation can be tuned such as to cancel the θ term in the Lagrangian. This then means that the equivalent expansion (4.8) must terminate for full QCD at the first term. But how can this be, when we know that gluon loops go like N_c^2 while the quark loops go as N_c? Let us make a spectral decomposition of (4.10)

$$U(p) = \sum_{\text{glueballs}} \frac{N_c^2 a_n^2}{p^2 + m_n^2} + \sum_{\text{mesons}} \frac{N_c b_n^2}{p^2 + M_n^2}, \tag{4.11}$$

where we have taken into account that the wave functions have the usual N_c scaling

$$\langle 0|\mathrm{Tr}F\tilde{F}|\text{glueball}\rangle \sim N_c, \qquad \langle 0|\mathrm{Tr}F\tilde{F}|\text{meson}\rangle \sim \sqrt{N_c}. \tag{4.12}$$

The requirement of vanishing QCD susceptibility χ when a massless quark is present in the theory requires that the meson part cancels out the glueball part. This means that there must be at least one state in the meson spectrum that has a mass $\sim 1/\sqrt{N_c}$. This is precisely our singlet η_0 state. If we assume this, then

$$U_{\mathrm{YM}}(0) = N_c \frac{b_{\eta_0}^2}{M_{\eta_0}^2}.$$

Via the anomaly equation (4.1) we relate the $F\tilde{F}$ wave function to the $\bar{q}\gamma_5 q$ wave function, i. e. the η_0 decay constant

$$\frac{g^2}{16\pi^2}\sqrt{N}b_{\eta_0} = \frac{g^2}{16\pi^2}\langle 0|F\tilde{F}|\eta_0\rangle = \frac{N_c}{2N_f}\langle 0|\partial_\mu J^\mu_{5,0}|\eta_0\rangle = \frac{N_c}{\sqrt{2N_f}}f_{\eta_0}\Delta M^2_{\eta_0}\,, \quad (4.13)$$

leading to

$$f^2_{\eta_0}\Delta M_{\eta_0^2} = 2N_f\chi_{\text{YM}}\,, \tag{4.14}$$

which is the Witten-Veneziano formula (4.6).

§ 4.2 EXPERIMENT

What can happen to the $U(1)_A$ symmetry in the medium? Topological susceptibility is governed by the existence of instantons in the QCD vacuum. As the tunnelling amplitude via individual instanton configuration goes as $e^{-S_E} \sim e^{-2\pi/\alpha_s}$ entering the perturbative regime, where α_s is small, suppresses the tunnelling. Therefore, it is expected that in the hot and dense medium effect of instantons are small and $U(1)_A$ symmetry would be restored.

The hot and dense medium created in heavy ion collisions presents a natural environment in searching for possible signals of such phenomena. For example, during the early stages of the most central Au-Au collisions at RHIC, temperatures of around $T \gtrsim 250-300$ MeV allow the formation of quark-gluon plasma. As the fireball expands and cools, quark and gluon condensates are formed, seeding the production of pseudoscalar mesons. If $U(1)_A$ is restored in such a medium, mass of the created η' should be lower than its vacuum value. Due to energy conservation, this leads to an increase in the number of η' 's created. This is the essence of the Kapusta, Kharzeev and McLerran's proposal on the return of the prodigal Goldstone boson [106], see also [107, 108, 109], [110, 111].

When thinking about a possible experimental signal one has to keep in mind that the η' has small scattering and annihilation cross section [106]. Thus, η''s produced with high momenta will leave the medium unaltered. By contrast, those produced with low momenta will remain in the medium until freeze-out and decay. These η' states have a chance to be altered by the medium allowing us to detect this effect through its decay channels.

Already in '93 Shuryak points that η' with low momenta should be copiously produced [107]. Now a recent theoretical analysis of the dipion data coming from the $\eta' \to \eta\pi\pi$ channel performed by Csörgő etal. [112, 113] claims that this is indeed the case. The gathered multiplicities origin from both STAR
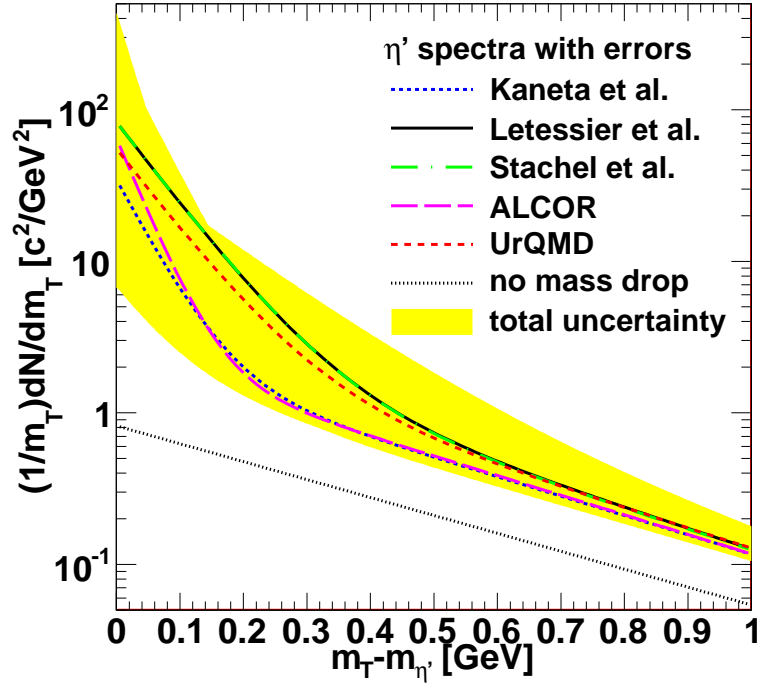
Figure 4.1: Spectrum of η' mesons as a function of momenta. Yellow band represents the reconstructed spectra from the scenario of a reduced η' mass. Figure from [113].

and PHENIX detectors at RHIC, with $\sqrt{s_{NN}}$ = 200 GeV for central Au-Au collisions. Their main result is summarized in Fig. 4.1. By analyzing the experimentally accessible intercept parameter of HBT correlations, through several popular models for hadron multiplicities, dipion multiplicity was extracted. At low transverse momenta, there is a region where one indeed observes the predicted enhancement. This leads to an indirect prediction of η' mass reduction of at least 200 MeV in the medium [112, 113].

§ 4.3 MODIFICATION OF THE WITTEN-VENEZIANO RELATION

Taken at face value, the experimental result [112, 113] is in direct conflict with the WVR. This is simple to explain. As we know from experiment that the anomaly generated mass is zero at some high T, this can be only achieved if χ_{YM} melts sooner than f_π. But that cannot be so. It is well known that YM conden-

sates are more resilient to medium effects than the ones of full QCD, if by nothing else than due to a smaller number of degrees of freedom. More specifically, while a typical YM temperature scale is around 250 MeV, the full QCD counterpart is around 150 MeV. Specifically this means, that when the pion swells, i. e. its decay constant reduces, χ_{YM} is still very much finite causing the anomaly induced η' mass to blow up!

χ_{YM} is related to the full QCD topological susceptibility χ via the Leutwyler-Smilga relation [114]

$$\chi = \frac{\chi_{YM}}{1 - \chi_{YM}\frac{N_f}{m\langle\bar{q}q\rangle_0}} \, , \tag{4.15}$$

where $\langle\bar{q}q\rangle_0$ is the quark condensate in the chiral limit, and

$$\frac{N_f}{m} = \sum_{q=u,d,s} \frac{1}{m_q} \, . \tag{4.16}$$

Note that when $m \to \infty$ we are back at $\chi = \chi_{YM}$. The relation is of course valid also in the opposite limit $m \to 0$, where we simply have $\chi = 0$ as stated previously. By the Di Vecchia-Veneziano relation [115]

$$\chi = -\frac{m\langle\bar{q}q\rangle_0}{N_f} + \mathscr{C}_m \, , \tag{4.17}$$

the same holds also for χ. This is merely a reflection of the fact that a single massless quark makes the effect of the anomaly unobservable. The correction factor $\mathscr{C}_m$ in this chiral-type expansion is essential to keep χ_{YM} finite when inserting (4.17) into (4.15).

Now the main point of this discussion is that the thermal behavior of χ is governed by that of the chiral condensate. This should not come as surprise, as the chiral transition is imprinted in the QCD partition function, and all the correlation functions calculated from it shall have the imprint of chiral transition on it as well. As a consequence, the chiral and $U(1)_A$ restorations are closely related. It is quite possible that the correction term $\mathscr{C}_m$ holds other types of condensates, making χ smaller, but still finite after the chiral transition. Nevertheless, it is quite important that already the effect of the chiral condensate is able to dictate the physics of $U(1)_A$ restoration.

Let us now invert (4.15)

$$\chi_{YM} = \frac{\chi}{1 + \chi\frac{N_f}{m\langle\bar{q}q\rangle_0}} \, , \tag{4.18}$$

as we want to examine it as a right hand side of the WVR. We proceed by replacing χ_{YM} in the WVR with the right hand side of (4.18), which we for clarity dub

$\tilde{\chi}$. The factor $\mathscr{C}_m$ is essentially unknown, but we can use the WVR to constrain it, obtaining

$$\mathscr{C}_m = \frac{m\langle \bar{q}q \rangle_0}{N_f} \left(1 - \chi_{\text{YM}} \frac{N_f}{m\langle \bar{q}q \rangle_0} \right)^{-1} \tag{4.19}$$

This is a nice feature, as it makes the WVR unaltered at $T = 0$.

For $T > 0$ we still choose to use $\tilde{\chi}$ instead of χ_{YM}, thus modifying the WVR. Now all the quantities need to be upgraded to their finite T counterparts. Specifically, the thermal behavior of $\mathscr{C}_m$ is unknown. Here we will stick to the scenario that the $U(1)_A$ transition is completely driven by the chiral one (although it need not be so), and propose an ansatz

$$\mathscr{C}_m(T) = \mathscr{C}_m(0) \left[\frac{\langle \bar{q}q \rangle_0(T)}{\langle \bar{q}q \rangle_0(0)} \right]^{\delta}, \tag{4.20}$$

where δ is left as a free parameter. To summarize, the thermal behavior of $\tilde{\chi}$ is [116, 117, 118]

$$\tilde{\chi}(T) = \frac{m\langle \bar{q}q \rangle_0(T)}{N_f} \left(1 - \frac{m\langle \bar{q}q \rangle_0(T)}{N_f \mathscr{C}_m(0)} \left[\frac{\langle \bar{q}q \rangle_0(0)}{\langle \bar{q}q \rangle_0(T)} \right]^{\delta} \right). \tag{4.21}$$

§ 4.4 MODELLING THE $\eta - \eta'$ SYSTEM

Up till now our procedure has been quite general. Qualitatively, we have established that modification of WVR via replacement $\chi_{\text{YM}} \rightarrow \tilde{\chi}$ ties the $U(1)_A$ restoration to chiral symmetry restoration. Now we would like to examine its quantitative features, by using a particular model.

For the meson masses and decay constants we follow [119] and use a bound state approach outlined in the previous Chapter. Medium calculations are facilitated by the separable model [79, 120] for the gluon propagator, see Eq. (3.4). Here we use the rank-2 Gaussian and Woods-Saxon model, see Eqs. (3.59) and (3.60).

We will work with several bases

- the flavor $q\bar{q}$ bases,

- the octet-singlet bases,
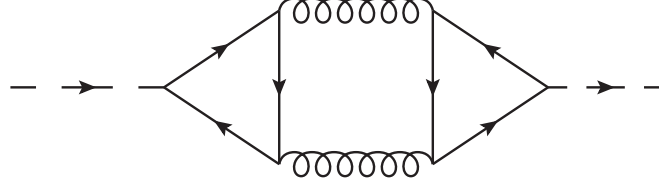
- and the strange-non–strange bases.

Figure 4.2: One possible gluon annihilation diagram leading to the anomalous part of the η_0 mass. The dashed lines denote the η_0 particle.

They are given through the following transformation matrices [119]:

$$
\begin{pmatrix} \pi^0 \\ \eta^8 \\ \eta^0 \end{pmatrix} = \frac{1}{\sqrt{6}} \underbrace{\begin{pmatrix} \sqrt{3} & -\sqrt{3} & 0 \\ 1 & 1 & -2 \\ \sqrt{2} & \sqrt{2} & \sqrt{2} \end{pmatrix}}_{S} \begin{pmatrix} u\bar{u} \\ d\bar{d} \\ s\bar{s} \end{pmatrix}
\tag{4.22}
$$

$$
\begin{pmatrix} \pi^0 \\ \eta_{NS} \\ \eta_S \end{pmatrix} = \frac{1}{\sqrt{2}} \underbrace{\begin{pmatrix} 1 & -1 & 0 \\ 1 & 1 & 0 \\ 0 & 0 & \sqrt{2} \end{pmatrix}}_{T} \begin{pmatrix} u\bar{u} \\ d\bar{d} \\ s\bar{s} \end{pmatrix} = \frac{1}{\sqrt{3}} \begin{pmatrix} \sqrt{3} & 0 & 0 \\ 0 & 1 & \sqrt{2} \\ 0 & -\sqrt{2} & 1 \end{pmatrix} \begin{pmatrix} \pi^0 \\ \eta^8 \\ \eta^0 \end{pmatrix}.
\tag{4.23}
$$

We split the contribution to the masses into anomalous and non-anomalous part [121]

$$
M^2 = M_{NA}^2 + M_A^2 \,,
\tag{4.24}
$$

where M^2 is to be understood as a 3×3 matrix. Non-anomalous masses M_{NA}^2 in the octet-singlet basis are given as follows

$$
M_{NA}^2 = \begin{pmatrix} M_\pi^2 & 0 & 0 \\ 0 & M_{88}^2 & M_{80}^2 \\ 0 & M_{08}^2 & M_{00}^2 \end{pmatrix} ,
\tag{4.25}
$$

where $M_\pi^2 = M_{u\bar{u}}^2 = M_{d\bar{d}}^2$, and

$$
\begin{aligned}
M_\pi^2 &= M_{u\bar{u}}^2 = M_{d\bar{d}}^2 \,, \\
M_{88}^2 &= \frac{2}{3}\left(M_{s\bar{s}}^2 + \frac{1}{2} M_\pi^2 \right) , \\
M_{00}^2 &= \frac{2}{3}\left(\frac{1}{2} M_{s\bar{s}}^2 + M_\pi^2 \right) .
\end{aligned}
\tag{4.26}
$$

All these quantities are calculated in the DSE-BSE approach [121].

The ladder approximation cannot handle M_A^2, as it lacks the possibility of a singlet quark-antiquark state annihilating into gluons. The diagram in Fig. 4.2 contains the lowest order process which, due to the triangle anomaly will lead to extra mass for the singlet η'. In total, this scheme [121] incorporates the anomaly effects only on the level of the masses, leaving the decay constants unaltered, as is dictated by the large N_c arguments [104].

In the octet-singlet basis, the anomaly is parametrized as

$$M_A^2 = S^T \begin{pmatrix} 0 & 0 & 0 \\ 0 & 0 & 0 \\ 0 & 0 & 3\beta \end{pmatrix} S = \beta \begin{pmatrix} 1 & 1 & 1 \\ 1 & 1 & 1 \\ 1 & 1 & 1 \end{pmatrix} \xrightarrow{SU(3) \to SU(2)} \beta \begin{pmatrix} 1 & 1 & X \\ 1 & 1 & X \\ X & X & X^2 \end{pmatrix}, \quad (4.27)$$

where the last step also includes the flavor breaking effects by using $X \simeq f_\pi / f_{s\bar{s}}$ [122] written in the flavor basis. The flavor breaking octet-singlet mass matrix is then

$$M_A^2 = S\beta \begin{pmatrix} 1 & 1 & X \\ 1 & 1 & X \\ X & X & X^2 \end{pmatrix} S^T = \beta \begin{pmatrix} 0 & 0 & 0 \\ 0 & \frac{2}{3}(1-X)^2 & \frac{\sqrt{2}}{3}(2-X-X^2) \\ 0 & \frac{\sqrt{2}}{3}(2-X-X^2) & \frac{1}{3}(2+X)^2 \end{pmatrix}. \quad (4.28)$$

Proceeding from the flavor basis to strange-non–strange basis we have

$$M_A^2 = T\beta \begin{pmatrix} 1 & 1 & X \\ 1 & 1 & X \\ X & X & X^2 \end{pmatrix} T^T = \beta \begin{pmatrix} 0 & 0 & 0 \\ 0 & 2 & \sqrt{2}X \\ 0 & \sqrt{2}X & X^2 \end{pmatrix}. \quad (4.29)$$

Note here that the anomaly does not effect π^0 in the isospin limit, permitting us to work in the $I = 0$ subspace from now on.

Rotating to the physical $\eta - \eta'$ basis

$$\begin{pmatrix} \eta \\ \eta' \end{pmatrix} = \underbrace{\begin{pmatrix} \cos\phi & -\sin\phi \\ \sin\phi & \cos\phi \end{pmatrix}}_{U} \begin{pmatrix} \eta_{NS} \\ \eta_S \end{pmatrix}, \quad (4.30)$$

leads to [119]

$$M^2 = U \begin{pmatrix} M_\pi^2 + 2\beta & \sqrt{2}\beta X \\ \sqrt{2}\beta X & M_{s\bar{s}}^2 + \beta X^2 \end{pmatrix} U^T = \mathrm{diag}(M_\eta^2, M_{\eta'}^2), \quad (4.31)$$

where

$$M_{\eta,\eta'}^2 = \frac{1}{2} \left(M_{\eta_{NS}}^2 + M_{\eta_S}^2 \mp \sqrt{M_{\eta_{NS}}^2 - M_{\eta_S}^2 + 8\beta^2 X^2} \right). \quad (4.32)$$

Here

$$M_{\eta_{NS}}^2 = M_\pi^2 + 2\beta, \qquad M_{\eta_S}^2 = M_{s\bar{s}}^2 + \beta X^2, \quad (4.33)$$
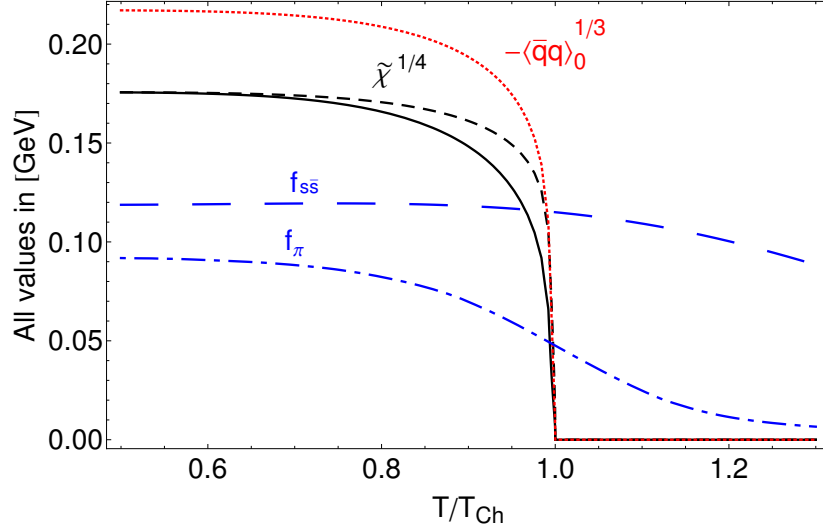
Figure 4.3: The relative-temperature dependences, on T/T_{Ch}, of $\widetilde{\chi}^{1/4}$, $\langle \bar{q}q \rangle_0^{1/3}$, f_π and $f_{s\bar{s}}$. The solid curve depicts $\widetilde{\chi}^{1/4}$ for $\delta = 0$ in Eq. (4.21), and the short-dashed curve is $\widetilde{\chi}^{1/4}$ for $\delta = 1$. At $T = 0$, the both $\widetilde{\chi}$'s are equal to $\chi_{\mathrm{YM}} = (0.1757\,\mathrm{GeV})^4$, the weighted average [120] of various lattice results for χ_{YM}.

are the non-physical strange-non–strange masses (the diagonal elements of first term in Eq. (4.31)). For completeness we also give the octet-singlet masses

$$M_{\eta_0}^2 = M_{00}^2 + \frac{1}{3}(2+X)^2\beta \qquad M_{\eta_8}^2 = M_{88}^2 + \frac{2}{3}(1-X)^2\beta \, , \qquad (4.34)$$

read off from diagonal elements of Eqs. (4.25) and (4.28).

Tracing the matrices in (4.31) leads to [119, 120]

$$\beta(2 + X^2) = M_\eta^2 + M_{\eta'}^2 - 2M_K^2 = \frac{2N_f}{f_\pi^2}\widetilde{\chi} \, , \qquad (4.35)$$

where we have used $M_{s\bar{s}}^2 = 2M_K^2 - M_\pi^2$. The last term in (4.35) is obtained from modified WVR, and thus enables us to relate the previously unknown parameter β to the topological susceptibility (4.21).

§ 4.5 RESULTS

The topological susceptibility, together with the required decay constants and the quark condensate is shown in Fig. 4.3. Already here one can see the physics
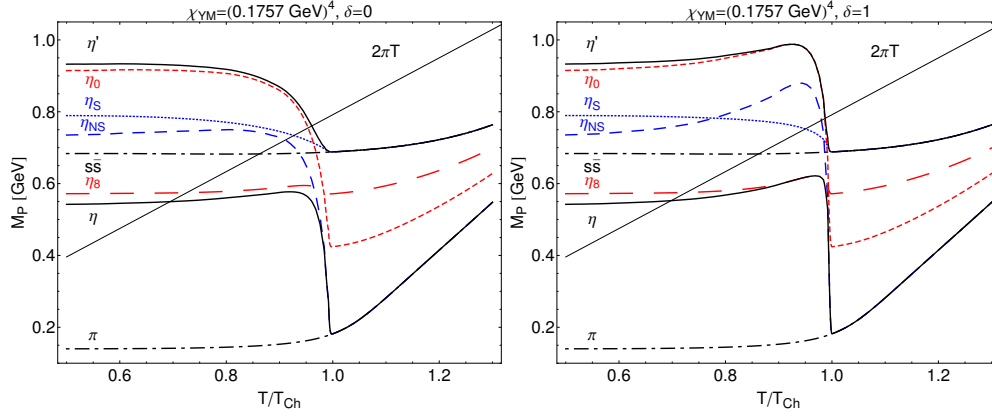
Figure 4.4: The relative-temperature dependence, on T/T_{Ch}, of the pseudoscalar meson masses for two $\widetilde{\chi}(T)$, with $\delta = 0$ (left panel) and with $\delta = 1$ (right panel). The straight line given by the Eletskii-Ioffe limit $2\pi T$ is twice the lowest Matsubara frequency.

at work: behavior of $\tilde{\chi}$ is governed by the condensate. So, while f_π is still finite, condensate is already zero, and the excess mass of η' vanishes.

The next Fig. 4.4 is our main result [116, 117]. We show masses as functions of temperature scaled to the chiral restoration temperature T_{Ch}. First of all, we see that at $T = 0$ the η and η' are almost degenerate with the unphysical η_8 and η_0 states, respectively. That is, the mixing angle between these states is small, which is why anomaly does not make η heavy as well. The strange-non–strange bases has its uses as well. If it were not for the anomaly, η_{NS} would be degenerate with π, while η_S would be degenerate with $s\bar{s}$. Increasing the temperature the anomalous contribution to various masses melts: η_{NS} and η_S degenerate with π and $s\bar{s}$, respectively, as reflected in (4.33). Furthermore, η' goes from being almost a pure η_0 state to being a $s\bar{s}$ (same as η_S) state. Accordingly, η degenerates with π (same as η_{NS}). This behavior was conjectured some time ago by Pisarski and Wilczek [23]. The residual splitting of η_0 and η_8 at high T has its origin in flavor breaking.

Our most dramatic result is a significant mass drop of the η' particle, as is now established by the analysis of Csörgő etal. The plots are shown for $\delta = 0$ and $\delta = 1$ of Eq. (4.21). Using δ significantly higher than 1 leads us to an opposite, unfavorable scenario where the mass of η' increases rather than drops. This is easily established from (4.21) where the influence of condensate on the high T behavior of $\tilde{\chi}$ diminishes as one increases δ.

5

Thermodynamics of covariant chiral quark models

In this chapter we move focus to the phase diagram and thermodynamic quantities like the pressure or the entropy in quark models which employ Lorentz covariant effective gluon interactions. For the phase diagram the influence of medium-induced Lorentz symmetry breaking on the critical end-point is examined. Also, some results on the phase diagram which can be obtained analitically are highlighted.

As we have seen in Chap. 3, a sufficiently strong interaction is required in order to break chiral symmetry. Such an interaction leaves a dramatic mark on the spectrum of the theory: the quark singularities move off-shell into the complex plane [123, 124, 125, 126, 127, 128, 129, 130], where they may remain poles, or even mutate into cuts. This is a very general consequence, seen in many models. Moreover, it is a desirable property: off-shell states can be thought of as a means to model confinement, via the property of positivity violation [13, 14].

Thermodynamics counts states. Here we would like to explore what are the consequences of counting the states seen in the complex plane of the quark propagator. We are especially interested in the low temperature behavior of such a theory, and a mechanism for regaining the perturbative quark singularity structure at sufficiently high temperatures.

Explicit calculations will be performed for $N_f = 2$ separable models, defined in Sec. 3.6.

§ 5.1 PHASE DIAGRAM

We approach the phase diagram from an analytic and a numerical perspective. The analytic perspective serves to understand several features observed in a full numerical calculations. We will start by discussing the splitting of $a - c$
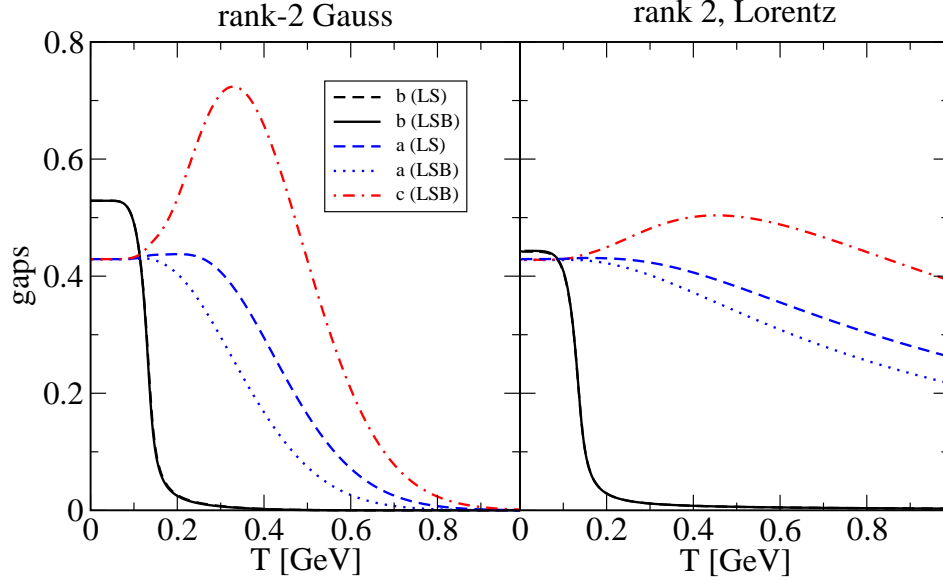
Figure 5.1: We illustrate the effect of LSB in rank-2 Gaussian (left) and rank-2 Lorentzian model (right) at $\mu = 0$. For simplicity, the system has been solved without the PL. The full (dashed) black curves represent the mass gap b, in the LSB (LS) case. The dotted (dashed) blue curve is the mean-field a in the LSB (LS), and the mean-field c is given by the dash-dotted red curve.

mean-fields at finite temperature, i. e. by discussing medium induced Lorentz symmetry breaking.

Medium induced Lorentz symmetry breaking   In Sec. 3.3 we argued for the possibility of the most general structure of the quark propagator (3.25). We solve the corresponding DSEs (3.27)-(3.29) (without the PL) at finite temperature for rank-2 Gaussian (3.55) and a rank-2 Lorentzian (3.61) model. Alternatively, we impose Lorentz symmetry by hand via $a = c$ and solve the corresponding truncated DSEs. The numerical results for both setups, Lorentz symmetry breaking (LSB) (full lines) and Lorentz symmetric (LS) (dashed lines) are shown in Fig. 5.1.

By comparing the mass gaps, given by the black curves, it is plain that there is barely an influence of solving the system by acknowledging the extra mean-field $a \neq c$, as the dashed and the full lines almost overlap. On the contrary, in Fig. 5.1, there is a clear difference between a and c mean fields defining a region where $O(4)$ symmetry is violated. This difference is a reflection of the
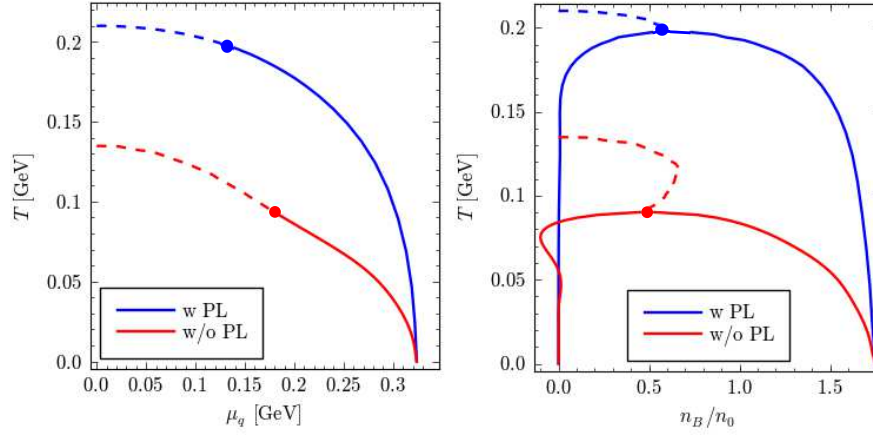
Figure 5.2: The left panel shows the phase diagram in the $T - \mu$ plane for rank-1 Gaussian model. The lower, red curve is the case without the PL, while the upper, blue curve is the case with the PL. Dashed line represents crossover, while the full line is the first order phase transition, with the critical end point denoted by a dot. On the right panel we have the same phase diagram, but in the $T - n_B$ plane, where n_B is the baryon number density. $n_0 = 0.16$ fm^{-3} is the nuclear matter density. The region in the middle is the coexistence region between the chirally broken, and the chirally restored phase.

$R^3 \times S^1$ structure of the spacetime manifold, and was already observed in DSE separable model studies, e. g. [99, 79]. At low temperatures the thermal circle S^1 is large, and Lorentz symmetry is approximately valid. With the increase in the temperature, a and c split, the difference is starting to be pronounced around the phase transition as the gap equations form a coupled system. Namely, since around the phase transition the mass gap suffers a significant drop, this must be reflected in changes of the gaps a and c. We see that the particular behavior of the mean fields is "causal", governing the inequality $a < c$.

From Fig. 5.1 we conclude that the splitting is much stronger for rank-2 Gauss; in the region $0.2 \, \text{GeV} \lesssim T \lesssim 0.6 \, \text{GeV}$ c develops a pronounced peak, whereas a monotonously descends. The value of a in the LS case can then be understood to provide a "mean value" between these two behaviors. The most distinct characteristic of the mean fields in set C is the finite value of a and c, referring to highly non-perturbative quarks even at $T \approx 1$ GeV!

Landau analysis   For simplicity we work in the chiral limit, and we put the PL equal to its conjugate $\Phi = \bar{\Phi}$. In this case the phase transition at $\mu = 0$ is

second order, and also $\Phi = \bar{\Phi}$. The critical temperature is read off from a Landau expansion of the thermodynamic potential in terms of the mean field b

$$\Omega_{\text{reg}}(a,b,c,\Phi) = \Omega_{\text{reg}}(a,0,c,\Phi) + \frac{1}{2}\left(\frac{\partial \Omega^2_{\text{reg}}}{\partial b^2}\right)_{b=0} b^2 + \cdots, \qquad (5.1)$$

more precisely from the point where the sign flip of the second derivative of the thermodynamic potential occurs. For rank-1 this is easily calculated to be

$$t_c = \left[\frac{24}{d_q}\left(\frac{1}{g_c} - \frac{1}{g}\right)\right]^{1/2}, \qquad (5.2)$$

where $t = T/\Lambda_0$ and $g = 2D_0/9\Lambda_0^2$ and g_c is the critical value dependent on the profile of the form-factor, see end of Sec. 3.2. Observe that while t_c will decrease by increasing the number of d. o. f., it will increase if the coupling g is stronger.

Let us now explore the consequences of generalizing (5.2) by the PL and by a non trivial wave function renormalization (WFR), i. e. for rank-2 class of models. In the first case, we obtain

$$t_c(\Phi) = \frac{t_c}{\left[1 - \frac{2}{\pi^2}\arccos\left(\frac{3\Phi-1}{2}\right)\right]^{1/2}}. \qquad (5.3)$$

For example, we have the limiting case $t_c(1) = t_c$, and $t_c(0.5) \simeq 1.17 t_c$, understanding that the PL acts to increase the critical temperature. The effect of non trivial WFR may be put in a analytic form in the local limit $\mathscr{F}_{0,1}(p^2) \to \theta(\Lambda_0^2 - \mathbf{p}^2)$. Then we have

$$t_c(a,c) = \frac{(1+a)^{3/2}}{(1+c)^{1/2}} t_c. \qquad (5.4)$$

Here now $t_c(0.5, 0.5) = 3/2 t_c$ and $t_c(0.5, 1) \simeq 1.3 t_c$, illustrating that even though WFR can increase the critical temperature, the splitting between the mean-fields a and c will tend to compensate this effect. Indeed, such a splitting is a medium induced breaking of Lorentz symmetry, and due to causality reasons progresses in such a way that $a < c$ [131]. As the gap equations (3.27)-(3.29) form a coupled system, the splitting is linked to the temperature scale of chiral restoration. This is what we observe on Fig. 5.1.

At small but finite μ, the line of the second order chiral phase transition takes an ellipsoidal shape. In rank-1 model

$$\frac{\pi^2}{3} t_c(\bar{\mu})^2 + \bar{\mu}^2 = \frac{8\pi^2}{d_q}\left(\frac{1}{g_c} - \frac{1}{g}\right), \qquad (5.5)$$

showing that introducing the density, or equivalently the chemical potential $\bar{\mu} = \mu/\Lambda_0$, reduces the critical temperature in accordance with our intuition:

a denser system enters the restored phase with less thermal agitation. The physics may be best captured by the curvature κ, a quantity that may be readily measured on the lattice [132], defined as

$$\frac{t_c^2(\bar{\mu})}{t_c^2(0)} = 1 - \kappa \frac{\bar{\mu}^2}{t_c^2(\bar{\mu})} \ . \tag{5.6}$$

In the simplest rank-1 case we have $\kappa = 3/\pi^2$. Note that this is a rather universal quantity as it does not depend on the profile of the form-factors, nor on the value of the coupling. Introducing the PL alters the curvature in the following manner

$$\kappa(\Phi) = \frac{\kappa}{1 - \frac{2}{\pi^2} \arccos\left(\frac{3\Phi-1}{2}\right)} \ . \tag{5.7}$$

Thus, the PL increases not only the critical temperature, but also the curvature of the critical line. On the other hand, in the local limit of rank-2 models it is easy to show that the curvature is not affected.

If the coupling is strong enough, the second order phase transition present at finite T and $\mu = 0$ might end up in the first order phase transition in the opposite regime: at finite μ and $T = 0$. This coupling should of course be stronger than the critical coupling g_c. In the local version of the model it can be analitically computed. First of all, assuming that the phase transition is second order at $T = 0$, Landau analysis yields

$$\bar{\mu}_c = \left[\frac{8\pi^2}{d_q} \left(\frac{1}{g_c} - \frac{1}{g} \right) \right]^{1/2} \ . \tag{5.8}$$

Compare this with the critical temperature at $\mu = 0$, given by Eq. (5.2). Second order phase transition will turn into the first order phase transition when the derivative $\partial b / \partial \mu$ has an infinite slope. This function will have a pole if the following condition is satisfied

$$\mu = \sqrt{\Lambda_0^2 + b^2} \cosh\left(\frac{\Lambda_0}{\sqrt{\Lambda_0^2 + b^2}} \right) - \Lambda_0 \sinh\left(\frac{\Lambda_0}{\sqrt{\Lambda_0^2 + b^2}} \right) . \tag{5.9}$$

Equating this with (5.8) and putting $b = 0$ yields

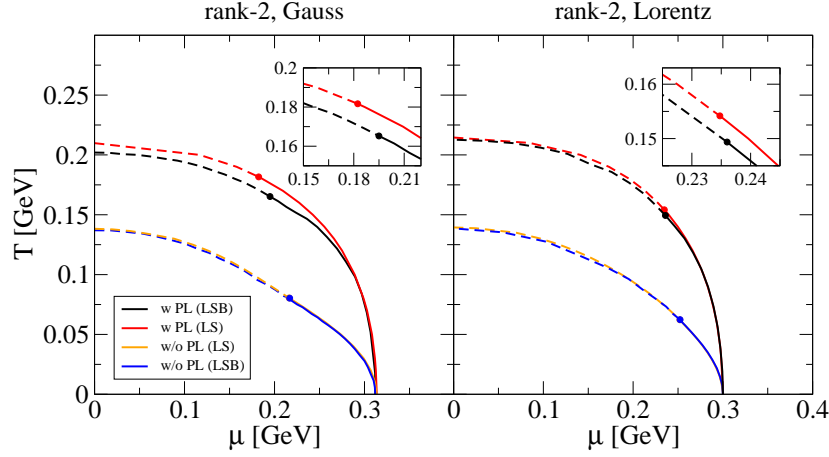$$g_c' = \frac{g_c}{1 - \frac{1}{e^2}} \ . \tag{5.10}$$

Figure 5.3: Phase diagram for rank-2 models. The lower pair of curves on both plots denote the phase diagram without PL, while in the upper pair of curves PL has been included as a dynamical variable. In the lower pair, the blue curve is the LS case, while the yellow curve is the LSB case. In the higher pair, the lower, black curve is the LSB case, while the higher red curve is the LS case.

Numerical results   By calculating the peak of the chiral susceptibility (3.38) we trace a line in $T - \mu$ plane separating the chirally broken and the chirally restored phase. For the simplest Gaussian rank-1 model, results are shown on the left panel in Fig. 5.2. Due to the finite current quark masses, chiral symmetry is explicitly broken, and at finite temperature there is no real phase transition, but a crossover behavior, denoted by the dashed curve. Increasing the chemical potential, one reaches the critical end point (CEP) after which the transition is first order.

Phase diagram for rank-1 Gaussian model with the PL is calculated by using the polynomial form of the PL potential (3.46). PL introduces two major changes in the phase diagram: first of all the temperature for the chiral restoration is higher, as anticipated from Eq. (5.3). Second, due to the fact that the phase transition in pure YM is first order, the CEP in the coupled system is somewhat closer to the T axis.

A first order transition implies a jump in the derivatives of the partition function, as e. g. the density. For example, in the chiral limit, the chirally broken phase at $T = 0$ has zero density, while the density in the chirally restored phase is finite. The region of densities in between represents a coexistence between two phases. This is what is plotted on the right panel of Fig. 5.2, where the phase diagram is given in the $T - n_B$ plane, with n_B the baryon number

density $n_B = n/3$, n being the quark number density. We normalize n_B to the density of nuclear matter $n_0 = 0.16 \text{ fm}^{-3}$. As the CEP is higher when the PL is included, the coexistence region at finite temperature is also higher. Notice the wiggles in the density for the red curve: this is imprint of the complex mass singularities of the quark propagator which will be discussed in the following Section. In particular, there is region around $T \sim 0.05$ to $T \sim 0.1$ GeV, where the density is negative. With the PL, this behavior is much improved, and the density is positive, as shown by the blue curve.

For rank-2 models the phase diagram is shown on Fig. 5.3. In our calculations we have used the rank-2 Gaussian (3.55) and the rank-2 Lorentzian (3.61) model. For the PL potential we have used the logarithmic form (3.48). First we observe that rank-2 models in general favor a CEP somewhat higher in μ and lower in T. Second, we have investigated the influence of Lorentz symmetry breaking on the position of the CEP. The curves shown in red and in yellow are results of Ref. [133], while the black and blue curves are results of Ref. [131]. We observe that LSB can, to a small extent, change the critical temperature, as announced by Eq. (5.4), but this behavior is not dramatic. Moreover, we find that the CEP does not change appreciably. The reason behind this is that the mass gap itself, which dictates the chiral phase transition is almost unchanged by introducing LSB, see Fig. 5.1.

§ 5.2 THERMODYNAMICS IN THE COMPLEX MASS POLE REPRESENTATION

We treat the simplest case, where we propose that the quark propagator has an infinite series of complex conjugate mass poles (CCMPs). There are several occurrences where such a structure has been found and put to use [128, 134, 135, 136].

The starting point is the 2PI thermodynamic potential (3.15) where we concentrate on the so-called kinetic part

$$\Omega_{\text{kin}} = -\frac{d_q}{2} T \sum_{n=-\infty}^{+\infty} \int \frac{d^3 p}{(2\pi)^3} \log \left[\mathbf{p}^2 A^2(\tilde{p}_n^2) + \tilde{\omega}_n^2 C^2(\tilde{p}_n^2) + B^2(\tilde{p}_n^2) \right] . \qquad (5.11)$$

We assume a series of CCMP quartets $\pm m_k = \pm m_k^R \pm i m_k^I$ and $\pm m_k^* = m_k^R \mp i m_k^I$. At $\mathbf{p} = 0$ these are the singularities of the quark propagator. At $\mathbf{p} \neq 0$ we have

$$\mathscr{E}_k^2 = \mathbf{p}^2 + m_k^2 , \qquad (5.12)$$

with the complex energy $\mathscr{E}_k = \epsilon_k + i\gamma_k$ so that

$$
\epsilon_k = \frac{1}{\sqrt{2}} \left\{ (m_k^R)^2 - (m_k^I)^2 + \mathbf{p}^2 + \sqrt{\left[(m_k^R)^2 - (m_k^I)^2 + \mathbf{p}^2 \right]^2 + 4(m_k^R)^2 (m_k^I)^2} \right\}^{1/2} ,
$$
$$
\gamma_k = \frac{m_k^R m_k^I}{\epsilon_k} .
$$
$$(5.13)$$

Knowing the analytic structure, Matsubara summation can be performed. Let us mention only the essential steps, and look at the simplifed case when $\mu = 0$. By introducing the generalized Fermi-Dirac function

$$
n(z) = (1 + e^{\beta z})^{-1} ,
$$
$$(5.14)$$

having simple poles precisely at $z = i\tilde{\omega}_n$, the Matsubara sum gets an interpretation as a sum over residues these poles. This allows us to use a master formula for Matsubara summation [77]

$$
-2\pi i T \sum_{n=-\infty}^{+\infty} \log[\mathscr{D}(i\tilde{\omega}_n)] = \int_{i\infty}^{-i\infty} dz \log[\mathscr{D}(z)]
$$
$$
+ \int_{-i\infty+\delta}^{i\infty+\delta} dz\, n(z) \log[\mathscr{D}(z)] - \int_{-i\infty-\delta}^{i\infty-\delta} dz\, n(z) \log[\mathscr{D}(z)] ,
$$
$$(5.15)$$

where $\delta > 0$ is infinitesimal and

$$
\mathscr{D}(z) = \mathbf{p}^2 A^2 (\mathbf{p}^2, -z^2) - z^2 C^2 (\mathbf{p}^2, -z^2) + B^2 (\mathbf{p}^2, -z^2) .
$$
$$(5.16)$$

The $\mathbf{p}^2$ dependence in (5.16) is omitted for brevity. The first term in (5.15) is just the vacuum contribution, while the second can be evaluated to

$$
\int_{-i\infty+\delta}^{i\infty+\delta} dz\, n(z) \log[\mathscr{D}(z)] = T \oint_{\mathscr{C}} dz \log\left[1 + e^{-\beta(z-\mu)} \right] \frac{\mathscr{D}'(z)}{\mathscr{D}(z)}
$$
$$
= T(-2\pi i) \sum_{k, \epsilon_k > 0} \left\{ \log\left[1 + e^{-\beta \mathscr{E}_k} \right] + \log\left[1 + e^{-\beta \mathscr{E}_k^*} \right] \right\} ,
$$
$$(5.17)$$

where $\mathscr{C}$ is the curve made by closing the straight line $\mathrm{Re}(z) = \delta$ with large semicircle at $\mathrm{Re}(z) > 0$, $|z| \to \infty$. In the second step partial integration was used. The third term can be evaluated in the same manner leading to

$$
\Omega_{\mathrm{kin}} = \Omega_{\mathrm{zpt}} - \frac{d_q}{2} T \sum_{k=1}^{\infty} \int \frac{d^3 p}{(2\pi)^3} \Big\{ \log\left[1 + e^{-\beta(\mathscr{E}_k - \mu)} \right] + \log\left[1 + e^{-\beta(\mathscr{E}_k^* - \mu)} \right]
$$
$$
+ \log\left[1 + e^{-\beta(\mathscr{E}_k + \mu)} \right] + \log\left[1 + e^{-\beta(\mathscr{E}_k^* + \mu)} \right] \Big\} ,
$$
$$(5.18)$$

where finite chemical potential μ was restored in an obvious manner. The divergent zero-point energy contribution Ω_{zpt} is given as (3.18).

By combining the logarithms, (5.18) can be cast in a more transparent form

$$\Omega_{\text{kin}} = \Omega_{\text{zpt}} - \frac{d_q}{2} T \sum_{k=1}^{\infty} \int \frac{d^3 p}{(2\pi)^3} \left\{ \log \left[1 + 2 e^{-\beta(\epsilon_k - \mu)} \cos(\beta \gamma_k) + e^{-2\beta(\epsilon_k - \mu)} \right] \right.$$
$$\left. + \log \left[1 + 2 e^{-\beta(\epsilon_k + \mu)} \cos(\beta \gamma_k) + e^{-2\beta(\epsilon_k + \mu)} \right] \right\} . \tag{5.19}$$

Note now that the oscillating cosine functions in the thermodynamic potential could render quark matter unstable. Their origin is traced back to the appearance of imaginary parts γ_k of the CCMPs.

We propose [137] to remedy this issue by introducing the PL in the system. In the background field approximation for the PL this amounts to a modification of (5.14)

$$n(z) \to \left\{ 1 + e^{\beta[z - i(\lambda_3 \phi_3 + \lambda_8 \phi_8)]} \right\}^{-1} , \tag{5.20}$$

where $\phi_{3,8}$ are the background gauge fields. For details see Sec. 3.

Following the same steps as before, and working out the non-trivial color trace, the kinetic contribution to the thermodynamic potential can be written as

$$\Omega_{\text{kin}} = \Omega_{\text{zpt}} - 2 N_f T \sum_{k=1}^{\infty} \int \frac{d^3 p}{(2\pi)^3} \left\{ \log \left[1 + 3\Phi e^{-\beta(\mathscr{E}_k - \mu)} + 3\bar{\Phi} e^{-2\beta(\mathscr{E}_k - \mu)} + e^{-3\beta(\mathscr{E}_k - \mu)} \right] \right.$$
$$\left. + \log \left[1 + 3\Phi e^{-\beta(\mathscr{E}_k^* - \mu)} + 3\bar{\Phi} e^{-2\beta(\mathscr{E}_k^* - \mu)} + e^{-3\beta(\mathscr{E}_k^* - \mu)} \right] + (\mu \to -\mu) \right\} . \tag{5.21}$$

In the special case of just one pair of real poles at $\pm m$, this expression is reduced to the corresponding term of the Polyakov-Nambu-Jona-Lasinio (PNJL) model (see, e.g., [94, 95, 96, 138]). The logarithms can be combined to obtain

$$\Omega_{\text{kin}} = \Omega_{\text{zpt}} - 2 N_f T \sum_{k=1}^{\infty} \int \frac{d^3 p}{(2\pi)^3} \left\{ \vphantom{\sum} \right.$$
$$\log \left[1 + 6\Phi \left(e^{-\beta(\epsilon_k - \mu)} \cos(\beta \gamma_k) + e^{-4\beta(\epsilon_k - \mu)} \cos(2\beta \gamma_k) \right) \right.$$
$$+ 6\bar{\Phi} \left(e^{-2\beta(\epsilon_k - \mu)} \cos(2\beta \gamma_k) + e^{-5\beta(\epsilon_k - \mu)} \cos(\beta \gamma_k) \right)$$
$$+ 9\Phi^2 e^{-2\beta(\epsilon_k - \mu)} + 9\bar{\Phi}^2 e^{-4\beta(\epsilon_k - \mu)}$$
$$+ 18\Phi\bar{\Phi} e^{-2\beta(\epsilon_k - \mu)} \cos(\beta \gamma_k) + 2 e^{-3\beta(\epsilon_k - \mu)} \cos(3\beta \gamma_k) + e^{-6\beta(\epsilon_k - \mu)} \right]$$
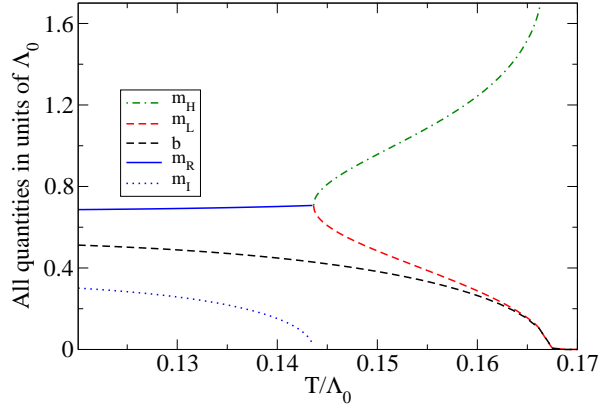$$\left. + (\mu \to -\mu) \right\} . \tag{5.22}$$

Figure 5.4: Temperature dependence of the lowest lying CCMPs in the chiral limit. m_R and m_I denote the real and imaginary part.

Comparing this with Eq. (5.19), we see that now the dominant cosine terms are weighted by the PL. As a consequence, the pressure instabilities are highly suppressed in the confined phase: as long as Φ and $\bar{\Phi}$ are zero, there remains only one cosine term, which is, however, suppressed by the third power of the Boltzmann factor. In fact, the mechanism is basically the same as in the PNJL model, where the coupling to the PL suppresses the quark degrees of freedom at low T, but does not eliminate them entirely [95, 96, 138].

§ 5.3 INSTABILITIES IN NON-LOCAL CHIRAL QUARK MODELS

The dispersion relations $\mathcal{E}_k$ which enter Eq. (5.18) are governed by the analytic structure of the quark propagator, so that further insight can be obtained only by studying the thermal behavior of the quark propagator, i.e., by understanding how the CCMPs respond to a change in the temperature or density.

Parametrizing the analytic structure, say, from lattice studies at finite T is very demanding. In this case the analytic structure is also somewhat arbitrary as the quark propagator is known only at a finite number of points, allowing for different meromorphic forms [128]. For the present purpose we will therefore study a specific model as an example case. More precisely, we consider a class of separable DSE models the rank-1 Gaussian model, already provided in Sec. 3.6, and rank-2 Gaussian and rank-2 Lorentzian model.

Rank-1 Gaussian model For this kind of separable models, it was already observed in the literature that pressure instabilities appear in certain regions of the T-μ plane in Refs. [97, 139, 140, 141, 142]. The aim of the present section is to demonstrate that these instabilities are driven by the presence of the CCMPs, and then to study the effect of the PL. Results from a full numerical study will be confronted with a calculation where we restrict ourselves only to a finite number of CCMPs, demonstrating that the instability region is actually completely dominated by the first quartet.

The size of the gap b determines whether the model will have complex singularities. In the chiral limit, the critical value is given by [139, 140, 141] $b_c = \Lambda_0/\sqrt{2e}$. This means that if the temperature is high enough, gap will be small enough to admit real poles. But, these are not the only singularities, as a Gaussian regulator admits an infinite number of poles. However, only the lowest ones (closest to the origin in the complex plane) are linked to the physical states encountered at high temperature. For them, call them $m_{L,H}$, also an analytic form is possible

$$m_{L,H}^2(b) = -\frac{1}{2}W_{0,-1}(-2b^2/\Lambda_0^2) \, , \tag{5.23}$$

where $W_{0,-1}(x)$ are the two branches of the Lambert W-function. The notation suggest that the light state, $m_L \to 0$, and the heavy state, $m_H \to \infty$, as $b \to 0$, as can be inferred from analytic properties of the Lambert W-function. Even though only m_L is physical, one should not ignore m_H as it would create unphysical discontinuities in the thermodynamics. Namely, as the temperature increases, the complex poles fuse into $m_{L,H}$, as illustrated in Fig. 5.4 so the number of degrees of freedom should be preserved below and above this point.

The thermodynamic potential in a CCMP parametrization is given as

$$\Omega_{\text{reg}} = \Omega_{\text{cond}} + \Omega_{\text{zpt}}^{\text{reg}} + \Omega_{\text{kin}} - \Omega_{\text{zpt}} \, , \tag{5.24}$$

where we put $a = 0$, and where for Ω_{kin} (5.19) and (5.22) is used for the case without and with the PL, respectively. We make an approximation by restricting ourselves to the case with only the first and the first plus second quartet. We calculate the pressure scaled to its Stefan-Boltzmann (SB) value without (3.39) and with (3.40) gluon degrees of freedom.

The results for the model without PL are displayed in Fig. 5.5. The most striking features are the oscillations, which signal the thermodynamic instabilities, we have anticipated from the cosine terms in Eq. (5.19). They turn out to be particularly troublesome, as there are not only temperature regions where the pressure drops with increasing temperature, but where it gets even negative.[1] Comparing the three panels of the figure, the results seem to be rather

---

[1]Let us recall that we defined the vacuum pressure to be zero, so this result is clearly unphys-
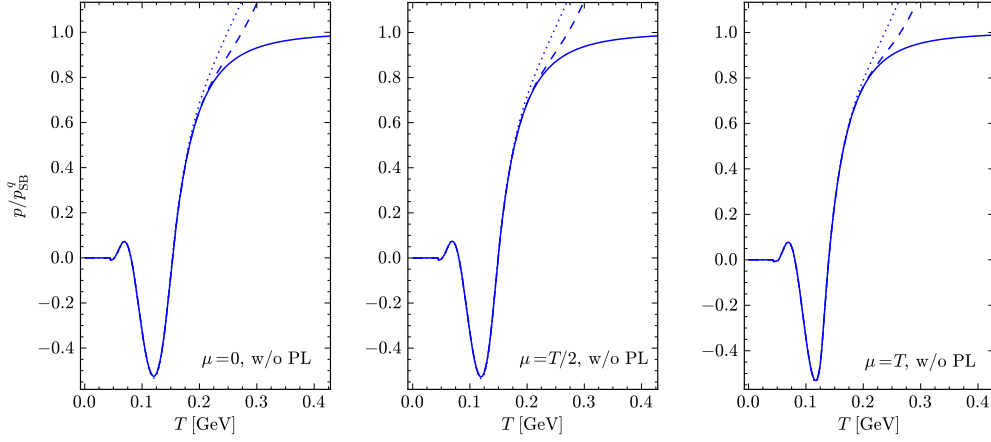
Figure 5.5: Scaled pressure p/p_{SB}^{q} as a function of temperature, for a system without the PL. The full line is the complete numerical calculation, while the dotted and the dashed lines correspond to the approximation accounting for the first and the first plus second quartet of poles, respectively.
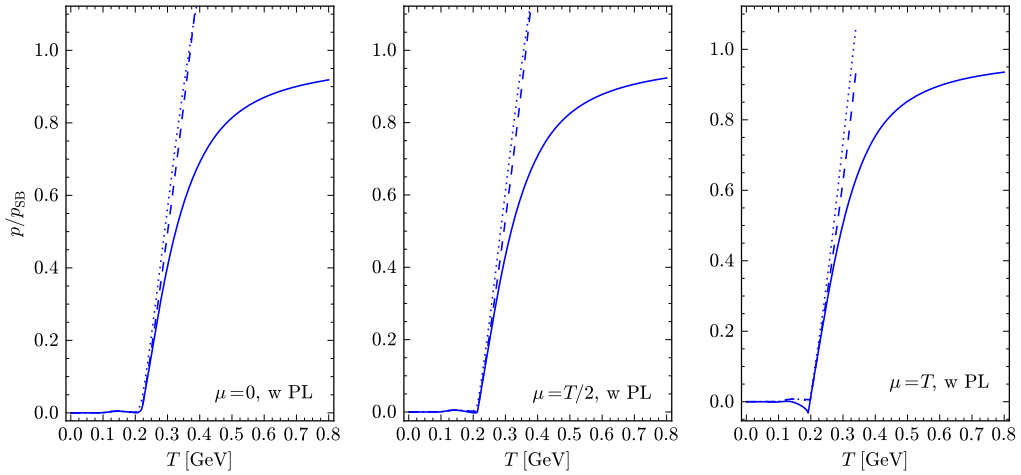

Figure 5.6: Scaled pressure p/p_{SB} as a function of temperature, for a system with the PL. Line styles as in Fig. 5.5.

independent of the ratio μ/T. We should keep in mind, however, that the pressure is scaled by the SB value, which is larger for larger values of μ/T. Taking this into account, the instabilities grow with the chemical potential, since the Boltzmann factors are even less effective in damping the oscillating terms. This results in a rather large negative pressure for $\mu/T = 1$.

For comparison we show again the results obtained when we only take into account the lowest-lying poles. In agreement with our findings for the mass gap, we observe that, at low temperatures and more importantly, in the region of the instability, the pressure given by just the first quartet is an excellent approximation. The oscillations of the pressure can thus be understood quantitatively from the temperature dependence of b shown in Fig. 5.4. In particular, at T around $0.1\Lambda_0$, the mass gap drops below b_c, so that the lowest quartet splits into two real doublets and no longer yields an oscillating behavior.

At high temperatures, the full numerical result for the pressure (solid lines) approaches the SB limit, whereas the restriction to the first quartet (dotted) strongly overshoots this limit and is not a good approximation in this regime. The inclusion of the second quartet (dashed line) leads to some improvement but fails as well to reproduce the SB limit as well.

Introducing the PL leads to a dramatic improvement of the EoS. As demonstrated on Fig. 5.6, the oscillations are strongly suppressed. Since the PL does not eliminate all the cosine terms completely (see Eq. (5.22)), residual wiggles are still present on the results for $\mu/T = 0, 1/2$, while at $\mu/T = 1$ also a slightly negative pressure is observed in the full numerical calculation.

Rank-2 models There are several differences when discussing rank-2 vs. rank-1 analytic structure and the impact of CCMPs on the thermodynamics. A mayor one is that in this case the gap is undercritical, both in the Gaussian and the Lorentz case under consideration. This results in a monotonous behavior in the low temperature, chirally broken phase. Second, in the Gaussian case, there is also an issue of criticality for a.

We now elaborate on these two points. The analysis is facilitated further by considering the case $\Lambda_0 = \Lambda_1$. With $a = 0$ two real poles exist, as shown on Fig. 5.7. Any $a > 0$ brings an extra pole b/a from infinity. As a increases, this singularity in turn coalesces with the first two at $a = a_c = 2/e^{3/2} \simeq 0.446$, after which point only one real singularity is present for all values of b. At the same time, the threshold b_c rises as a function of a, until it hits

$$b_c(a_c) = \frac{\Lambda_0}{\sqrt{2}} \left(\frac{3}{e}\right)^{3/2} . \tag{5.25}$$
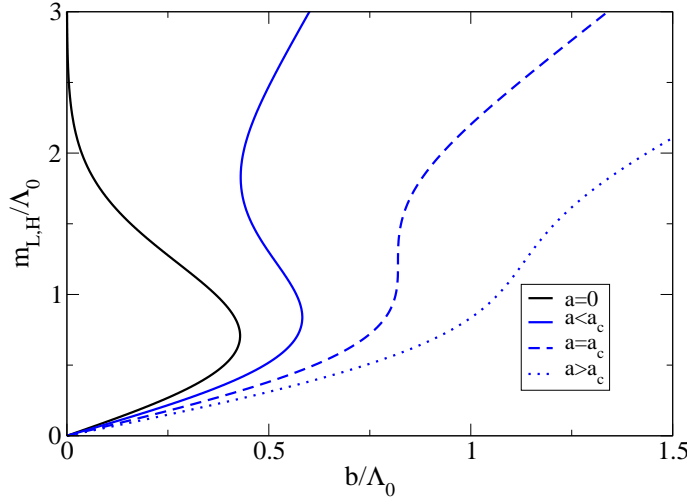
ical.

Figure 5.7: Scaled singularities in the limiting $m = 0$ and $\Lambda_0 = \Lambda_1$ case of a Gaussian rank-2 model as a function of the scaled mass gap b for several different value of a. Note that for $a = 0$ we are back at the rank-1 scenario with a heavy and a light state. This is preserved up to $a = a_c$.

The outcome is that in rank-2 it is easier for the physical mass gap (set by low energy phenomenology) to be undercritical. A concrete calculation for set B with $\Lambda_0 = \Lambda_1$ yields $b = 0.497$ GeV and $b_c(0.430) = 0.652$ GeV confirming that indeed the gap is undercritical.

The meanfields a, c do not follow any symmetry breaking-restoration pattern - they die out around the scale $T \sim \Lambda_1$, which is much higher than T_{Ch}. This is a good and a bad point. It is a good point because the finiteness of these fields means quarks are still strongly coupled, and provide a very simplistic manner to think about a strongly coupled QGP. It is a bad point because the analytic structure of the quark propagator is such that there are extra unwanted singularities in the complex plane. In the chiral limit and in the simplifying scenario when $a = c$ of Gaussian rank-2 case they are double poles in the complex plane. They severely affect the Equation of State [131].

In Fig. 5.8 we show the entropy (3.35) to give an explicit example. This is a full calculation where we use physical quark masses. First we observe that there is indeed no negative pressure in the low T chirally broken phase both for the Gaussian and for the Lorentzian regulator. At high T, chiral symmetry is restored, gap is almost zero, and the the Gaussian form factor shows a massive oscillation, very much in complete conflict to a monotonous rise seen on
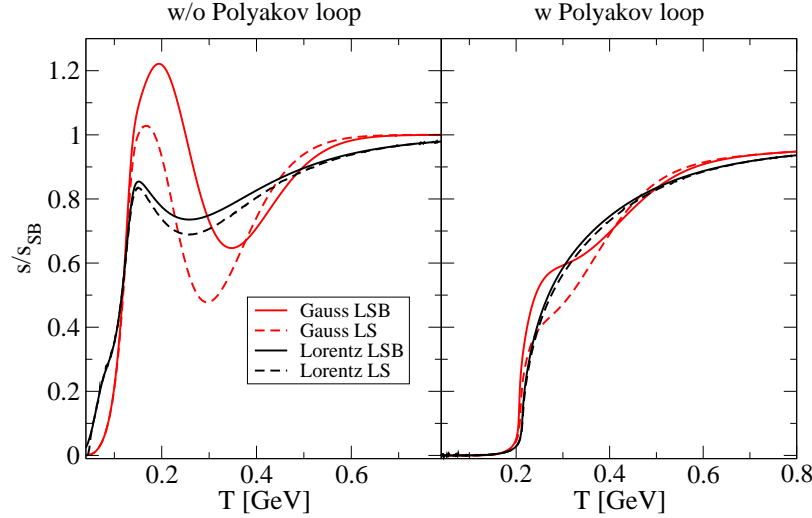
Figure 5.8: The plots show scaled entropy as a function of temperature for rank-2 Gauss and Lorentzian models.

the lattice [143]. Moreover, as we have double poles, the SB limit is eventually exceeded. This unsatisfactory result is readily improved with the Lorentz parametrization; the oscillation is somewhat reduced, giving an entropy within the SB bound, over the whole temperature range.

Introducing the PL to the system again leads to a dramatically improved behavior [131]. The PL is very successful in taming the oscillations in a theory with CCMPs, as its value is zero in the low temperature, confined phase. As the confinement transition is coincident with the chiral one, the only poles that the PL is able to strongly suppress are the ones present before the chiral transition. Therefore, the oscillation in Gaussian model, due to the double poles, is still present, albeit largely reduced. For the Lorentzian model, the oscillation was smaller to begin with, so when the PL smooths that out, all what is left is again a monotonous rise, as observed by the black curve on the right panel of Fig. 5.8.

In addition, we have studied also a degenerate scenario, where we have enforced by hand Lorentz symmetry on the level of the quark propagator by setting $a = c$. This is the LS (Lorentz symmetry) case, given in Fig. 5.8. A more complete Lorentz symmetry breaking scenario where $a \neq c$ is denoted by LSB. Our results show that although the mean-fields a and c significantly differ in the high temperature phase, the EoS is not very much affected.

§ 5.4 MAIN POINTS AND DISCUSSION

Singularities in the complex plane are usually seen as favourable property for modelling confining interactions. However, if a model exhibiting such a property is promoted to finite T and μ then these singularities might lead to a thermodynamic instability. That is not hard to grasp; although Matsubara formalism discretizes the imaginary energy axis, through elementary complex analysis, it is in fact sensitive to the structure in the whole complex plane. States are poles, cuts, non-analyticities in general, and every one of them is accounted for in the partition function.

One of the major points shown here is that even these covariant confining models may have problems in the low T domain. The theory may be unstable in the sense of Le Chatelier, second temperature derivative of the partition function being less than zero. We have found that one possible way out is to couple the model to the PL. This in effect betters the gluon sector of the theory, and at the same time has a very convenient property to stabilize the system.

PL was introduced in NJL models to mimic confinement, i. e. to make quarks statistically unfavorable. nlNJL model has confinement built in, via positivity violation criteria. What is the motivation then for coupling the PL in these models? We are of opinion that the issue of thermodynamic (in)stability makes a compelling point.

Finally, when discussing the instability several interesting issues are left open:

- Fully coupled system of quarks and gluons may very well hold some analytic structure, related to confinement. If yes, then it appears that these structures conspires in some very complicated way at finite T so that we do not see the oscillations (in fact, we know from lattice they do not belong there).

- Should we really count complex singularities in thermodynamics? After all, the physical degrees of freedom in the low T phase are not quarks and gluons, but mesons and baryons. These are the states one should count. Then, the failure of the model description might be searched for simply in the lack of description beyond the mean-field. This is similar as in pure YM where Savvidy encountered a tachyonic mode in a mean-field description [144, 145]. It is interesting to note that also in this case the PL acts as a "stabilizer", i.e., by suppressing the original tachyonic modes [146, 147]. Unfortunately, this program is also not entirely successful as new unstable modes arise [146, 147]. Let us also mention that, at least in this model, it is not possible to omit these states by hand. Since some of them are connected to the massless singularity in the high T phase, it means that we would loose this physical state.

- Should we really have complex singularities in the propagators? What is confinement then? There is really no proof that these structures exist, it may very well be that the quark propagator is an entire function, as discussed e. g. in [148, 149]. But an entire function is either a constant or it has a singularity at infinity. If that is really the case for the quark propagator, then the gluon sector of the theory must have such a profound back-reaction on matter as to reconstruct its pertubative analytic structure at high T.

- In the simple model used here, the running of the quark mass is set to mimic the lattice data. But the lattice data is given only in the Euclidean axis of the complex plane. A priori it is not clear which function should be used, and more importantly whether such a function should be used in the whole complex plane. Most probably it should not, which leads to the possibility that the complex poles might be somewhere else, but also that they are merely an artifact. Quoting Georges Ripka [89]: "*Our ignorance as how to continue propagators in the complex plane reflects our ignorance of the confining mechanism.*". It would thus be highly desirable to get a handle on the quark (or the gluon) propagator in the whole complex plane. An initiative in that direction has been taken [150, 151, 152].

6

Aspects of the Mott transition in covariant models

According to the interpretation of the experimental results from CERN-SPS, RHIC and LHC, the quark-gluon plasma created in the heavy ion collisions is a strongly correlated liquid [153, 154]. This means not only that correlations are important for a description of a QGP phase, but even more important to describe the phase transition itself.

Nowadays, lattice studies are able to confirm this very natural paradigm: the Equation of State in the low temperature domain, where chiral symmetry is still broken, reveals hadrons as active degrees of freedom [143]. As an additional confirmation, the Hadron Resonance Gas model put forward by Rolf Hagedorn in '65 [155], correctly saturates lattice data in this low T region [156, 157, 158]. With such hindsight, we understand that a realistic theoretical prediction of the QCD phase diagram must go beyond the mean-field and include mesons and baryons as active degrees of freedom. For example, Refs. [159, 160] showed that a correct description of the chemical freeze-out data, through the melting of the quark condensate, is possible only when the backreaction of hadron degrees of freedom is included. Already activating few low lying states, the π and σ mesons, has important repercussions on the phase diagram: functional renormalization group studies show that fluctuations smear out the border between phases, and wash out the critical end-point [161, 162].

Returning back to the Hadron Resonance Gas, we understand that it is a viable scenario only up to some point: the Hagedorn limiting temperature [155]. In other words, at some point hadrons have to melt into their constituents: quarks and gluons. The present Chapter aims at understanding the QCD phase transition through the description of melting hadrons. This is the QCD Mott transition, pictorially described on Fig. 6.1; by increasing the temperature hadron wave functions start to overlap, leading to a crowded phase space due to the
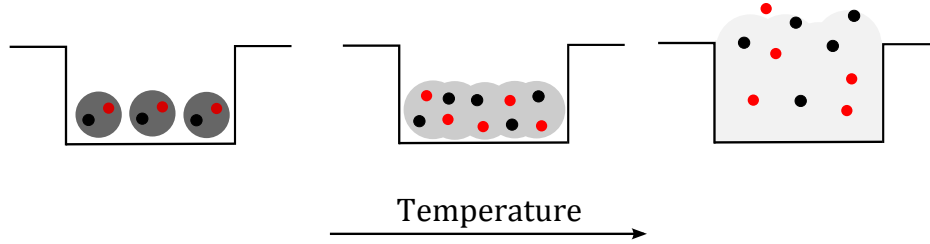
Figure 6.1: A cartoon of the Mott transition. Color shades indicate strength of the interaction.

Pauli principle, forcing quarks to occupy higher states, finally to merge in the continuum. Initial works were performed by Hüfner etal. [163, 164, 165] in the NJL model. Recently, this activity was renewed in the PNJL model [166] with the emphasizes on the role of the Levinson theorem at finite T by Blaschke etal. [167] and with diquarks at finite T and μ [168].

   We will use the separable DSE model coupled to the PL described in Chapter 3 for a initial beyond mean field study. In particular we will be interested in asking to what extent does the bound state description of the π and σ mesons survive the chiral and deconfinement phase transition.

§ 6.1   MESONS AT FINITE TEMPERATURE

At this point we discuss the thermal behaviour of mesonic degrees of freedom. We expect that non-local interactions, such as the one present in the separable model might induce new features particularly into the picture of meson dissociation in the plasma. The aim is to deduce qualitative influence of the non-local interactions on the aspect of Mott physics concerning resonance broadening, and also to discuss the effects of the WFR channel.

   The in-medium features of correlations are encoded in the meson polarization function (3.41). For calculations, we will be using models introduced already in Sec. 3.6 rank-1 Gaussian model (3.54), rank-2 Gaussian (3.55) and Lorentzian (3.55) models, as well as the Instanton Liquid type model (3.65). We also use the logarithmic PL potential (3.48). When calculating meson properties, we will restrict ourselves to the leading covariant description.

Meson masses   In principle they can be obtained from its Bethe-Salpeter equation at zero meson momentum $\mathbf{P} = 0$, see Eq. (3.14)

$$1 - \frac{2D_0}{9}\Pi_M(-im_M^{\text{pole}}, 0) = 0 \,, \tag{6.1}$$

where m_M^{pole} denotes the dynamical, pole mass. While such calculations are straightforward in local NJL models, the covariant approach presents technical difficulties. In the high temperature phase, some quark propagator singularities become real, so that kinematical thresholds might be opened, see the previous Section, esp. Fig. 5.4, making the polarization loop a complex function. A complete analysis therefore requires performing Matsubara summation analytically. Via residue calculus this will in principle lead to a double summation over all the singularities present in the propagator, requiring that their behaviour first needs to be traced as a function of the mean fields a, b, c. While this approach might be possible for rank-1 models, it is technically rather challenging for rank-2 models.

We circumvent this difficulty by following Refs. [99, 169, 79, 170] and calculating spatial or screening masses given by solving the equation

$$1 - \frac{2D_0}{9}\Pi_M(0, -i m_M^{\text{spat}}) = 0 \ . \tag{6.2}$$

This simplification is supported by a calculation in local NJL models [171, 172] where a careful comparison of both screening and pole masses lead to the following conclusion: at low temperatures, below the chiral restoration temperature, the screening masses closely follow the dynamical ones. However, at temperatures above the chiral restoration, screening masses were found to be somewhat higher in value, asymptotically approaching the $2\pi T$ Eletskii-Ioffe limit. It should be emphasized that both the screening and the pole masses were found to follow the expected pattern of chiral symmetry breaking and restoration.

Meson widths The width is obtained by renormalizing the meson propagator. For simplicity, if we take the vacuum propagator in Euclidean space and expand it around $P^2 = -m_M^2$

$$\Delta(P^2) = \frac{1}{-\frac{1}{G_S} + \Pi_M(P^2)} \rightarrow \frac{g_{M\bar{q}q}^2}{P^2 + m_M^2 + i\Gamma_M m_M} \ , \tag{6.3}$$

where Γ_M is the meson width

$$\Gamma_M = g_{M\bar{q}q}^2 \frac{\text{Im}(\Pi_M)}{m_M} \ , \tag{6.4}$$

and $g_{M\bar{q}q}$ is the effective quark-meson coupling, or the meson wave function renormalization

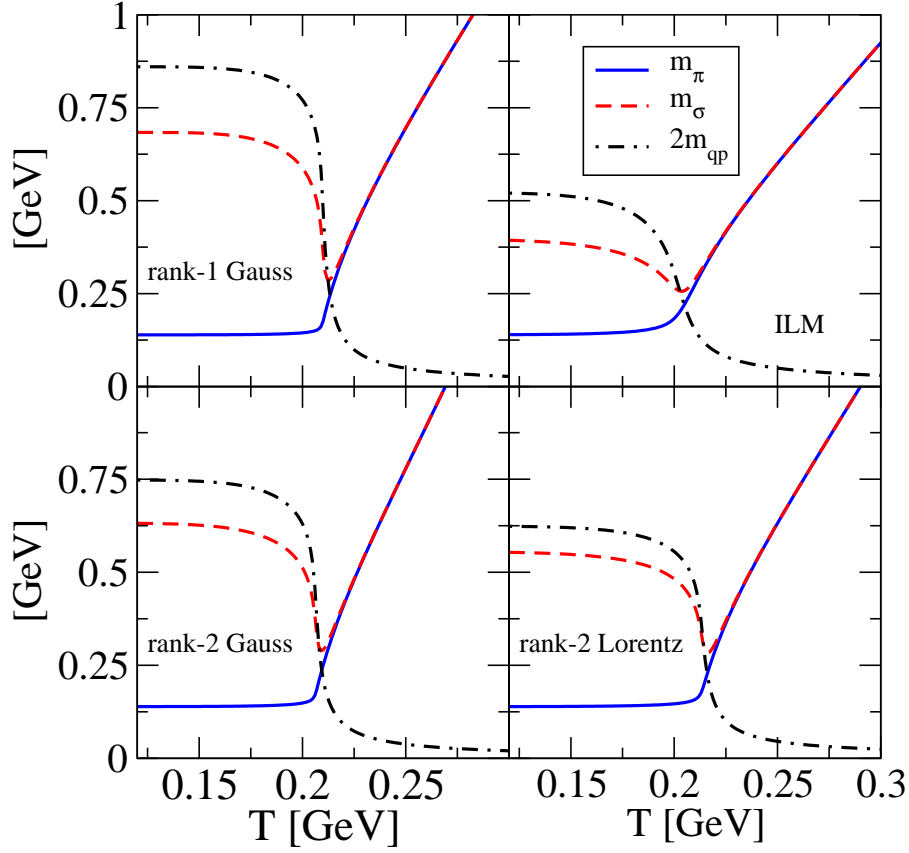$$g_{M\bar{q}q}^2 = \left[\frac{\partial \text{Re}(\Pi_M)}{\partial P^2} \right]_{P^2 = -m_M^2}^{-1} \ . \tag{6.5}$$

Figure 6.2: The panels display masses for π and σ mesons for different sets. The results for rank-2 models are given only for the LSB case.

In order to obtain $\text{Im}(\Pi_M)$ in a covariant setup we anticipate the following idealized scenario. At low temperatures all the singularities in the models are either complex or real, but in both cases they are at least of the order of the scale of the regulators $f(p^2)$ and $g(p^2)$, which is out of reach as a continuum threshold. In fact, by an elaborate analytic continuation (see, *e.g.*, [173, 174, 169]) one can avoid thresholds for complex poles. Increasing the temperature, the mass gap drops, and all the masses of non-physical states move out to infinity, with only one physical quark degree of freedom remaining.

This is indeed supported by a more detailed analysis of rank-1, see Sec. 5.3, and illustrated on Fig. 5.4, where the thermal evolution of the lowest lying singularities is shown. For rank-2 there are still complex singularities at $T > T_c$ but,

as already mentioned, they do not enter in a calculation of $\text{Im}(\Pi_M)$. Adopting the reasoning of [169], the imaginary part is developed only in the case of real poles. In the case when several real poles are present, as is e. g. the case in rank-1 (see Fig. 5.4), we take into account only those poles that continuously evolve to current quark mass. In the high temperature phase these will be equal to m_{qp}, where m_{qp} is the quark quasi-particle mass (i. e. the dynamical mass at zero momentum)

$$m_{qp} = \frac{m + b}{1 + c} , \tag{6.6}$$

These are just the states obtained in the local approximation to the model, with energies

$$E_{qp} = \sqrt{v_{qp}^2 \mathbf{p}^2 + m_{qp}^2} , \qquad v_{qp} = \frac{1 + a}{1 + c} . \tag{6.7}$$

For real poles we can apply the usual $i\epsilon$ prescription

$$\text{Im}[\Pi_M(-iP_0, 0)] = \frac{1}{2i} [\Pi_M(-i(P_0 + i\epsilon), 0) - \Pi_M(-i(P_0 - i\epsilon), 0)] , \tag{6.8}$$

where the bosonic Matsubara frequencies were analytically continued to $iv_m \to P_0$, and where the imaginary part will be calculated at $\mathbf{P} = 0$.

§ 6.2   CALCULATION OF THE IMAGINARY PART

For clarity, we study the case where $\mu = 0$, $\phi_3 = 0$. The integrand of the polarization function takes the following form

$$\pi_M(z) = \mathscr{F}_0^2(-z^2 + \mathbf{p}^2) \frac{K_M(-z^2, \mathbf{p}^2, -P_0^2, 0)}{\mathscr{D}(-z_+^2, \mathbf{p}^2)\mathscr{D}(-z_-^2, \mathbf{p}^2)} , \tag{6.9}$$

where $z_\pm = z \pm \frac{P_0}{2}$, and where we suppressed the $\mathbf{p}$ and P_0 dependence of π_M for brevity. Master formula for Matsubara summation is then

$$-2\pi i T \sum_{n=-\infty}^{\infty} \pi_M\left(i\omega_n - \frac{iv_m}{2}\right) = \int_{i\infty}^{-i\infty} dz\, \pi_M(z)$$
$$+ \int_{-i\infty+\delta}^{i\infty+\delta} dz\, \pi_M(z) n(z_+) - \int_{-i\infty-\delta}^{i\infty-\delta} dz\, \pi_M(z) n(-z_+) , \tag{6.10}$$

where on the left hand side we used translational invariance. It is crucial to observe that the integrals can be performed using the information on the singularity structure of the propagator in the whole complex plane. Although these

can be rather complicated, we shall assume that at some not too high temperature the only singularities are simple poles at m_{qp}. Then, the only singularities of the propagator that we need to worry about are $\pm E_{\mathrm{qp}}^{\pm}$, where E_{qp} is given by (6.7) and $E_{\mathrm{qp}}^{a} = E_{\mathrm{qp}} + aP_0/2$, with $a = \pm$.

Evaluating the first integral by closing the contour with a large semicircle in the region $\mathrm{Re}(z) > 0$ we obtain

$$\int_{i\infty}^{-i\infty} dz\, \pi_M(z) = 2\pi i \sum_{a=\pm} \mathrm{Res}(E_{\mathrm{qp}}^a)\,,$$

where

$$\mathrm{Res}(E_{\mathrm{qp}}^a) = -\frac{\mathscr{F}_0^2(-(E_{\mathrm{qp}}^a)^2 + \mathbf{p}^2)}{2E_{\mathrm{qp}}} \frac{K_M(-(E_{\mathrm{qp}}^a)^2,\mathbf{p}^2,-P_0^2,0)}{\mathscr{D}'(-E_{\mathrm{qp}}^2,\mathbf{p}^2)\mathscr{D}(-(E_{\mathrm{qp}}+aP_0)^2,\mathbf{p}^2)}\,. \tag{6.11}$$

Here we denoted

$$\mathscr{D}'(p^2) = \partial\mathscr{D}/\partial p^2\,. \tag{6.12}$$

Since the distribution function $n(z)$ has poles only on the imaginary axis, the evaluation of the remaining integrals is performed in a similar way. The only subtle step is acknowledging that $n(z \pm P_0) = n(z \pm i\nu_m) = n(z)$. For (6.10) we obtain

$$T\sum_{n=-\infty}^{\infty} \pi_M\left(i\omega_n - \frac{i\nu_m}{2}\right) = -[1 - 2n(E_{\mathrm{qp}})]\sum_{a=\pm}\mathrm{Res}(E_{\mathrm{qp}}^a)\,, \tag{6.13}$$

where we have used that $\mathrm{Res}(E_{\mathrm{qp}}^a) = -\mathrm{Res}(-E_{\mathrm{qp}}^a)$.

The imaginary part develops from the point where $E_{\mathrm{qp}} = P_0/2$. In order to obtain (6.8) it is sufficient to calculate

$$\mathrm{Res}(E_{\mathrm{qp}}^- + i\epsilon) - \mathrm{Res}(E_{\mathrm{qp}}^- - i\epsilon) = -\frac{\mathscr{F}_0^2(-(E_{\mathrm{qp}}^-)^2 + \mathbf{p}^2)}{2E_{\mathrm{qp}}}\frac{K_M(-(E_{\mathrm{qp}}^-)^2,\mathbf{p}^2,-P_0^2,0)}{\mathscr{D}'(-E_{\mathrm{qp}}^2,\mathbf{p}^2)}$$
$$\times\left[\frac{1}{\mathscr{D}(-(E_{\mathrm{qp}}-P_0+i\epsilon)^2,\mathbf{p}^2)} - \frac{1}{\mathscr{D}(-(E_{\mathrm{qp}}-P_0-i\epsilon)^2,\mathbf{p}^2)}\right]\,, \tag{6.14}$$

where we have used the fact that the only discontinuities arise from the denominator. By expanding around $E_{\mathrm{qp}} = P_0/2$,

$$\mathscr{D}(-(E_{\mathrm{qp}}-P_0-i\epsilon)^2,\mathbf{p}^2) \to 2P_0(E_{\mathrm{qp}}^- \mp i\epsilon)\mathscr{D}'(-P_0^2/4,\mathbf{p}^2)\,,$$

and using the Plemelj formula, the following discontinuity developes

$$\mathrm{Res}(E_{\mathrm{qp}}^- + i\epsilon) - \mathrm{Res}(E_{\mathrm{qp}}^- - i\epsilon) = \frac{\mathscr{F}_0^2(-(E_{\mathrm{qp}}^-)^2 + \mathbf{p}^2)}{4P_0 E_{\mathrm{qp}}}\times$$
$$\frac{K_M(-(E_{\mathrm{qp}}^-)^2,\mathbf{p}^2,-P_0^2,0)}{\mathscr{D}'(-E_{\mathrm{qp}}^2,\mathbf{p}^2)\mathscr{D}'(-P_0^2/4,\mathbf{p}^2)}(-2i\pi)\delta(E_{\mathrm{qp}}^-)\,. \tag{6.15}$$

Plugging (6.15) into (6.13) and back into the original formula (3.41) for the polarization function yields

$$\text{Im}[\Pi_M(-iP_0)] = \frac{d_q}{16\pi}[1 - 2n(P_0/2)]\sqrt{1 - \left(\frac{2m_{\text{qp}}}{P_0}\right)^2}$$

$$\times \mathscr{F}_0^2\left(\frac{P_0^2}{4} - m_{\text{qp}}^2\right)\frac{K_M\left(0, \frac{P_0^2}{4} - m_{\text{qp}}^2, -P_0^2, 0\right)}{\left[\mathscr{D}'\left(-\frac{P_0^2}{4}, \frac{P_0^2}{4} - m_{\text{qp}}^2\right)\right]^2}\theta\left(\frac{P_0}{2} - m_{\text{qp}}\right).$$

(6.16)

Introducing the chemical potential and the PL is now a simple matter. By generalizing $2n(z) \to n_+^{\Phi}(z) + n_-^{\Phi}(z)$ one arrives at

$$\text{Im}[\Pi_M(-iP_0, 0)] = \frac{d_q}{16\pi}\left[1 - n_+^{\Phi}(P_0/2) - n_-^{\Phi}(P_0/2))\right]\sqrt{1 - \left(\frac{2m_{\text{qp}}}{P_0}\right)^2}$$

$$\times \mathscr{F}_0^2\left(\frac{P_0^2}{4} - m_{\text{qp}}^2\right)\frac{K_M\left(0, \frac{P_0^2}{4} - m_{\text{qp}}^2, -P_0^2, 0\right)}{\left[\mathscr{D}'\left(-\frac{P_0^2}{4}, \frac{P_0^2}{4} - m_{\text{qp}}^2\right)\right]^2}\theta\left(\frac{P_0}{2} - m_{\text{qp}}\right).$$

(6.17)

In order to obtain $\text{Im}(\Pi_M)$ for ILM follows by making the replacement (3.45) by taking into account that the quasi-particle states are on-shell

$$\mathscr{F}_0^2\left(\frac{P_0^2}{4} - m_{\text{qp}}^2\right) \to r^4(-m_{\text{qp}}^2).$$

(6.18)

Notice that as the quasi-particle mass goes to the current quark mass, in the ILM model this prefactor $r^4(-m_{\text{qp}}^2) \to 1$. On the other hand, in sets A - C, ignoring the small current mass, we will still be left with $\mathscr{F}_0^2\left(P_0^2/4\right)$. Thus, if the meson mass grows with temperature (as will be the case after the chiral restoration) since the regulators are decreasing functions of momenta, it appears that the imaginary part can in this case drastically decrease.

It is interesting to discuss the local limit, where we obtain

$$K_M \simeq \frac{P_0^2}{4}(1+c)^2 + \left(\frac{P_0^2}{4} - m_{\text{qp}}^2\right)(1+a)^2 \pm m_{\text{qp}}^2, \qquad \mathscr{D}' \simeq (1+c)^2.$$

(6.19)

	r-1 Gauss	r-2 Gauss	r-2 Lorentz	ILM
b [MeV]	424	429	442	284
b_c [MeV]	317	557	m	391
T_{cont} [MeV]	208	0	0	0
T^{π}_{Mott} [MeV]	213	209	216	204
T^{σ}_{Mott} [MeV]	212	208	214	202

Table 6.1: The table collects vacuum values of the mass gaps b, the critical values b_c at which the physical continuum moves from the real axes, together with the respective temperature T_{cont} where this happens, for all pertinent models. We also provide the Mott temperatures for π and σ mesons. Note that for rank-1 Gauss model the physical mass gap is overcritical, while for rank-2 Gauss it is undercritical. For rank-2 Lorentz, the imaginary part develops continuously from the current quark mass m. Therefore, the continuum is present in rank-2 Gauss, rank-2 Lorentz as well as in the ILM already at $T = 0$.

Furthemore, by taking $a, c \rightarrow 0$, we reproduce the local NJL result [166]

$$
\text{Im}[\Pi_M(-iP_0, 0)] \rightarrow \frac{d_q}{16\pi} \left[1 - n^{\Phi}_+(P_0/2) - n^{\Phi}_-(P_0/2) \right]
$$
$$
\times \sqrt{1 - \left(\frac{2m_{\text{qp}}}{P_0} \right)^2} \left[\frac{P_0^2}{4} - m_{\text{qp}}^2 \pm m_{\text{qp}}^2 \right] \theta \left(\frac{P_0}{2} - m_{\text{qp}} \right).
\tag{6.20}
$$

On the other hand, by using (6.19), in the chiral limit we obtain

$$
\frac{K_M}{(\mathscr{D}')^2} \rightarrow \frac{P_0^2}{4} \frac{1}{(1+c)^2} \left(1 + v_{\text{qp}}^2 \right).
\tag{6.21}
$$

This result shows that introducing wave function renormalization can significantly reduce the imaginary part. In addition, if LSB by the medium is acknowledged, owing to the fact that $v_{\text{qp}} < 1$, the imaginary will be even more reduced.

§ 6.3 DISCUSSION OF RESULTS

In local NJL, see e. g. [166] and 3D nlNJL studies [76], it is shown that $g_{M\bar{q}q}$ is a slowly reducing function of the temperature. Hence, to get an idea on the meson width also in a 4D nlPNJL setup, we make a rough approximation by replacing the thermal dependence of the quark-meson coupling $g_{M\bar{q}q}$ by its vacuum value. With this our scheme of extracting the meson widths is complete.

On Fig. 6.2 we plot the sigma and pion spatial masses, as calculated from (6.52). Besides the spatial meson masses, it is instructive to show the "continuum" states defined by $2m_{qp}$, where m_{qp} is given by (6.6). Strictly speaking, these states need not be present as actual singularities of the quark propagator up to some high temperature, as was previously discussed.

Returning to our canonical example in rank-1 Gauss, the continuum states are developed only after the temperature where $b = b_c$ (see the discussion in Sec. 5.3). For finite current quark mass, this happens at $T_{cont} = 208$ MeV. Now, from Fig. 6.2 we observe that the Mott temperatures for both π and σ are *higher*, *i.e.*, $T_{Mott}^{\pi} = 213$ MeV, $T_{Mott}^{\sigma} = 212$ MeV, thus a posteriori justifying our assumptions. This is also the situation in all other models, i. e. rank-2 Gauss rank-2 Lorentz and ILM. The complete set of values of Mott and continuum temperatures is collected in Table 6.1.

If we proceed to extrapolate the meaning of m_{qp} also to low temperatures, one could argue a seemingly generic property of the nl-NJL model. In contrast to its local version, the σ meson is bound in the vacuum and at low temperatures, as already observed, *e.g.*, in [76] and [175].

We see that introducing wave function renormalization lowers the continuum according to the Eq. (6.6). Also the σ meson mass is reduced, which one would naively agree to from the local setting where $m_\sigma \simeq 2m_{qp}$. The meson screening masses are joining at the chiral restoration temperature, and tend to rise steeply beyond that point, approaching 1 GeV already around $T \simeq 300$ MeV, with the steepest rise for set B. The results for the ILM model single out because of its small mass gap, which in turn leads to a smoother transition into the chirally restored phase. As a further consequence, the sigma meson mass is almost twice reduced in the vacuum.

We calculate the widths by using spatial masses in Eq. (6.4), and in Eq. (6.17) by replacing $P_0 \to m_M^{spat}$, instead of the more accepted m_M^{pole}. This certainly introduces an error in our calculation, but since the qualitative behavior of both spatial and dynamical masses is the same it will nevertheless provide a useful study. Since the Mott transition happens rather close to the chiral transition, the pion and the sigma meson are approximately degenerate, so it is sufficient to focus only on the pion. For the quark-meson couplings we calculate their vacuum values from Eq. (6.5), providing the values collected in Table 6.2.

Fig. 6.3 shows the main result of this Section. For rank-1 and rank-2 models, the widths follow a generic pattern. In the low temperature region, we find a steep rise, mostly due to the meson mass itself: see e. g. the local and the chiral limit (6.21), where one has a quadratic dependence on the meson mass in the imaginary part of the polarization loop. But, since in the non-local models, the complete imaginary part, and therefore the width is multiplied by the reg-
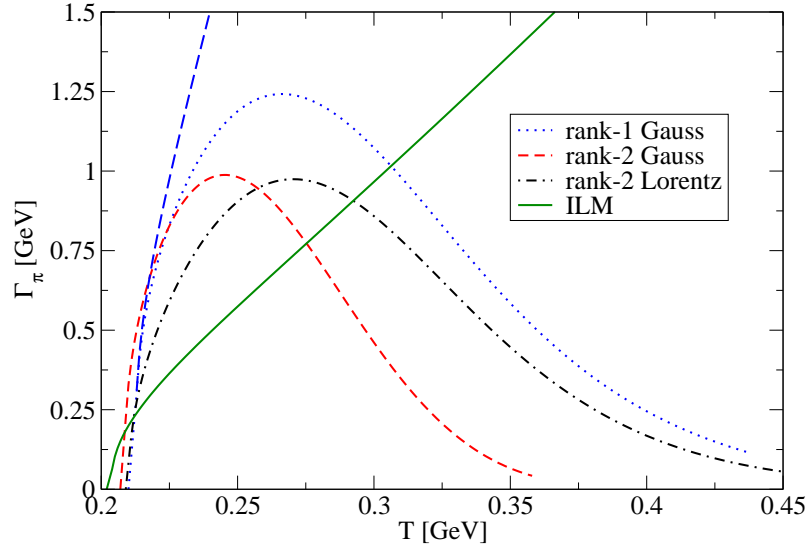
Figure 6.3: The figure displays the approximate pion widths calculated from Eqs. (6.4) for all pertinent models.

ulator, it is this factor that dictates the high temperature behavior. Namely, as $\mathscr{F}_0(p^2)$ is a rapidly decreasing function of momenta (see Sec. 3.6), and because for sets rank-1 and rank-2 models, the argument is a rising function of the temperature, it eventually overwhelms the quadratic dependence, and provide a characteristic decrease in the width. Therefore, in the high temperature phase, the width drops to zero. Of course, this behaviour is somewhat exaggerated due to the fact that the screening masses steeply rise with the temperature, making the decline of Γ_π more dramatic. Nevertheless, this behaviour should be considered as generic to this class of models. In that regard, let us also comment on the fact that, as announced previously, the width in overall gets somewhat reduced when the WFR channel is introduced. This is demonstrated by the red and black curves in Fig. 6.3.

In Ref. [176] we have attempted a calculation where the pre-factor

$$\mathscr{F}_0^2 \left(\frac{P_0^2}{4} - m_{\text{qp}}^2 \right) \tag{6.22}$$

from the imaginary part of the polarization loop (6.17) was omitted by hand. Indeed in that case we have obtained monotonous widths, confirming that it is this prefactor that makes the width rapidly decrease in the high temperature regime. This is shown on Fig. 6.3, where we have taken the simplest rank-1

Gauss model as an example. The width is calculated by the same formula (6.4), but omitting (6.22) we obtain the long-dashed blue curve.

–	r1-Gauss	r-2 Gauss	r-2 Lorentz	ILM
$g_{\pi\bar{q}q}$	4.62	5.74	4.74	2.47

Table 6.2: Quark-pion couplings at $T = 0$.

The result we obtain for the ILM calculation of the width is completely different: due to the fact that the form-factor in this case has a different momentum partitioning in the polarization loop, see Eq. (3.45) and Eq. (6.18), there is no dependence on the meson mass in the regulator, and its effect at high temperatures is highly suppressed. This results in a monotonous rise of Γ_π, shown by the green curve, in the low, as well as in the high temperature region.

To conclude, we have calculated the spatial meson masses, and in addition presented a detailed derivation and a discussion of the widths in the covariant version of nonlocal models. We emphasize that the latter was completely absent from the literature, although the model itself is present in the community for more than two decades. The basic problem is the covariance of the approach. More precisely, the fact that it is defined in Euclidean space, makes "Minkowski-quantities" like the dynamical meson masses and widths, difficult to obtain. Since we do not claim that we have solved this hard problem[1], our results bear a qualitative significance. Thus, given the roughness of our approximations we can state the following. First, the meson widths, as calculated in our approximation are not strongly affected by the shape of the regulator that is used. Second, introducing WFR and LSB reduces the widths to some extent, and third; the most interesting result comes from investigating the different ways non-local interactions can be introduced. For rank-1 and rank-2 models, the widths rapidly decline at high temperatures. On the other hand, if the non-locality is introduced via ILM the width is a rising function of temperature. It should be noted that the latter result is also similar to what is seen in local [166], or 3D non-local [76] NJL studies.

---

[1] A first step in solving it would be to map the analytic structure of the quark propagator in the complex plane. This is a highly non-trivial task, addressed only very recently [150, 151, 152].

Concluding remarks

As QCD is nonperturbative at low energies, we have studied its properties via effective models, incorporating quarks (and gluons) as active degrees of freedom.

For the $\gamma^* \to \pi^+ \pi^0 \pi^-$ process we have provided an alternative scenario for the explanation of the only existing experimental point so far by incorporating the effect of vector mesons. The relevant amplitude was built up from quark triangle and box loop. Moreover, we have predicted the behavior of the form-factor for the momentum range explored at ongoing and future experiments at CEBAF and COMPASS.

$\eta - \eta'$ complex is a fascinating arena to study symmetries of QCD, in particular their thermal appearance. Due to the pseudoscalar $\eta - \eta'$ states being strongly influenced by the gluonic content of the theory, we obtain a unique insight into a relation between the chiral and the $U(1)_A$ symmetry, at zero and finite temperature.

In order to explain the analysis of experimental data on η' multiplicity on heavy ion collisions, we have found that a modification of the Witten-Veneziano relation was necessary. We have understood that this modification entails a connection between the restoration of $U(1)_A$ and the chiral symmetry of QCD. In this scenario, the mass of the η' particle was reduced in the chirally restored phase.

A thermodynamical instability was identified in a general class of covariant quark models at one-loop level. We have partially resolved this problem already at the mean field level: by coupling the quarks to the Polyakov loop. With the Polyakov loop as an essential element, we proceed to study thermodynamics in more realistic models, incorporating also wave function renormalization. We have made a mean field study of the $T - \mu$ phase diagram and concluded that the critical-point is only slightly affected by the medium induced Lorentz symmetry breaking.

The fate of hadronic matter in extreme environments, e.g., in the interior of compact stars, or in the early universe, remains one of the most interesting unanswered questions today. Experiments at RHIC and LHC established the

existence of quark-gluon plasma in the high temperature, low density regime. While there are many theoretical predictions for the QCD phase diagram in the regime of high densities as well, one awaits for upcoming heavy-ion experiments at NICA and FAIR to steer the theoretical community in the right direction. So far most of the calculations are performed in the mean field, where hadrons provide only a uniform background. But, from lattice studies of the Equation of State, or from the Hadron Resonance Gas picture, it is clear that they should be dynamically involved.

As a first step beyond the mean field we have studied meson dissociation in two flavor separable DSE model. We have been able to map the structure of the polarization loop in the complex energy plane. Our results show that while separable models yield a width that is dropping to zero in the high temperature regime, the Instanton Liquid Model was able to provide a more satisfactory scenario. Such an unexpected sensitivity to model details shows that a more appropriate way to study bound states, resonances and the Mott transition in QCD might be by using a model defined in the Coulomb gauge.

Prošireni sažetak

Kvantna kromodinamika (QCD, od engl. Quantum Chromodynamics) je baždarna $SU(3)$ kvantna baždarna teorija kvarkova i gluona. Eksplicitno, klasični Lagranžijan za N_f okusa je dan sa

$$\mathscr{L} = -\sum_{i=1}^{N_f} \bar{q}(\gamma^\mu \mathscr{D}_\mu + m_i)q - \frac{1}{2}\mathrm{Tr}(F^{\mu\nu}F_{\mu\nu}) + \frac{\theta}{16\pi^2}\mathrm{Tr}(\tilde{F}^{\mu\nu}F_{\mu\nu})\,, \tag{6.23}$$

gdje su q kvarkovska te $F_{\mu\nu}$ baždarna polja. Interakcija se dobiva iz kovarijantne derivacije

$$\mathscr{D}_\mu = \partial_\mu + ig A_\mu \tag{6.24}$$

ali isto iz ne-Abelove strukture teorije

$$F_{\mu\nu} = \partial_\mu A_\nu - \partial_\nu A_\mu + g[A_\mu, A_\nu]\,, \tag{6.25}$$

gdje A_μ predstavlja matricu u $SU(3)$ prostoru. Parametri teorije su kvarkovske mase m_i, baždarno vezanje g te kut θ.

Na niskim energija kvarkovi i gluoni postoje samo u stanjima bez boje: mezonima i barionima. Činjenica da do sada nije primjećen slobodan kvark ili gluon u detektoru je poznata kao *zatočenje*. O fizikalnoj manifestaciji neperturbativne fizike svjedoči lomljenje približne $SU(N_f)_L \times SU(N_f)_R$ kiralne simetrije QCD-a.

Izrazita nelinearnost teorije u infracrvenom području nalaže primjenu neperturbativnih tehnika pri računanju observabla. To su QCD na rešetci, funkcionalne metode i efektivni modeli. U ovom radu bavimo se efektivnim modelima.

Na kvarkovskoj razini, Higgsov mehanizam Standardnog Modela daje u i d kvarkovima samo malu *strujnu* masu reda ~ 5 MeV-a. Konstituentna kvarkovska masa generirana dinamičkim lomljenjem kiralne simetrije se tada može definirati kao $\sim m_N/3$ ili $m_\rho/2$.

QCD fazni dijagram izražava se preko temperature T i barionskog kemijskog potencijala μ_B, vidi sliku Fig. 6.4. Na niskim T i $\mu_B = 0$ mezoni igraju
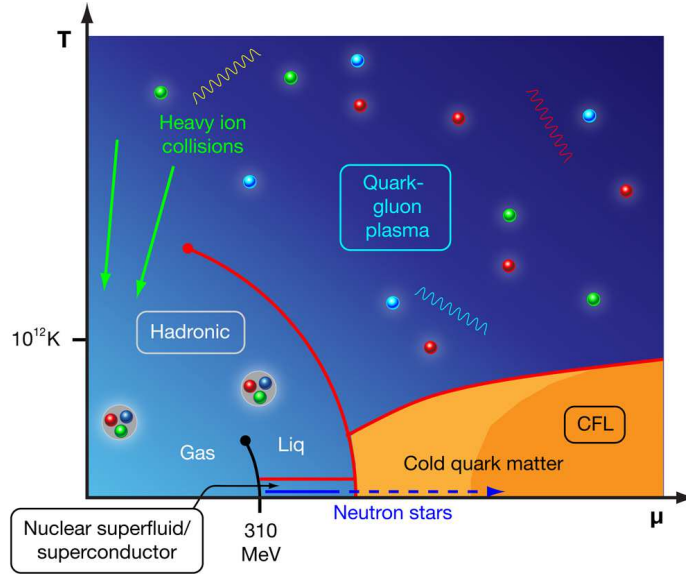
Figure 6.4: Ilustracija faznog dijagrama QCD-a, A. Stonebraker.

ulogu aktivnih stupnjeva slobode. U području $T = 0$ te niskog μ_B dominira nuklearna materija. Pretpostavlja se da je, zbog svojstva asimptotske slobode, osnovno stanje na visokim T i/ili visokim μ_B plazma kvarkova i gluona.

Za predvidjeti QCD fazni dijagram koriste se neperturvbativne tehnike kao što je račun na rešetci te funkcionalne metode. Za opisati QCD fazni dijagram koristi se mnoštvo modela, svaki gdje svaki od njih pažljivo opisuje pojedinu fazu, pomoću stupnjeva slobode koji u toj fazi dominiraju. Isti modeli se potom koriste da da bi predvidjeli moguće granice među fazama. Za detaljni pregled može se konzultirati [21].

Kemijska slika otapanja hadrona pruža intuitivan opis faznog prijelaza. Mogućnost opisivanja faznog prijelaza na taj način zahtijeva mikroskopsko razumijevanje disocijacije hadrona, što pak zahtijeva razumijevanje njihove formacije, što se konačno svodi na razumijevanje zatočenja. Slijedi da se, unutar kemijske slike, na ovaj način može razumijeti potreba za opisom hadrona preko vezanih stanja.

AKSIJALNA ANOMALIJA I $\gamma^* \to 3\pi$ PROCES

U fizici elementarnih čestica postoje procesi, koji se ne bi dešavali, ili bili iznimno potisnuti, u odsustvu kvantnih korekcija. Daleko najpoznatiji primjer

takvog procesa je $\pi^0 \to \gamma\gamma$. Naime, on je u potpunosti određen takozvanom Adler-Bell-Jackiw (ABJ) kvantnom anomalijom [32, 33]. Za teoriju kao što je bezmasena kvantna elektrodinamika Adler i suradnici pronašli su da aksijalna struja $J_5^\mu = \bar\psi \gamma^\mu \gamma_5 \psi$ nije sačuvana

$$\partial_\mu J_5^\mu = 2 \frac{e^2}{16\pi^2} \tilde{F}_{\mu\nu} F^{\mu\nu} \, . \tag{6.26}$$

Proces $\gamma^* \to 3\pi$ su prvi analizirali Aviv i Zee [36]. Pronašli su da u niskoenergetskom i kiralnom limesu prikladan zapis amplitude za ovaj proces je dan kao

$$A_\gamma^{3\pi} = \frac{e \, N_c}{12\pi^2 f_\pi^3} = 9.72 \pm 0.09 \, \text{GeV}^{-3} \, . \tag{6.27}$$

Jedina eksperimentalno mjerena vrijednost ovog procesa je dana '86 mjerenjem na Serpkhuovu [37]

$$F_\gamma^{3\pi}(\text{expt}) = 12.9 \pm 0.9 \pm 0.5 \, \text{GeV}^{-3} \, . \tag{6.28}$$

Jasno je postojanje diskrepance između ovog i teorijskog rezultata (6.27).

Za račun faktora oblika procesa koristimo model konstituentne kvarkovske petlje (CQL, od engl. constituent quark loop), vezanjem kvarkovskih struja na pionska polja [47], [48, 49, 50, 51], [46, 52]. U ovom problemu također razmatramo situaciju u kojoj pionski par može izaći iz procesa kroz raspad vektorske rezonance.

Relevantni članovi efektivnog Lagranžijana dani su s

$$\mathcal{L}_{\text{eff}} = -\bar{q}(\slashed{\partial} + M_q + \dots)q + \mathcal{L}_{\text{int}} + \mathcal{L}_{\text{VMD2}} + \mathcal{L}_{\rho\pi\pi} \, , \tag{6.29}$$

gdje je $q = (u, d)^T$, te M_q konstituentna masa.

Član $\mathcal{L}_{\text{int}}$ je dan s

$$\mathcal{L}_{\text{int}} = -2i g_{\pi\bar{q}q} \bar{q} \gamma_5 \pi q + i g_{\rho\bar{q}q} \bar{q} \gamma^\mu \rho_\mu q \, , \tag{6.30}$$

dok

$$\mathcal{L}_{\rho\pi\pi} = 2i G_{\rho\pi\pi} \text{Tr}([\pi, (\partial_\mu \pi)] \rho^\mu) \, , \tag{6.31}$$

Elektromagnetizam se uključuje koristeći model dominacije vektorskih mezona (VMD, od engl. vector meson dominance) [56]

$$\mathcal{L}_{\text{VMD2}} = \frac{e m_\rho^2}{g_{\rho\gamma}} A^\mu \left(\rho_\mu^0 + \frac{1}{3} \omega_\mu \right) \, . \tag{6.32}$$

Dani pristup nazivamo CQL-VMD model.

Feynmanova pravila daju amplitudu

$$\mathcal{M}_\gamma^{3\pi} = \epsilon_\mu(\mathbf{q},\sigma)\, p_{1\nu}\, p_{2\rho}\, p_{3\lambda}\, \epsilon^{\mu\nu\rho\lambda}\, F_\gamma^{3\pi}(p_1,p_2,p_3)\,. \tag{6.33}$$

Četverokutni i trokutni doprinos faktoru oblika su

$$F_\Diamond(p_1,p_2,p_3) = \frac{1}{3}\frac{eN_c}{6\pi^2}\frac{g_{\pi\bar{q}q}^3}{M_q^3}\frac{m_\rho^2}{m_\rho^2+q^2}$$
$$\times \left[\widetilde{D}_0(p_1,p_2,p_3) + \widetilde{D}_0(p_1,p_3,p_2) + \widetilde{D}_0(p_2,p_1,p_3)\right],\quad (6.34)$$

$$F_\triangle^{\mathrm{res}}(p_1,p_2,p_3) = \frac{1}{2}\frac{eN_c}{6\pi^2}\frac{g_{\pi\bar{q}q}}{M_q}\frac{g_{\rho\bar{q}q}^2}{m_\rho^2}\frac{m_\rho^2}{m_\rho^2+q^2}$$
$$\times \left[\frac{m_\rho^2}{m_\rho^2-s}\widetilde{C}_0(p_1,p_2) + \frac{m_\rho^2}{m_\rho^2-t}\widetilde{C}_0(p_2,p_3) + \frac{m_\rho^2}{m_\rho^2-u}\widetilde{C}_0(p_1,p_3)\right].\quad (6.35)$$

Uz izmjenu trokutnog doprinosa ne-rezonantnom Weinberg-Tmmozawa interakcijom ukupan trokutni doprinos $F_\triangle = F_\triangle^{\mathrm{res}} + F_\triangle^{\mathrm{WT}}$ amplitudi glasi

$$F_\triangle(p_1,p_2,p_3) = \frac{1}{2}\frac{eN_c}{6\pi^2}\frac{g_{\pi\bar{q}q}}{M_q}\frac{g_{\rho\bar{q}q}^2}{m_\rho^2}\frac{m_\rho^2}{m_\rho^2+q^2}$$
$$\times \left[\frac{s}{m_\rho^2-s}\widetilde{C}_0(p_1,p_2) + \frac{t}{m_\rho^2-t}\widetilde{C}_0(p_2,p_3) + \frac{u}{m_\rho^2-u}\widetilde{C}_0(p_1,p_3)\right].\quad (6.36)$$

Time ukupni faktor oblika dan s $F_\gamma^{3\pi} = F_\triangle + F_\Diamond$ poštuje Wess-Zumino-Witten ograničenje.

Slike 6.5, 6.6 prikazuju normalizirani faktor oblika $\widetilde{F}_\gamma^{3\pi} = F_\gamma^{3\pi}/A_\gamma^{3\pi}$. Za konstitentne mase u i d kvarka koristimo $M_q \approx m_p/3 \approx 330$ MeV, ali također dozvoljavamo da se njena vrijednost može i nešto promijeniti.

Usporedba faktora oblika izračunatih u CQL i CQL-VMD pristupu pokazuje da prisustvo rezonance povećava njenu vrijednost na neiščezavajućim impulsima. Drugo, povećanjem M_q smanjuje se vrijednost $\widetilde{F}^{3\pi}$ na određenom impulsu, jednostavno zbog toga jer je to jedina masena skala u petlji.

Slike demonstriraju da CQL model nije kompatibilan s (skromnim) eksperimentalnim podacima, ali proširenje modela s vektorskim mezonima (CQL–VMD), je. Unatoč tome, alternativni pristup koji koristi kiralnu perturbacijsku teoriju također zadovoljava eksperimentalno ograničenje jednom kada se korekcije pionskih petlji, te elektromagnetske korekcije pažljivo uzmu u obzir [39]. Stoga, bar u kinematičkom području kojeg pokriva Serpukhov moguća su alternativna objašnjenja, bez uključenja vektorskih mezona.
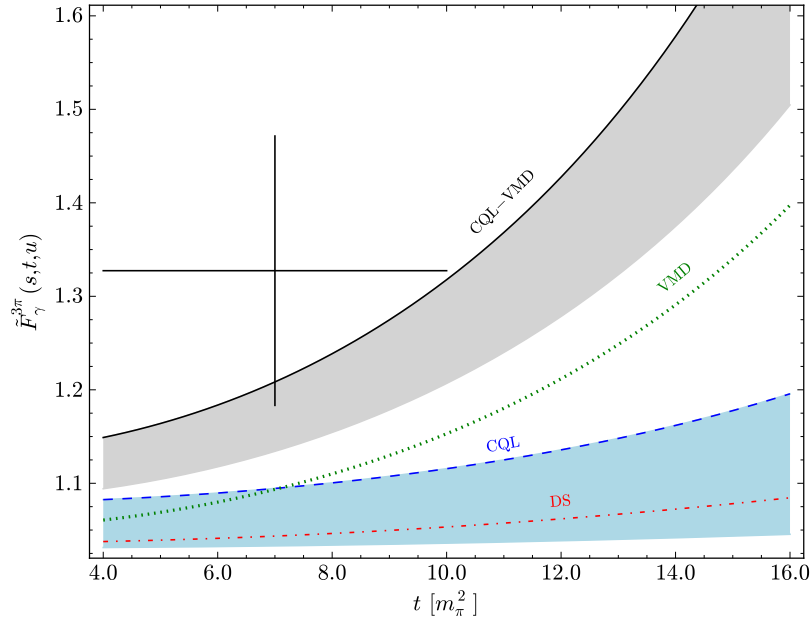
Figure 6.5: Faktori oblika $\tilde{F}_\gamma^{3\pi}(s,t,u)$ raznih pristupa su dani preko Mandelstamove varijable t. Gornje zasijenjeno područje pokriva rezultate CQL–VMD pristupa za konstituentne mase između $M_q = 360$ MeV (gornji rub) i $M_q = 565.69$ MeV što je skala DSE pristupa iz Ref. [71] (donji rub). Donje zasijenjeno područje pokriva rezultate CQL modela [46] za isti interval M_q. Usporedba je dana s rezultatima "modificiranog" VMD-a [61, 70] (zelena točkasta krivulja) i DS pristupa [71] (crvena, crtkano-točkasta krivulja). Eksperimentalna točka s Serpkhuova [37] je ustvari prosječna vrijednost dobivena iz ukupnog udarnog presjeka.

U eksperimentu COMPASS, gdje će viši impulsi biti istraženi, očekuje se da vektorski mezoni mogu igrati bitnu ulogu. Eksperimenti koji istražuju anomalne procese za teže čestice kao što su $\eta(\eta') \to 2\pi\gamma$ raspadi [54, 55] odvijaju se u režimu vektorskih rezonanci, čime $\gamma^* \to 3\pi$ koji uključuje vektorske mezone također postaje koristan.

η, η' U MEDIJU I WITTEN-VENEZIANO RELACIJA

Osim uobičajene kiralne grupe $SU(N_f)_L \times SU(N_f)_R$, QCD s bezmasenim kvarkovima je invarijantan i na $U(1)_A$ simetriju, gdje su sva kvarkovska polja pomnožena zajedničkim faktorom $e^{i\alpha\gamma_5}$. Najlakši pseudoskalarni $SU(3)$ singlet je η'
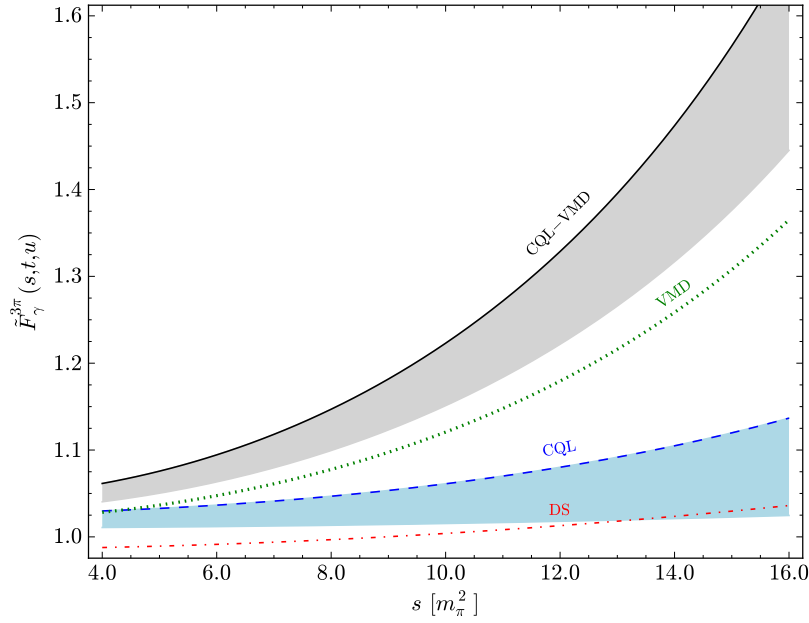
Figure 6.6: Isto kao i u prethodnoj slici 6.5, ali za CEBAF kinematiku, gdje dva izlazna piona na ljusci mase su π^+ and π^0. Faktor oblika je dan kao funkcija Mandelstamove varijable s. Za π^-, koji nije na ljusci mase, koristimo $p_3^2 = m_\pi^2$. Također fiksiramo $t = -m_\pi^2$.

čestica. Ali sa svojom masom od otprilike 1 GeV, jednostavno je pretežak da bi se razmatrao kao Goldstoneov bozon sponatno slomljene $U(1)_A$ [100].

Na kvantnoj razini $U(1)_A$ je slomljena eksplicitno, s obzirom na to da korespondirajuća Nötherina struja $J_{5,0}^\mu = \bar{q} t_0 \gamma^\mu \gamma_5 q$ nije očuvana

$$\partial_\mu J_{5,0}^\mu = 2N_f \omega(x), \quad \omega(x) = \frac{g^2}{16\pi^2} \mathrm{Tr}(\tilde{F}_{\mu\nu} F^{\mu\nu}). \tag{6.37}$$

Witten-Veneziano relacija (WVR) [103, 104] je nisko-energetski teorem dobiven u limesu velikog N_c, koji kaže da dodatna masa singletne komponente η_0 pseudoskalarnog polja η' dolazi od infracrvenih korelacija gustoće topološkog naboja $\omega(x)$

$$M_{\eta'}^2 + M_\eta^2 - 2M_K^2 = \frac{2N_f}{f_\pi^2} \chi_{\mathrm{YM}}, \tag{6.38}$$

gdje je χ_{YM} topološka susceptibilnost Yang-Mills teorije

$$\chi_{\mathrm{YM}} = \int d^4 x \langle 0 | T(\omega(x)\omega(0)) | 0 \rangle. \tag{6.39}$$

Prisutnost instantona u QCD vakuumu generira konačnu topološku susceptibilnost. S obzirom na to da pojedinačna instantonska konfiguracija daje amplitudu tuneliranja koja ide kao $e^{-S_E} \sim e^{-2\pi/\alpha_s}$ u perturbativnom režimu gdje je α_s mali, očekuje se da je tuneliranje potisnuto. Stoga, također se očekuje da su u vrućem i gustom mediju efekti instantona također mali te da je $U(1)_A$ simetrija restaurirana.

Već '93 Shuryak ukazuje da bi η' na malim impulsima trebala biti izrazito producirana [107]. Recentna teorijska analiza dipionskog spektra u $\eta' \to \eta\pi\pi$ kanalu od strane Csörgő i suradnika [112, 113] tvrdi da je to uistinu slučaj, vodeći time na indirektno predviđanje redukcije mase η' za bar 200 MeV-a u mediju.

Konkretno govoreći, eksperimentalni rezultat [112, 113] je u direktnom konfliktu s WVR. χ_{YM} je vezana na topološku susceptibilnost QCD-a preko Leutwyler-Smilga relacije [114]

$$\chi_{\text{YM}} = \frac{\chi}{1 + \chi \frac{N_f}{m\langle \bar{q}q \rangle_0}} \, , \tag{6.40}$$

Od koristi će biti i Di Vecchia-Veneziano relacija [115]

$$\chi = -\frac{m\langle \bar{q}q \rangle_0}{N_f} + \mathscr{C}_m \, , \tag{6.41}$$

koja ukazuje da je termalna ovisnost χ u prvoj aproksimaciji upravljana kiralnim kondenzatom. Kao posljedica, kiralna i $U(1)_A$ restauracija bi trebale biti vezane.

U slijedećem koraku zamijenjujemo χ_{YM} u VWR sa desnom stranom (6.40), što zbog jasnoće označamo $\tilde{\chi}$. Za $T > 0$ koristimo $\tilde{\chi}$ umjesto χ_{YM}, čime modificiramo WVR. Ovdje ostajemo pri scenariju da je u $U(1)_A$ prijelaz u potpunosti određen kiralnim (iako to ne mora biti nužno tako), te predlažemo slijedeću formu za nepoznatu konstantu C_m

$$\mathscr{C}_m(T) = \mathscr{C}_m(0) \left[\frac{\langle \bar{q}q \rangle_0(T)}{\langle \bar{q}q \rangle_0(0)} \right]^{\delta} \, . \tag{6.42}$$

U konačnici, termalno ponašanje $\tilde{\chi}$ je [116, 117, 118]

$$\tilde{\chi}(T) = \frac{m\langle \bar{q}q \rangle_0(T)}{N_f} \left(1 - \frac{m\langle \bar{q}q \rangle_0(T)}{N_f \mathscr{C}_m(0)} \left[\frac{\langle \bar{q}q \rangle_0(0)}{\langle \bar{q}q \rangle_0(T)} \right]^{\delta} \right) \, . \tag{6.43}$$

Pri računu mezonskih masa i konstantni raspada slijedimo [119] koristeći pristup preko vezanih stanja. Račun u mediju pojednostavljen je računanjem
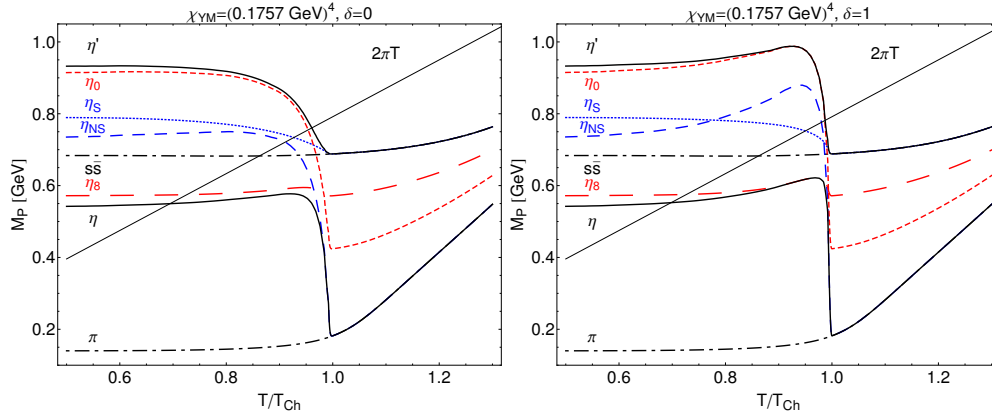
Figure 6.7: Relativna temperaturna ovisnost, on T/T_{Ch}, masa pseudoskalarnih mezona za dva slučaja $\widetilde{\chi}(T)$, s $\delta = 0$ (lijeva slika) te $\delta = 1$ (desna slika). Pravac $2\pi T$ je dvostruka osnovna Matsubarina frekvencija.

sa separabilnom interakcijom [79, 120] za gluonski propagator. Sve tražene veličine izračunate su u DSE-BSE pristupu [121].

Slika 6.7 predstavlja naš glavni rezultat [116, 117, 118]. Mase su dane kao funkcija temperature, koja je normirana na temperaturu kiralne restauracije T_{Ch}. Kao prvo, vidimo da na $T = 0$ η i η' su skoro degenerirani s nefizikalnim η_8 i η_0 stanjima, respektivno. Točnije, kut miješanja između ovih stanja je mali, što je ujedno i razlog zašto anomalija ne čini i η stanje teškim.

Najznačajniji rezultat je znatan pad u masi η' čestice, u skladu s analizom Csörgő i suradnika.

TERMODINAMIKA KOVARIJANTNIH KVARKOVSKIH MODELA

U ovom odjeljku usredotočiti ćemo se na QCD fazni dijagram i termodinamičke veličine kao što su pritisak odnosno entropija u kvarkovskim modelima koji koriste Lorentz kovarijantne efektivne gluonske interakcije. Za fazni dijagram, utjecaj lomljenja Lorentzove simetrije uzrokovane medijem na kritičnu točku će biti istražen.

Termodinamika broji stanja. Istražujemo koje su termodinamičke posljedice uzimanja u obzir stanja iz kompleksne ravnine kvarkovskog propagatora. Preciznije, interesira nas niskotemperaturno ponašanje takve teorije, te mehanizam
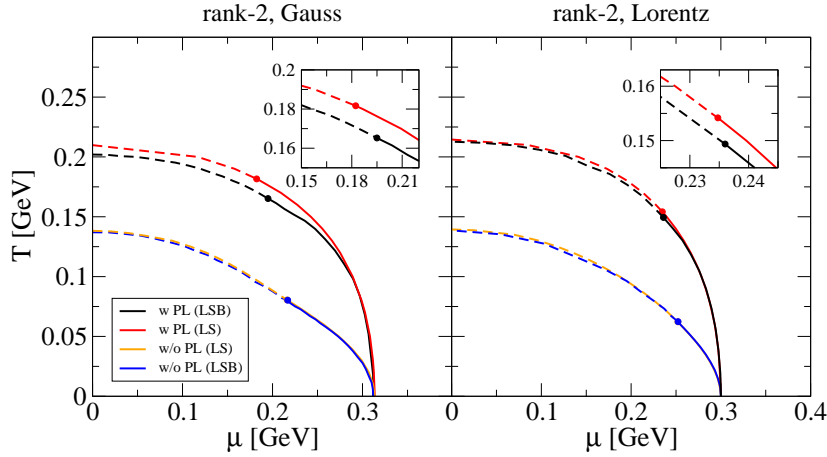
Figure 6.8: Fazni dijagram za modele ranga 2. Donji par krivulja na obje slike prikazuje kiralni prijelaz bez Polyakovljeve petlje, dok gornji par krivulja prikazuje fazni dijagram s Polyakovljevom petljom. U donjem paru, plava krivulja daje fazni dijagram uz umjetno nametnutu Lorentzovu simetriju, dok žuta krivulja uzima u obzir da je Lorentzova simetrija slomljena u mediju. Za gornji par, gornja, crvena krivulja je izračunata u aproksimaciji Lorentzove simetrije, dok je crna krivulja dana za slučaj kada je Lorentzova simetrija slomljena u mediju.

za uspostavljanje kiralnog kvarkovskog singulariteta na dovoljno visokim temperaturama.

Računajući vrh kiralne susceptibilnosti iscrtavamo liniju u $T - \mu$ ravnini koja odvaja kiralno slomljenu te kiralno simetričnu fazu. Za modele ranga 2 fazni dijagam je prikazan na slici 6.8. U računima koristili smo Gaussijanske, odnosno Lorentzijanske form faktore ranga 2. Koristimo logaritamski potencijal za Polyakovljevu petlju. Primjećujemo da uzimanje u obzir lomljenja Lorentzove simetrije u mediju daje mali pomak u poziciji kritične točke. Fizikalno, srednja polja vektorskog doprinosa kvarkovskom propagatoru se ne miješaju znatno s skalarnim doprinosom. Drugim riječima, kako ta polja nisu osjetljiva na kiralne transformacije, promjena u kritičnoj točci je mala.

Nadalje diskutiramo termodinamičke veličine kao što je pritisak u slučaju kad kvarkovski propagator ima kompleksno konjugirane polove. Promatramo najjednostavniju situaciju u kojoj propagator ima niz od moguće beskonačno kompleksno konjugiranih masenih polova prvog reda. U literaturi postoji mnoštvo primjera gdje se sreće upravo takva situacija [128, 134, 135, 136].

Početna točka je dvočestično ireducibilni termodinamički potencijal, gdje

se usredotočujemo na kinetički doprinos

$$\Omega_{\text{kin}} = -\frac{d_q}{2}T\sum_{n=-\infty}^{+\infty}\int\frac{d^3p}{(2\pi)^3}\log\left[\mathbf{p}^2A^2(\tilde{p}_n^2) + \tilde{\omega}_n^2C^2(\tilde{p}_n^2) + B^2(\tilde{p}_n^2)\right].\qquad(6.44)$$

Kada je $\mathbf{p} = 0$, singularitete označavamo s $\pm m_k = \pm m_k^R \pm i m_k^I$ i $\pm m_k^* = m_k^R \mp i m_k^I$. Za $\mathbf{p} \neq 0$ imamo

$$\mathscr{E}_k^2 = \mathbf{p}^2 + m_k^2,\qquad(6.45)$$

za kompleksne energije $\mathscr{E}_k = \epsilon_k + i\gamma_k$ tako da

$$\epsilon_k = \frac{1}{\sqrt{2}}\left\{(m_k^R)^2 - (m_k^I)^2 + \mathbf{p}^2 + \sqrt{\left[(m_k^R)^2 - (m_k^I)^2 + \mathbf{p}^2\right]^2 + 4(m_k^R)^2(m_k^I)^2}\right\}^{1/2},$$

$$\gamma_k = \frac{m_k^R m_k^I}{\epsilon_k}.$$

$$(6.46)$$

Tada se kinetički član u termodinamičkom potencijalu može zapisati kao

$$\Omega_{\text{kin}} = \Omega_{\text{zpt}} - \frac{d_q}{2}T\sum_{k=1}^{\infty}\int\frac{d^3p}{(2\pi)^3}\left\{\log\left[1 + e^{-\beta(\mathscr{E}_k - \mu)}\right] + \log\left[1 + e^{-\beta(\mathscr{E}_k^* - \mu)}\right]\right.$$
$$\left. + \log\left[1 + e^{-\beta(\mathscr{E}_k + \mu)}\right] + \log\left[1 + e^{-\beta(\mathscr{E}_k^* + \mu)}\right]\right\},$$
$$(6.47)$$

Ako udružimo logaritme, u mogućnosti smo dobiti nešto transparentniju formu

$$\Omega_{\text{kin}} = \Omega_{\text{zpt}} - \frac{d_q}{2}T\sum_{k=1}^{\infty}\int\frac{d^3p}{(2\pi)^3}\left\{\log\left[1 + 2e^{-\beta(\epsilon_k - \mu)}\cos(\beta\gamma_k) + e^{-2\beta(\epsilon_k - \mu)}\right]\right.$$
$$\left. + \log\left[1 + 2e^{-\beta(\epsilon_k + \mu)}\cos(\beta\gamma_k) + e^{-2\beta(\epsilon_k + \mu)}\right]\right\}.$$
$$(6.48)$$

Primjetimo da sada oscilatorna kosinus funkcija u termodinamičkom potencijalu može učiniti kvarkovsku materiju nestabilnom. Porijeklo oscilatorne funkcije vidimo u postojanju imaginarnog doprinosa γ_k masenih polova.

Kao moguće rješenje ovog problema predlažemo [137] uključenje Polyakovljeve petlje u sustav. U aproksimaciji srednjeg polja za Polyakovljevu petlju to se svodi na modifikaciju Fermi-Diracove distribucije

$$n(z) \rightarrow \left\{1 + e^{\beta[z - i(\lambda_3\phi_3 + \lambda_8\phi_8)]}\right\}^{-1},\qquad(6.49)$$

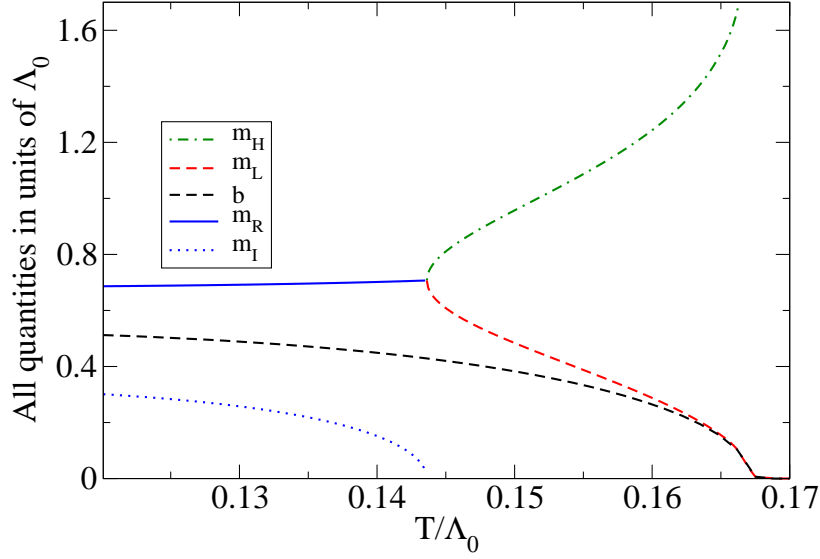gdje su $\phi_{3,8}$ pozadinska baždarna polja.

Figure 6.9: Temperaturna ovisnost najnižih kompleksno konjugiranih masenih polova u kiralnom limesu za separabilni model ranga 1 s Gaussijanskim faktorom oblika.

Usrednjavanjem po boji, kinetički doprinos termodinamičkom potencijalu može se napisati kao

$$
\begin{aligned}
\Omega_{\text{kin}} = {} & \Omega_{\text{zpt}} - 2N_f T \sum_{k=1}^{\infty} \int \frac{d^3 p}{(2\pi)^3} \Bigg\{ \\
& \log\Big[1 + 6\Phi\Big(e^{-\beta(\epsilon_k - \mu)} \cos(\beta\gamma_k) + e^{-4\beta(\epsilon_k - \mu)} \cos(2\beta\gamma_k) \Big) \\
& + 6\bar{\Phi}\Big(e^{-2\beta(\epsilon_k - \mu)} \cos(2\beta\gamma_k) + e^{-5\beta(\epsilon_k - \mu)} \cos(\beta\gamma_k) \Big) \\
& + 9\Phi^2 e^{-2\beta(\epsilon_k - \mu)} + 9\bar{\Phi}^2 e^{-4\beta(\epsilon_k - \mu)} \\
& + 18\Phi\bar{\Phi} e^{-2\beta(\epsilon_k - \mu)} \cos(\beta\gamma_k) + 2e^{-3\beta(\epsilon_k - \mu)} \cos(3\beta\gamma_k) + e^{-6\beta(\epsilon_k - \mu)} \Big] \\
& + (\mu \rightarrow -\mu) \Bigg\} .
\end{aligned}
\tag{6.50}
$$

Uspoređujući s izrazom (6.48), vidimo da su dominantni kosinusni članovi zasijenjeni s Polyakovljevom petljom. Kao posljedica, nestabilnosti u pritisku su znatno potisnute u zatočenoj fazi, tj. dok god su Φ i $\bar{\Phi}$ nula.

Za eksplicitnu demonstraciju nestabilnosti promatramo specifični model. Preciznije, promatramo klasu separabilnih Dyson-Schwinger modela. Kao što je već primjećeno u literaturi nestabilnosti u pritisku pojavljuju se u određenim
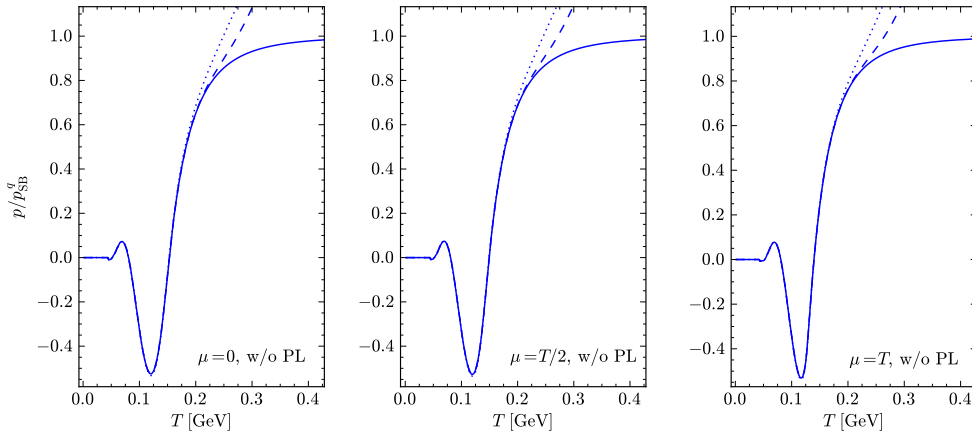
Figure 6.10: Skaliran pritisak p/p_{SB}^q kao funkcija temperature, za sistem bez Polyakovljeve petlje. Puna krivulja predstavlja puno numeričko rješenje, dok točkasta i crtkana krivulja predstavljaju aproksimaciju koja uzima u obzir prvi, odnosno prvi te naredni kvartet polova, respektivno.

područjima $T-\mu$ ravnine [97, 139, 140, 141, 142]. Cilj trenutne studije je demonstracija da je uzrok tih nestabilnosti pojava kompleksih masa, te pokazati kakav je efekt Polyakovljeve petlje.

Termodinamički potencijal u reprezentaciji kompleksno konjugiranih masenih polova dan je kao

$$\Omega_{\text{reg}} = \Omega_{\text{cond}} + \Omega_{\text{zpt}}^{\text{reg}} + \Omega_{\text{kin}} - \Omega_{\text{zpt}} , \qquad (6.51)$$

gdje promatramo slučaj u kojem se vektorski dio fermionskog propagatora ne renormalizira, te gdje za Ω_{kin} koristimo (6.48) i (6.50) u slučaju sa i bez Polyakovljeve petlje, respektivno. Krenuti ćemo od aproksimacije u kojoj radimo ograničenje na slučaj u kojem imamo samo prvi, odnosno samo prvi i drugi kvartet polova. Računamo pritisak skaliran na svoju Stefan-Boltzmannovu vrijednost sa i bez gluonskih stupnjeva slobode.

Rezultati modela koji ne uključuje Polyakovljevu petlju su dani na slici 6.10. Najinteresantniji doprinos su oscilacije, koje signaliziraju termodinamičku nestabilnost, kao što je nagoviješteno kosinusnim članovima u (6.48). Posebno je problematično što pritisak nije monotona funkcija, nego je za neke temperature i negativan. Također je važno za naglasiti da je uzimanje u obzir samo najnižih polova odlična aproksimacija na niskim temperaturama te osobito u području nestabilnosti. Oscilacije u pritisku se stoga mogu kvalitativno razumijeti kroz temperaturnu ovisnost singulariteta sa slike 5.4. Nakon temperature od oko $0.1\Lambda_0$, maseni procjep padne ispod svoje kritične vrijednosti, čime
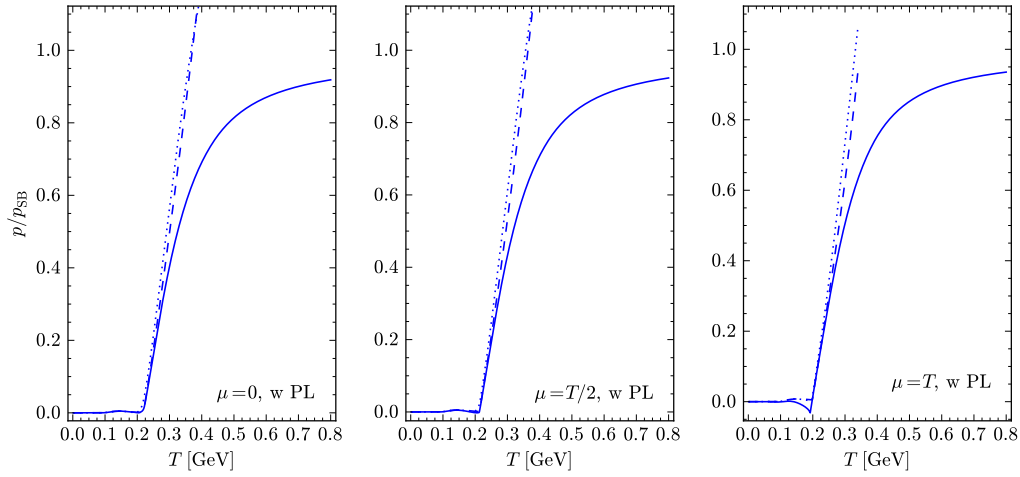
Figure 6.11: Kao i prethodna slika, samo u slučaju sa Polyakovljevom petljom.

kompleksni polovi postaju dva realna pola, nakon čega više nema oscilatornog ponašanja.

Uvođenje Polyakovljeve petlje vodi na dramatično poboljšanje. Na slici 6.11 demonstrirano je da su oscilacije izrazito potisnute. S obzirom na to da Polyakovljeva petlja ne eliminira sve kosinusne članove u potpunosti, rezidualne oscilacije su prisutne u rezultatima za $\mu/T = 0, 1/2$, dok se za $\mu/T = 1$ primjećuje negativan pritisak i u punom numeričkom računu.

Na slici 6.12 pokazujemo numerički dobivenu entropiju za modele ranga 2. Primjetimo prvo da nema negativnog pritiska u kiralno slomljenoj fazi za Gaussijanski kao ni za Lorentzijanski regulator. Na visokim T, kiralna simetrija je restaurirana, maseni procjep gotovo iščezavajući, te slučaj s Gaussovskim faktorom oblika pokazuje izrazitu oscilaciju, što je u konfliktu sa monotonim porastom iz računa na rešetci [143]. Štoviše, s obzirom na to da su polovi drugog reda, pritisak je u određenom području veći od Stefan-Boltzmannovog limesa. Ovaj nezadovoljavajući rezultat je poboljšan u slučaju Lorentzijanske parametrizacije; oscilacija je nešto reducirana, dajući entropiju unutar Stefan-Boltzmannove granice, na cijelom temperaturnom području.

Uključenje Polyakovljeve petlje opet unosi znantno poboljšanje [131]. Međutim, s obzirom na to da je Polyakovljeva petlja različita od nule u visokotemperaturnom području, tj. nakon faznog prijelaza, mehanizam više nije tako učinkovit. To je razlog zbog čega se npr. u Gaussijanskom modelu mogu i dalje vidjeti rezidualne oscilacije na desnoj strani slike 6.12.

Pri diskusiji nestabilnosti, nekoliko interesatnih pitanja ostaje otvoreno:

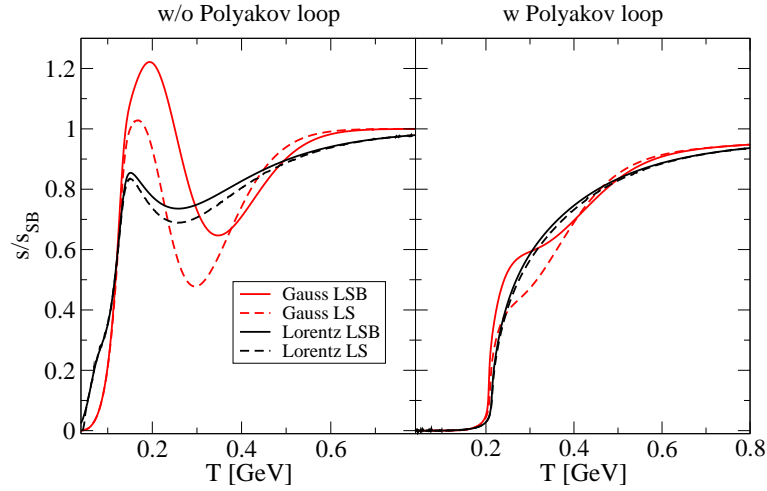- Vezani sustav kvarkova i gluona može imati neku netrivijalnu analitičku

Figure 6.12: Slike prikazuju skaliranu entropijju kao funkciju temperature za Gaussijanski i Lorentzijanski model ranga 2.

struktura, koja ima porijeklo u zatočenju. Ako da, onda je moguće da se te strukture na konačnoj temperaturi tako urote da ne vidimo oscilacije (zapravo, s računa na rešetci znamo da su nefizikalne).

- S druge strane, možemo se zapitati, želimo li zbilja ta stanja ubrajati u termodinamiku? Konačno, fizikalna stanja na niskoj T nisu kvarkovi i gluoni, nego mezoni i barioni. To su stanja koja bi trebala koja bi trebalo uzeti u obzir. Gledano na taj način, neuspjeh modela se može tražiti u nedostatku opisa koji ide iznad aproksimacije srednjeg polja. Primjetimo i to da, bar unutar ovih modela, nije moguće jednostavno rukom maknuti kompleksna stanja - neka od njih su povezana s fizikalnim singularitetom na visokim temperaturama, pa bi onda time izgubili i fizikalno stanje.

- Da li zbilja imamo kompleksna stanja u propagatoru? Nema nikakvog dokaza da te strukture uistinu i postoje, Iako je moguće npr. da je propagator cijela funkcija, kao što je diskutirano u npr. [148, 149]. Ali cijela funkcija je ili konstanta ili ima singularitet u beskonačnosti. Ako je to zbilja slučaj za kvarkovski propagator, onda povratna reakcija gluonskog sektora mora biti utoliko značajna da rekonstruira njegovu analitičku strukturu na visokim T.

- U jednostavnom modelu koji smo ovdje koristili, impulsna ovisnost kvarkovskog propagatora je takva da može razumno opisati rezultate s re-
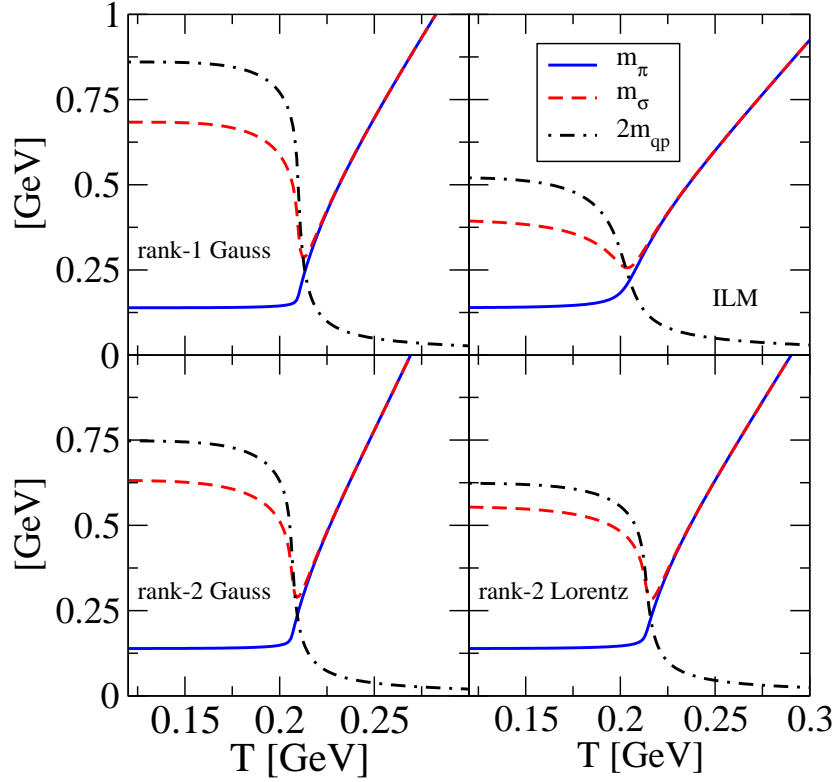
Figure 6.13: Panel prikazuje mase π i σ mezona za različite modele. Rezultati za Gaussijanski i Lorentzijanski model ranga 2 rješavamo puni sustav gdje je Lorentzova simetrija slomljena u mediju.

šetke. Ali rezultati s rešetke su dani samo na imaginarnoj (Euklidskoj) osi kompleksne ravnine. A priori nije jasno koja funkcija treba biti korištena, te da li ista funkcija mora biti korištena u cijeloj kompleksnoj ravnini. Najvjerojatnije ne mora biti tako, što onda vodi na mogućnost da su polovi u kompleksnoj ravnini možda samo posljedica našeg neznanja kvarkovskog propagatora u kompleksnoj ravnini.

Aspekti Mottovog prijelaza u kovarijantnim kvarkovskim modelima

U skladu s eksperimentalnim rezultatima s CERN-SPS, RHIC i LHC eksperimenta, kvark-gluon plazma stvorena u sudarima teških iona je jako korelirana tekućina [153, 154]. To znači da ne samo da su korelacije važne za opis te faze, nego su još i važnije za opis samog faznog prijelaza.

Recentne studije sa rešetke u stanju su potvrditi ovu veoma prirodnu paradigmu: jednadžba stanja na niskim temperaturama, gdje je kiralna simetrija slomljena, otkriva hadrone kao aktivne stupnjeve slobode [143]. Kao dodatna potvrda, model plina hadronskih rezonanci, postavljen od strane Rolf Hagedorna u '65 [155], ispravno saturira rezultate s rešetke u području niskih temperatura [156, 157, 158]. S takvim uvidom, razumijemo da realistično teorijsko predviđanje QCD faznog dijagrama mora ići dalje od aproksimacije srednjeg polja, i uključiti mezone i barione kao aktivne stupnjeve slobode. Npr. u referencama [159, 160] pokazano je da ispravan opis kemijskog zamrzavanja u kasnijoj fazi sudara teških iona, preko opisa topljenja kvarkovskog kondenzata, je moguć pod uvjetom da se uključi povratna reakcija hadronskih stupnjeva slobode. Zapravo, aktivirajući tek nekoliko najnižih stanja, kao što su npr. π i σ mezoni, ima važne posljedice na fazni dijagram: studije koje koriste funkcionalnu renormalizacijsku grupu ukazuju na to da fluktuacije mekšaju granice između faza, i miču kritičnu točku iz faznog dijagrama [161, 162].

Vraćajući se nazad na plin hadronskih rezonanci, razumijemo da on može predstavljati realni scenarij samo do neke točke: Hagedornove granične temperature [155]. Drugim riječima, u nekom trenutku hadroni se moraju disocirati u svoje konstituente: kvarkove i gluone. U tom smislu, postaje jasno da je moguće QCD fazni prijelaz razumijeti kroz disocijaciju hadrona.

Svojstva korelacija u mediju zapisana su u mezonskoj polarizacijskoj funkciji. U svrhu računa, koristiti ćemo separabilni model, kao model instantonske tekućine. Također koristimo logaritamski potencijal Polyakovljeve petlje.

Računamo prostorne mase rješavajući jednadžbu

$$1 - \frac{2D_0}{9}\Pi_M(0, -i m_M^{\text{spat}}) = 0 \,. \tag{6.52}$$

Ovo pojednostavljenje je podržano računima u NJL modelu [171, 172] gdje je pažljiva usporedba dinamičkih i prostornih masa napravljena, te je ustanovljeno da su kvalitativno i jedna i druga veličina veoma slične, u smislu da obje npr. demonstriraju degeneraciju jednom kada se kiralna simetrija restaurira. S druge strane, obje mase su i numerički slične u nisko temperaturnoj granici, dok na višim temperaturam, nakon kiralne restauracije, dinamičke mase su niže, a prostorne mase asimptotski odlaze u Eletskii-Ioffe $2\pi T$ granicu.
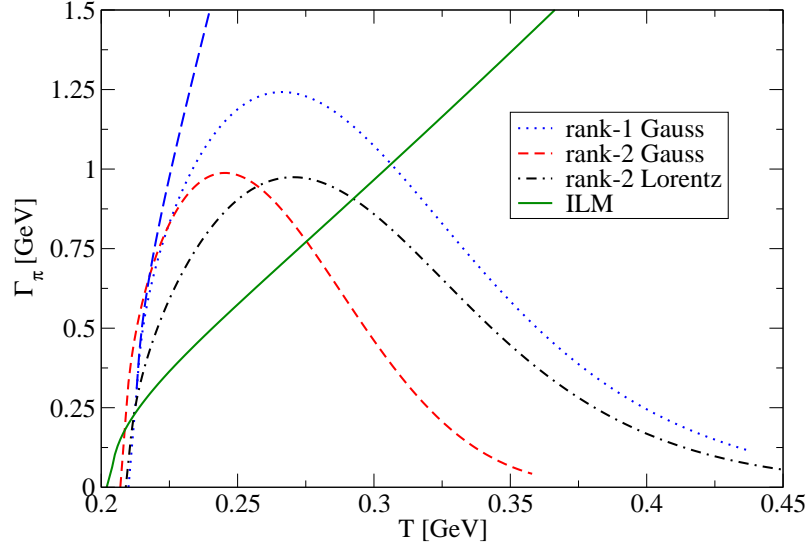
Figure 6.14: Slika prikazuje širinu raspada za pion izračunatu iz (6.54) za sve modele od interesa.

Ako radi jednostavnosti uzmemo vakuumski mezonski propagator u Euklidskom prostoru i razvijemo ga oko $P^2 = -m_M^2$, imamo

$$\Delta(P^2) = \frac{1}{-\frac{1}{G_S} + \Pi_M(P^2)} \rightarrow \frac{g^2_{M\bar{q}q}}{P^2 + m_M^2 + i\Gamma_M m_M}\,, \qquad (6.53)$$

gdje je Γ_M širina raspada

$$\Gamma_M = g^2_{M\bar{q}q} \frac{\mathrm{Im}(\Pi_M)}{m_M}\,, \qquad (6.54)$$

te $g_{M\bar{q}q}$ efektivno kvark-mezon vezanje Za realne polove, imaginarni dio možemo izračunati pomoću $i\epsilon$ preskripcije

$$\mathrm{Im}[\Pi_M(-iP_0, 0)] = \frac{1}{2i} \left[\Pi_M(-i(P_0 + i\epsilon), 0) - \Pi_M(-i(P_0 - i\epsilon), 0) \right]. \qquad (6.55)$$

Na slici 6.13 prikazane su prostorna masa pi i sigma mezona. Osim prostornih masa, interesantno je prikazati i kontinuum stanja definiran s $2m_{\mathrm{qp}}$ gdje je m_{qp} tzv. konstituentna masa, ovdje definirana kao masa kada impuls iščezava. Striktno govoreći ova stanja fizikalno nisu nužno prisutna na niskim temperaturama u smislu da su uistinu singulariteti kvarkovskog propagatora, kao što je slučaj na visokim temperaturama.

Računamo širine koristeći prostorne mase, tj. tako da zamijenimo $P_0 \to m_M^{\text{spat}}$. To sigurno unosi grešku u naš račun, ali s obzirom na to da je kvalitativno ponašanje prostornih i dinamičkih masa slično, korisno je napraviti aproksimativnu studiju. S obzirom na to da se Mottov prijelaz dešava relativno blizu kiralnog prijelaza, pion i sigma mezon su gotovo degenerirani u masi, tako da je dovoljno usredotočiti se na pion. Za kvark-mezon vezanje računamo njegovu vakuumsku vrijednost, koju koristimo i na konačnoj temperaturi.

Slika 6.14 je glavni rezultat ovog odjeljka. Za modele ranga 1 i ranga 2, širine pokazuju generičko ponašanje. Na niskim temperaturama, širina raspada monotono raste. Ali, s obzirom na to da u nelokalnim modelima, kompletni imaginarni dio, pa stoga i širina, je pomnožena s regulatorom, upravo to je faktor koji diktira visokotemperaturno ponašanje. Naime, kako je $\mathscr{F}_0(p^2)$ izrazito padajuća funkcija impulsa, te kako u modelima ranga 1 i ranga 2, argument je rastuća funkcija temperature, na visokim temperaturama širina raspada se smanjuje. Stoga, na visokim temperaturama, širina pada na nulu. Naravno, ovo ponašanje je u određenoj mjeri pretjerano, s obzirom na to očekujemo da dinamičke mase ne rastu tako izrazito s temperaturom kao prostorne. No, unatoč tome, kvalitativni trend je generički za cijelu klasu separabilnih modela.

U referenci [176] račun je napravljen u kojem je predfaktor

$$\mathscr{F}_0^2\left(\frac{P_0^2}{4} - m_{\text{qp}}^2\right) \tag{6.56}$$

iz imaginarnog dijela polarizacijske funkcije maknut rukom, u kojem slučaju dobijemo monotono rastuću širinu raspada, potvrđujući time da je uistinu taj predfaktor odgovoran za nefizikalno ponašanje na visokim temperaturama. To je i pokazano na slici 6.14, sa crtkanom plavom krivuljom.

Rezultat dobiven u modelu instantonske tekućine je kompletno drugačiji. S obzirom na činjenicu da faktor oblika u tom slučaju ima drugačiju particiju impulsa u polarizacijskoj funkciji, u njegovom argumentu nema funkcijske ovisnosti o mezonskoj masi, čime je njegov efekt na visokim temperaturama mali. To konačno daje monotoni rast širine Γ_π, prikazan s zelenom krivuljom, na niskim kao i na visokim temperaturama.

Zaključak

Kako je QCD neperturbativan na niskim energijama, izučavali smo njegova svojstva pomoću efektivnih modela, koja uključuju kvarkove i gluone kao aktivne stupnjeve slobode.

Za $\gamma^* \to \pi^+\pi^0\pi^-$ proces pružili smo alternativno scenarij za objašnjenje jedine postojeće eksperimentalne točke do sada tako da smo u model uključili

vektorske mezone. Predvidjeli smo ponašanje faktora oblika za raspon impulsa koji će biti istražen na već postojećim te budućim eksperimentima na CEBAFU i COMPASSU.

Da bi objasnili analizu eksperimentalnih podataka o η' multiplicitetu sa sudara teških iona, pronašli smo da je nužno modificirati Witten-Veneziano relaciju na konačnim temperaturama. Osnova za modifikaciju nam je bila veza između kiralne i $U(1)_A$ simetrije kvantne kromodinamike. U našem scenariju, masa η' čestice je reducirana u kiralno restauriranoj fazi.

Termodinamička nestabilnost je identificirana u općoj klasi kovarijantnih kvarkovskih modela na nivou jedne petlje. Uspjeli smo djelomično ukloniti nestabilnost već u aproksimaciji srednjeg polja: vezanjem kvarkova na Polyakovljevu petlju. S uključenjem Polykovljeve petlje kao esencijalnog elementa, izučavali smo termodinamiku realističnijih modela, koji uzimaju u obzir i renormalizaciju valne funkcije. Pokazali smo da je u računima prikladnije korisititi faktore oblika Lorentzijanskog tipa. Unutar aproksimacije srednjeg polja napravili smo studiju faznog dijagrama i zaključili da utjecaj lomljenja Lorentzove simetrije u mediju ima mali utjecaj na kritičnu točku kiralnog faznog prijelaza.

Kao prvi korak u studiji koja uključuje mezonske korelacije kroz njihovu podstrukturu, računali smo disocijaciju mezona u separabilnom Dyson-Schwinger modelu s dva kvarkovska okusa. Rezultati ukazuju da dok separabilni modeli daju širinu koja pada na visokim temperaturama, model instantonske tekućine daje znatno bolji opis u kojem širina monotono raste s temperaturom. Ovakva neočekivana osjetljivost na detalje modela pokazuje da bi proučavanje vezanih stanja u modelu QCD-a definiranom u Coulombovom baždarenju moglo biti prikladnije.

Bibliography

[1] M. Gell-Mann, Phys. Lett. **8** (1964) 214.

[2] E. D. Bloom, D. H. Coward, H. C. DeStaebler, J. Drees, G. Miller, L. W. Mo, R. E. Taylor and M. Breidenbach *et al.*, Phys. Rev. Lett. **23** (1969) 930.

[3] M. Breidenbach, J. I. Friedman, H. W. Kendall, E. D. Bloom, D. H. Coward, H. C. DeStaebler, J. Drees and L. W. Mo *et al.*, Phys. Rev. Lett. **23** (1969) 935.

[4] J. C. Pati and A. Salam, Phys. Rev. D **8** (1973) 1240.

[5] H. Fritzsch, M. Gell-Mann and H. Leutwyler, Phys. Lett. B **47** (1973) 365.

[6] S. Weinberg, Phys. Rev. Lett. **31** (1973) 494.

[7] D. J. Gross and F. Wilczek, Phys. Rev. Lett. **30** (1973) 1343.

[8] H. D. Politzer, Phys. Rev. Lett. **30** (1973) 1346.

[9] S. Durr, Z. Fodor, J. Frison, C. Hoelbling, R. Hoffmann, S. D. Katz, S. Krieg and T. Kurth *et al.*, Science **322** (2008) 1224

[10] O. Philipsen, Prog. Theor. Phys. Suppl. **174** (2008) 206

[11] F. Karsch, Lect. Notes Phys. **583** (2002) 209

[12] P. Petreczky, J. Phys. G **39** (2012) 093002

[13] C. D. Roberts and S. M. Schmidt, Prog. Part. Nucl. Phys. **45** (2000) S1

[14] R. Alkofer and L. von Smekal, Phys. Rept. **353** (2001) 281

[15] J. Berges, N. Tetradis and C. Wetterich, Phys. Rept. **363** (2002) 223

[16] H. Gies, Lect. Notes Phys. **852** (2012) 287

[17] S. Scherer and M. R. Schindler, Lect. Notes Phys. **830** (2012) pp.1.

[18] T. D. Cohen, Rev. Mod. Phys. **68** (1996) 599.

[19] M. B. Parappilly, P. O. Bowman, U. M. Heller, D. B. Leinweber, A. G. Williams and J. BZhang, Phys. Rev. D **73** (2006) 054504

[20] W. Kamleh, P. O. Bowman, D. B. Leinweber, A. G. Williams and J. Zhang, Phys. Rev. D **76** (2007) 094501 [arXiv:0705.4129 [hep-lat]].

[21] K. Fukushima and C. Sasaki, Prog. Part. Nucl. Phys. **72** (2013) 99

[22] A. M. Polyakov, Phys. Lett. B **72** (1978) 477.

[23] R. D. Pisarski and F. Wilczek, Phys. Rev. D **29** (1984) 338.

[24] M. Fukugita, M. Okawa and A. Ukawa, Phys. Rev. Lett. **63** (1989) 1768.

[25] A. Bazavov, T. Bhattacharya, M. Cheng, C. DeTar, H. T. Ding, S. Gottlieb, R. Gupta and P. Hegde *et al.*, Phys. Rev. D **85** (2012) 054503 [arXiv:1111.1710 [hep-lat]].

[26] U. W. Heinz and M. Jacob, nucl-th/0002042.

[27] H. Song, S. A. Bass, U. Heinz, T. Hirano and C. Shen, Phys. Rev. Lett. **106** (2011) 192301 [Erratum-ibid. **109** (2012) 139904]

[28] P. Foka [the ALICE Collaboration], J. Phys. Conf. Ser. **455** (2013) 012004.

[29] K. Rajagopal and F. Wilczek, In *Shifman, M. (ed.): At the frontier of particle physics, vol. 3* 2061-2151

[30] M. G. Alford, A. Schmitt, K. Rajagopal and T. Schäfer, Rev. Mod. Phys. **80** (2008) 1455

[31] M. E. Peskin and D. V. Schroeder, "An Introduction to quantum field theory," Reading, USA: Addison-Wesley (1995) 842 p

[32] S. L. Adler, Phys. Rev. **177** (1969) 2426.

[33] J. S. Bell and R. Jackiw, Nuovo Cim. A **60** (1969) 47.

[34] J. Wess and B. Zumino, Phys. Lett. B **37** (1971) 95.

[35] E. Witten, Nucl. Phys. B **223** (1983) 422.

[36] R. Aviv and A. Zee, Phys. Rev. D **5** (1972) 2372.

[37] Y. .M. Antipov, V. A. Batarin, V. A. Bezzubov, N. P. Budanov, Y. .P. Gorin, Y. .A. Gornushkin, S. P. Denisov and S. V. Klimenko *et al.*, Phys. Rev. D **36** (1987) 21.

[38] T. Hannah, Nucl. Phys. B **593** (2001) 577 [hep-ph/0102213].

[39] L. Ametller, M. Knecht and P. Talavera, Phys. Rev. D **64** (2001) 094009

[40] R. A. Miskimen, K. Wang, A. Yagneswaran (spokesmen),"Study of the Axial Anomaly using the $\gamma\pi^+ \to \gamma\pi^+$ Reaction Near Threshold", letter of intent, CEBAF-experiment 94-015.

[41] M. A. Moinester and V. Steiner,

[42] P. Abbon *et al.* [COMPASS Collaboration], Nucl. Instrum. Meth. A **577**, 455 (2007) [arXiv:hep-ex/0703049].

[43] D. G. Sutherland, Nucl. Phys. B **2** (1967) 433.

[44] M. Veltman, Proc. R. Soc. A **301** (1967) 107.

[45] D. Kekez and D. Klabucar, Phys. Lett. B **457** (1999) 359

[46] B. Bistrovic and D. Klabucar, Phys. Rev. D **61** (2000) 033006

[47] M. D. Scadron, Hackensack, USA: World Scientific (2007) 424 p

[48] T. Hakioglu, M. D. Scadron, Phys. Rev. **D42** (1990) 941-944.

[49] T. Hakioglu, M. D. Scadron, Phys. Rev. **D43** (1991) 2439-2442.

[50] R. Delbourgo and M. D. Scadron, Mod. Phys. Lett. A **10** (1995) 251

[51] R. Delbourgo, D. -s. Liu and M. D. Scadron, Int. J. Mod. Phys. A **14** (1999) 4331

[52] D. Kekez, D. Klabucar and M. D. Scadron, Fizika B **14** (2005) 13

[53] E. P. Venugopal and B. R. Holstein, Phys. Rev. D **57** (1998) 4397

[54] H. H. Adam *et al.* [WASA-at-COSY Collaboration], arXiv:nucl-ex/0411038.

[55] S. Schadmand [WASA-at-COSY Collaboration], AIP Conf. Proc. **1322**, 161 (2010).

[56] H. B. O'Connell, B. C. Pearce, A. W. Thomas and A. G. Williams, Prog. Part. Nucl. Phys. **39** (1997) 201

[57] G. 't Hooft and M. J. G. Veltman, Nucl. Phys. B **153** (1979) 365.

[58] S. Rudaz, Phys. Rev. D **10** (1974) 3857.

[59] L. Ametller, L. Bergstrom, A. Bramon and E. Masso, Nucl. Phys. B **228** (1983) 301.

[60] J. L. Basdevant, D. Bessis and J. Zinn-Justin, Nuovo Cim. A **60** (1969) 185.

[61] S. Rudaz, Phys. Lett. B **145** (1984) 281.

[62] T. D. Cohen, Phys. Lett. B **233** (1989) 467.

[63] S. Benic and D. Klabucar, Phys. Rev. D **85** (2012) 034042

[64] S. Weinberg, Phys. Rev. Lett. **17** (1966) 336.

[65] Y. Tomozawa, Nuovo Cim. A **46** (1966) 707.

[66] S. R. Cotanch and P. Maris, Phys. Rev. D **68** (2003) 036006

[67] P. Maris and P. C. Tandy, Phys. Rev. C **61** (2000) 045202

[68] M. V. Terent'ev, Phys. Lett. B **38** (1972) 419.

[69] M. V. Terentev, Usp. Fiz. Nauk **112** (1974) 37 [Sov. Phys. Usp. **17** (1974) 20].

[70] B. R. Holstein, Phys. Rev. **D53** (1996) 4099-4101.

[71] B. Bistrović and D. Klabučar, Phys. Lett. B **478** (2000) 127

[72] S. R. Coleman, "1/n," SLAC-PUB-2484.

[73] H. Ito, W. Buck and F. Gross, Phys. Rev. C **43** (1991) 2483.

[74] M. Buballa and S. Krewald, Phys. Lett. B **294** (1992) 19.

[75] D. Gomez Dumm, A. G. Grunfeld and N. N. Scoccola, Phys. Rev. D **74** (2006) 054026

[76] S. M. Schmidt, D. Blaschke and Y. .L. Kalinovsky, Phys. Rev. C **50** (1994) 435.

[77] J. I. Kapusta and C. Gale, Cambridge, UK: Univ. Pr. (2006) 428 p

[78] C. J. Burden, L. Qian, C. D. Roberts, P. C. Tandy and M. J. Thomson, Phys. Rev. C **55** (1997) 2649

[79] D. Horvatic, D. Blaschke, D. Klabucar and A. E. Radzhabov, Phys. Part. Nucl. **39** (2008) 1033

[80] J. M. Cornwall, R. Jackiw and E. Tomboulis, Phys. Rev. D **10** (1974) 2428.

[81] D. Diakonov and V. Y. .Petrov, Nucl. Phys. B **245** (1984) 259.

[82] T. Schäfer and E. V. Shuryak, Rev. Mod. Phys. **70** (1998) 323

[83] R. D. Bowler and M. C. Birse, Nucl. Phys. A **582** (1995) 655

[84] R. S. Plant and M. C. Birse, Nucl. Phys. A **628**, 607 (1998).

[85] R. T. Cahill and S. M. Gunner, Austral. J. Phys. **50** (1997) 103

[86] P. C. Tandy, Prog. Part. Nucl. Phys. **39** (1997) 117

[87] T. Hatsuda and T. Kunihiro, Phys. Rept. **247**, 221 (1994).

[88] M. Buballa, Phys. Rept. **407**, 205 (2005).

[89] G. Ripka, Oxford, UK: Clarendon Pr. (1997) 205 p

[90] M. R. Frank and T. Meissner, Phys. Rev. C **53** (1996) 2410

[91] W. Broniowski, [hep-ph/9909438].

[92] E. -M. Ilgenfritz and J. Kripfganz, Z. Phys. C **29** (1985) 79.

[93] A. Gocksch and M. Ogilvie, Phys. Rev. D **31** (1985) 877.

[94] K. Fukushima, Phys. Lett. B **591** (2004) 277

[95] C. Ratti, M. A. Thaler and W. Weise, Phys. Rev. D **73** (2006) 014019

[96] S. Roessner, C. Ratti and W. Weise, Phys. Rev. D **75** (2007) 034007

[97] D. Blaschke and P. C. Tandy, in Proceedings of the International Workshop on "Understanding deconfinement in QCD", Ed. by D. Blaschke, F. Karsch and C.D. Roberts, World Scientific, Singapore (2000), p. 218; [arxiv: nucl-th/9905067].

[98] S. Noguera and N. N. Scoccola, Phys. Rev. D **78**, 114002 (2008).

[99] D. Blaschke, G. Burau, Y. .L. Kalinovsky, P. Maris and P. C. Tandy, Int. J. Mod. Phys. A **16**, 2267 (2001).

[100] S. Weinberg, Phys. Rev. D **11** (1975) 3583.

[101] A. A. Belavin, A. M. Polyakov, A. S. Schwartz and Y. .S. Tyupkin, Phys. Lett. B **59** (1975) 85.

[102] G. 't Hooft, Phys. Rev. D **14** (1976) 3432 [Erratum-ibid. D **18** (1978) 2199].

[103] E. Witten, Nucl. Phys. B **156** (1979) 269.

[104] G. Veneziano, Nucl. Phys. B **159** (1979) 213.

[105] A. V. Manohar, "Large N QCD," hep-ph/9802419.

[106] J. I. Kapusta, D. Kharzeev and L. D. McLerran, Phys. Rev. D **53** (1996) 5028

[107] E. V. Shuryak, Comments Nucl. Part. Phys. **21** (1994) 235

[108] T. D. Cohen, Phys. Rev. D **54** (1996) 1867

[109] S. H. Lee and T. Hatsuda, Phys. Rev. D **54** (1996) 1871

[110] J. Schaffner-Bielich, Phys. Rev. Lett. **84** (2000) 3261

[111] P. Costa, M. C. Ruivo, C. A. de Sousa and Y. .L. Kalinovsky, Phys. Rev. D **70** (2004) 116013

[112] T. Csorgo, R. Vertesi and J. Sziklai, Phys. Rev. Lett. **105** (2010) 182301

[113] R. Vertesi, T. Csorgo and J. Sziklai, Phys. Rev. C **83** (2011) 054903

[114] H. Leutwyler and A. V. Smilga, Phys. Rev. D **46** (1992) 5607.

[115] P. Di Vecchia and G. Veneziano, Nucl. Phys. B **171** (1980) 253.

[116] S. Benic, D. Horvatic, D. Kekez and D. Klabucar, Phys. Rev. D **84** (2011) 016006

[117] S. Benic, D. Horvatic, D. Kekez and D. Klabucar, Acta Phys. Polon. Supp. **5** (2012) 941 [arXiv:1207.3068 [hep-ph]].

[118] D. Klabucar, S. Benic, D. Horvatic and D. Kekez, Acta Phys. Polon. Supp. **6** (2013) 3, 935 [arXiv:1311.1052 [hep-ph]].

[119] D. Kekez and D. Klabucar, Phys. Rev. D **73** (2006) 036002

[120] D. Horvatic, D. Klabucar and A. E. Radzhabov, Phys. Rev. D **76** (2007) 096009

[121] D. Klabucar and D. Kekez, Phys. Rev. D **58** (1998) 096003

[122] D. Klabucar, D. Kekez and M. D. Scadron, J. Phys. G **27** (2001) 1775

[123] G. Krein, C. D. Roberts and A. G. Williams, Int. J. Mod. Phys. A **7** (1992) 5607.

[124] C. J. Burden, C. D. Roberts and A. G. Williams, Phys. Lett. B **285** (1992) 347.

[125] S. J. Stainsby and R. T. Cahill, Int. J. Mod. Phys. A **7** (1992) 7541.

[126] C. J. Burden, Phys. Rev. D **57** (1998) 276.

[127] V. N. Gribov, Eur. Phys. J. C **10** (1999) 91.

[128] R. Alkofer, W. Detmold, C. S. Fischer and P. Maris, Phys. Rev. D **70** (2004) 014014.

[129] D. Dudal, J. A. Gracey, S. P. Sorella, N. Vandersickel and H. Verschelde, Phys. Rev. D **78** (2008) 065047.

[130] D. Dudal, M. S. Guimaraes, L. F. Palhares and S. P. Sorella, arXiv:1303.7134 [hep-ph].

[131] S. Benic, D. Blaschke, G. A. Contrera and D. Horvatic, arXiv:1306.0588 [hep-ph].

[132] O. Kaczmarek, F. Karsch, E. Laermann, C. Miao, S. Mukherjee, P. Petreczky, C. Schmidt and W. Soeldner *et al.*, Phys. Rev. D **83** (2011) 014504

[133] G. A. Contrera, M. Orsaria and N. N. Scoccola, Phys. Rev. D **82** (2010) 054026

[134] M. S. Bhagwat, M. A. Pichowsky, C. D. Roberts and P. C. Tandy, Phys. Rev. C **68** (2003) 015203

[135] B. C. Tiburzi, W. Detmold and G. A. Miller, Phys. Rev. D **68** (2003) 073002

[136] H. Chen, W. Yuan, L. Chang, Y. -X. Liu, T. Klahn and C. D. Roberts, Phys. Rev. D **78** (2008) 116015

[137] S. Benic, D. Blaschke and M. Buballa, Phys. Rev. D **86** (2012) 074002

[138] K. Fukushima, Phys. Rev. D **77**, 114028 (2008) [Erratum-ibid. D **78**, 039902 (2008)].

[139] I. General, D. Gomez Dumm and N. N. Scoccola, Phys. Lett. B **506** (2001) 267.

[140] D. Gomez Dumm and N. N. Scoccola, Phys. Rev. D **65** (2002) 074021.

[141] D. Gomez Dumm and N. N. Scoccola, Phys. Rev. C **72** (2005) 014909.

[142] M. Loewe, P. Morales and C. Villavicencio, Phys. Rev. D **83** (2011) 096005.

[143] S. Borsanyi, Nucl. Phys. A904-905 **2013** (2013) 270c

[144] G. K. Savvidy, Phys. Lett. B **71** (1977) 133.

[145] N. K. Nielsen and P. Olesen, Nucl. Phys. B **144** (1978) 376.

[146] P. N. Meisinger and M. C. Ogilvie, Phys. Lett. B **407** (1997) 297.

[147] P. N. Meisinger and M. C. Ogilvie, Phys. Rev. D **66** (2002) 105006.

[148] H. J. Munczek and A. M. Nemirovsky, Phys. Rev. D **28**, 181 (1983).

[149] G. V. Efimov and S. N. Nedelko, Phys. Rev. D **51** (1995) 176.

[150] S. Strauss, C. S. Fischer and C. Kellermann, Phys. Rev. Lett. **109** (2012) 252001

[151] A. Windisch, R. Alkofer, G. Haase and M. Liebmann, Comput. Phys. Commun. **184** (2013) 109

[152] A. Windisch, M. Q. Huber and R. Alkofer, Phys. Rev. D **87** (2013) 065005

[153] E. V. Shuryak, Nucl. Phys. A **750** (2005) 64

[154] U. A. Wiedemann, Nucl. Phys. A904-905 **2013** (2013) 3c

[155] R. Hagedorn, Nuovo Cim. Suppl. **3** (1965) 147.

[156] F. Karsch, K. Redlich and A. Tawfik, Phys. Lett. B **571** (2003) 67

[157] F. Karsch, K. Redlich and A. Tawfik, Eur. Phys. J. C **29** (2003) 549

[158] P. Huovinen and P. Petreczky, Nucl. Phys. A **837** (2010) 26

[159] D. B. Blaschke, J. Berdermann, J. Cleymans and K. Redlich, Phys. Part. Nucl. Lett. **8** (2011) 811

[160] D. Blaschke, J. Berdermann, J. Cleymans and K. Redlich, Few Body Syst. **53** (2012) 99

[161] T. K. Herbst, J. M. Pawlowski and B. -J. Schaefer, Phys. Lett. B **696** (2011) 58

[162] T. K. Herbst, J. M. Pawlowski and B. -J. Schaefer, Phys. Rev. D **88** (2013) 014007

[163] J. Hufner, S. P. Klevansky, P. Zhuang and H. Voss, Annals Phys. **234** (1994) 225.

[164] P. Zhuang, J. Hufner and S. P. Klevansky, Nucl. Phys. A **576** (1994) 525.

[165] J. Hufner, S. P. Klevansky and P. Rehberg, Nucl. Phys. A **606** (1996) 260.

[166] H. Hansen, W. M. Alberico, A. Beraudo, A. Molinari, M. Nardi and C. Ratti, Phys. Rev. D **75**, 065004 (2007).

[167] A. Wergieluk, D. Blaschke, Y. .L. Kalinovsky and A. Friesen, arXiv:1212.5245 [nucl-th].

[168] D. Blaschke, D. Zablocki, M. Buballa and G. Roepke, arXiv:1305.3907 [hep-ph].

[169] A. Scarpettini, D. Gomez Dumm and N. N. Scoccola, Phys. Rev. D **69**, 114018 (2004).

[170] G. A. Contrera, D. G. Dumm and N. N. Scoccola, Phys. Rev. D **81**, 054005 (2010).

[171] W. Florkowski and B. L. Friman, Z. Phys. A **347**, 271 (1994).

[172] W. Florkowski and B. L. Friman, Acta Phys. Polon. B **25** 49 (1994).

[173] R. E. Cutkosky, P. V. Landshoff, D. I. Olive and J. C. Polkinghorne, Nucl. Phys. B **12**, 281 (1969).

[174] M. Bhagwat, M. A. Pichowsky and P. C. Tandy, Phys. Rev. D **67** (2003) 054019.

[175] D. Horvatic, D. Blaschke, D. Klabucar and O. Kaczmarek, Phys. Rev. D **84**, 016005 (2011).

[176] S. Benic and D. Blaschke, Acta Phys. Polon. Supp. **6** (2013) 947

Sanjin Benić - Curriculum Vitae

Born 21. August 1982, Pula, Croatia

Address, phone, e-mail

Bijenička cesta 32, Department of Physics, Faculty of Science, 10 002 Zagreb, Croatia
00 385 01 460 5582
sanjinb@phy.hr

Education

2000 - 2008 Undergraduate Study at the Department of Physics, Faculty of Science, University of Zagreb, Croatia
direction: Theoretical Physics

2008 Diploma Thesis: "Some Anomalous Processes of Pseudoscalar Hadrons"
advisor: Prof. D. Klabučar

2009 - present Graduate Study at the Department of Physics, Faculty of Science, University of Zagreb, Croatia
direction: Particle Physics

Research interests

Quark matter. Continuum models of Quantum chromodynamics. QCD phase diagram. Applications to astrophysics, heavy ion collisions and early universe.

List of publications

1. S. Benić, D. Blaschke, G. A. Contrera and D. Horvatić, *Medium induced Lorentz symmetry breaking effects in nonlocal PNJL models*, arXiv:1306.0588 [hep-ph].

2. S. Benić, *Physical interpretation of the dressed Polyakov loop in the Nambu–Jona-Lasinio model*, Phys. Rev. D **88** (2013), 077501.

3. S. Benić, D. Blaschke and M. Buballa, *Thermodynamic Instabilities in Dynamical Quark Models with Complex Conjugate Mass Poles*, Phys. Rev. D

86 (2012) 074002.

4. S. Benić and D. Klabučar, *Axial anomaly and the interplay of quark loops with pseudoscalar and vector mesons in the $\gamma* \rightarrow \pi^+\pi^0\pi^-$ process*, Phys. Rev. D **85** (2012) 034042.

5. S. Benić, D. Horvatić, D. Kekez and D. Klabučar, *η' Multiplicity and the Witten-Veneziano relation at finite temperature*, Phys. Rev. D **84** (2011) 016006.

Conference proceedings

1. D. Blaschke, D. E. A. Castillo, S. Benić, *Mass-radius constraints for compact stars and a critical endpoint*, PoS CPOD 2013 (2013) 063.

2. S. Benić and D. Blaschke, *Finite temperature Mott transition in a nonlocal PNJL model*, Acta Phys. Polon. Supp. **6** (2013) 947.

3. D. Klabučar, S. Benić, D. Horvatić, D. Kekez, *η' multiplicity and Witten-Veneziano relation at $T > 0$*, Acta Phys. Polon. Supp. **6** (2013) 947.

4. D. Blaschke, D. E. A. Castillo, S. Benić, G. Contrera and R. Łastowiecki, *Nonlocal PNJL models and heavy hybrid stars*, PoS ConfinementX (2012) 249.

5. S. Benić, D. Horvatić, D. Kekez and D. Klabučar, *Restoration of singlet axial symmetry at finite temperature*, Acta Phys. Polon. Supp. **5** (2012) 941.

Working experience

2009 - present Research/Teaching Assistant at the Department of Physics, Faculty of Science, University of Zagreb, Croatia

2009 - present associate on the project Elementary particles, field theory and cosmology under the Contract No. 119-0982930-1016 of Ministry of Science, Education and Sports of Croatia

Teaching

2009 - present *Quantum mechanics, Relativistic quantum mechanics* (exercises)

2009 - 2010 *Selected chapters of nuclear physics and particle physics* (exercises)

2011 - present *Mathematical methods of physics* (exercises)

Stays abroad

01.10.2008–28.02.2009. Research Study at the Faculty of Physics, University of Vienna (*Vienna, Austria*)

Participation in Schools and conferences

2009
25.05.–29.05. International School on selected topics in Particle Physics (*Ljubljana, Slovenia*)

2010
27.11.–29.11. 6th Vienna Central European Seminar (*Vienna, Austria*)

10.03.–12.03. Spring Workshop in Theoretical Particle Physics (*Heviz, Hungary*)

24.05.–28.05. International School on selected topics in Particle Physics (*Ljubljana, Slovenia*)

2011
26.02.–04.03. Winter School in Theoretical Physics (*Schladming, Austria*)

03.05.–12.05. Compstar School and Workshop (*Catania, Italy*)
(talk: Restoration of the $U(1)_A$ symmetry in hot strongly interacting matter)

19.05.–21.05. 28th Max Born Symposium (*Wrocław, Poland*)
(poster: Restoration of singlet axial symmetry at finite T)

06.06.–17.06. Summer School on Particle Physics (*Trieste, Italy*)

2012

04.02.–11.02. 48th Karpacz Winter School of Theoretical Physics (*Ładek Zdroj, Poland*)
(talk and poster: Thermodynamic instability in non-local chiral quark models)

25.02.–02.03. Winter School in Theoretical Physics (*Schladming, Austria*)
(poster: Thermodynamic instability in non-local chiral quark models)

13.04.–15.04. 30th Max Born Symposium (*Wrocław, Poland*)

28.08.–08.09. Helmholtz International Summer School (*Dubna, Russia*)
(talk and poster: Thermodynamic instabilities in non-local chiral quark models)

24.09.–28.09. CompStar School (*Zadar, Croatia*)
(talk: Covariant non-local NJL models at finite μ: some results and applications for hybrid stars)

30.11.–02.12. 9th Vienna Central European Seminar (*Vienna, Austria*)

18.12.–20.12. Mini-Symposium (*Wrocław, Poland*)
(talk: Mesonic correlations in non-local NJL model-status report)

2013

03.02.–09.02. Excited QCD (*Sarajevo, Bosnia and Herzegovina*)
(talk: Mesonic correlations in non-local NJL model-status report)

14.04.–24.05. Doctoral Training Programme (*Trento, Italy*)
(talk: Heavy hybrid stars in non-local PNJL model)

27.06.–28.06. Austria-Croatia-Hungary-Triangle Workshop (*Bildungshaus Schloss Retzhof, Leitring, Austria*)
(talk: Heavy hybrid stars in non-local PNJL model)

14.06.–16.06. 31st Max Born Symposium (*Wrocław, Poland*)
(talk: Hybrid stars from lattice constrained nonlocal PNJL model,
poster: Lorentz symmetry breaking effects in non-local PNJL models beyond the mean field)

30.08.–04.09. Summer workshop for theoretical physics (*Rab, Croatia*)
(talk: Physical interpretation of the dressed Polyakov loop in the NJL model)

09.09.–13.09. Topics in Cosmology (*Prague, Czech Republic*)

Member of the organizing committee of schools and conferences

24.09.2012.–28.09.2012. CompStar School (*Zadar, Croatia*)